MALATYA TURGUT ÖZAL UNIVERSITY

NATURENGS

MTU Journal of Engineering and Natural Sciences

Volume: 1 Issue: 2 - December 2020

https://dergipark.org.tr/tr/pub/naturengs

www.naturengs.com

MALATYA TURGUT ÖZAL UNIVERSITY

NATURENGS

MTU Journal of Engineering and Natural Sciences

Volume: 1 / Issue: 2 / December - 2020

We are delighted to present the second issue of the journal NATURENGS owned by Malatya Turgut Özal University. MTU Journal of Engineering and Natural Sciences – NATURENGS is a double-blind peer-reviewed, open-access international journal which will publish electronically two times in a year by the Malatya Turgut Özal University from June 2020.

We set out with the desire to create an environment where scientific and / or technological studies carried out in universities, industry and other research institutions will be shared. We aim to advance by giving priority to studies involving scientific and / or technological originality.

Manuscripts submitted for publication are analyzed in terms of scientific quality, ethics and research methods in terms of its compliance by the Editorial Board representatives of the relevant areas. Then, the abstracts of the appropriate articles are sent to at least two different referees with a well-known in scientific area. If the referees agree to review the article, full text in the framework of the privacy protocol is sent. By the decisions of referees, either directly or corrected article is published or rejected. Confidential reports of the referees in the journal archive will be retained for ten years. All post-evaluation process is done electronically on the internet.

In the journal's publication policy, we would like to state that we will not compromise on quality. In this process, we know that we have undertaken important tasks, especially the selection of referees and monitoring of evaluations. Our journal is indexed in Cite Factor, ASOS, DRJI and ESJI international databases. We will work with the devotion to get our journal into the TR-Index and then the Science Citation Index database as soon as possible.

We would like to thanks our Rector, Prof. Dr. Aysun Bay KARABULUT, who encouraged and supported the establishment of our journal. In addition, we would like to thank all the Authors and Referees who contributed to this issue.

Assist. Prof. Aydan AKSOĞAN KORKMAZ
On behalf of the Editorial Board

MALATYA TURGUT ÖZAL UNIVERSITY

NATURENGS

MTU Journal of Engineering and Natural Sciences

Volume: 1 / Issue: 2 / December- 2020

ISSN: 2717-8013

Contact Information

MTU Journal of Engineering and Natural Sciences – NATURENGS,

Malatya Turgut Özal University, 44210, Battalgazi/Malatya, TURKEY

Phone: +90-422 846 12 55, Fax: +90-422 846 12 25,

e-mail: naturengs@ozal.edu.tr

web: https://dergipark.org.tr/tr/pub/naturengs

MALATYA TURGUT ÖZAL UNIVERSITY

NATURENGS

MTU Journal of Engineering and Natural Sciences

Volume: 1 / Issue: 2 / December- 2020

ISSN: 2717-8013

MTU Journal of Engineering and Natural Sciences – NATURENGS
Volume: 1 / Issue: 2 / December - 2020

CONTENTS

NATURENGS
MTU Journal of Engineering and Natural Sciences
https://dergipark.org.tr/tr/pub/naturengs
DOI: 10.46572/nat.2020.12

The Generalized Odd Nakagami-G Family of Distributions: Properties and Applications

Ibrahim ABDULLAHI[1*], Job OBALOWU[2]

[1]Department of Mathematics and Statistics, Faculty of Science, Yobe State University, 620, Yobe, Nigeria.
[2]Department of Statistics, Faculty of Physical Science, University of Ilorin, 240003, Kwara, Nigeria.

(**Received:** 15.08.2020; **Accepted:** 01.10.2020)

ABSTRACT: In this study, the Generalized Odd Nakagami-G distribution has been empirically investigated using Frechet distribution as the baseline distribution. Some mathematical statistics properties viz: quantile function, moments, probability-weighted moment, entropies, and order statistics were derived among others. The method of maximum likelihood estimation is suitable for the derivation of estimators of the distribution parameters. And the Generalized odd Nakagami Frechet (GONak-Fr) distribution gives the best fit vis-a-vis its competitors via application to real life data sets.

Keywords: GONak-G, GONak-Fr, Probability-weighted moment, Entropies, Order statistics.

1. INTRODUCTION

There have been recent developments focus on generalized odd classes of continuous distributions by adding at least one shape parameters to the baseline distribution, has led mathematical statistician researcher to make of the new flexible distributions and studying the properties of these distributions and using these distributions to model data in many applied areas which include engineering, biological studies, environmental sciences and economics. Numerous methods for generating new families of distributions have been proposed [1] by many researchers.
The beta-generalized family of distribution was developed, Kumaraswamy generated a family of distributions [2], Beta-Nakagami distribution [3], Weibull generalized family of distributions [4], Additive Weibull generated distributions [5], Kummer beta generalized family of distributions [6], the Exponentiated-G family [7], the Gamma-G (type I) [8], the Gamma-G family (type II) [9], the McDonald-G [10], the Log-Gamma-G [11], A new beta generated Kumaraswamy Marshall-Olkin-G family of distributions with applications [12], Beta Marshall-Olkin-G family [13] and Logistic-G family [14].

In this paper, the so-called generalized odd Nakagami generator and the corresponding family of distributions are called generalized odd Nakagami (GONak-G) family of distributions. To the best of the researcher's knowledge, it is new in the literature.

*Corresponding Author: ibworld@ysu.edu.ng
ORCID number of authors: [1] 0000-0002-7280-3035, [2] 0000-0001-5232-1509

2. CONSTRUCTIONS OF THE GENERALIZED ODD NAKAGAMI DISTRIBUTION

The Generalized Odd Nakagami-G distribution (GONak-G) would be made

$$F\left(x;\lambda,\beta,\tau,\eta\right)=\int_0^{\frac{G(x;\eta)^{\tau}}{1-G(x;\eta)^{\tau}}}\frac{2\lambda^{\lambda}}{\Gamma\left(\lambda\right)\beta^{\lambda}}t^{2\lambda-1}e^{-\frac{\lambda t^2}{\beta}}dt \tag{1}$$

$$F\left(x.\lambda,\beta,\eta\right)=\gamma_{*}\left\{\lambda,\frac{\lambda}{\beta}\left[\frac{G\left(x;\eta\right)^{\tau}}{\left(1-G\left(x;\eta\right)^{\tau}\right)}\right]^2\right\} \tag{2}$$

where

$$\gamma_{*}\left\{\lambda,\frac{\lambda}{\beta}\left[\frac{G\left(x;\eta\right)^{\tau}}{\left(1-G\left(x;\eta\right)^{\tau}\right)}\right]^2\right\}=\frac{1}{\Gamma\left(\lambda\right)}\left\{\lambda,\frac{\lambda}{\beta}\left[\frac{G\left(x;\eta\right)^{\tau}}{\left(1-G\left(x;\eta\right)^{\tau}\right)}\right]^2\right\}$$

where $\lambda,\beta,\tau>0$ are three additional parameters, η is the parameter for baseline *G(x)* and $\gamma\left(\sigma,x\right)=\int v^{\sigma-1}e^{-v}\partial v$ is the incomplete gamma function. By differentiation, the probability density function (pdf) of the GONak-G distribution will be obtained as follows:

$$f\left(x;\lambda,\beta,\tau,\eta\right)=\frac{2\lambda^{\lambda}\tau g\left(x\right)G\left(x\right)^{2\lambda\tau-1}}{\Gamma\left(\lambda\right)\beta^{\lambda}\left(1-G\left(x\right)^{\tau}\right)^{2\lambda+1}}e^{-\frac{\lambda}{\beta}\left(\frac{G(x;\eta)^{\tau}}{1-G(x;\eta)^{\tau}}\right)^2} \tag{3}$$

The survival function hazard rate function (hrf) is given by

$$S\left(x;\lambda,\beta,\tau,\eta\right)=1-\gamma_{*}\left\{\lambda,\frac{\lambda}{\beta}\left[\frac{G\left(x;\eta\right)^{\tau}}{\left(1-G\left(x;\eta\right)^{\tau}\right)}\right]^2\right\} \tag{4}$$

$$h\left(x;\lambda,\beta,\tau,\eta\right)=\frac{\frac{2\lambda^{\lambda}\tau g\left(x\right)G\left(x\right)^{2\lambda\tau-1}}{\Gamma\left(\lambda\right)\beta^{\lambda}\left(1-G\left(x\right)^{\tau}\right)^{2\lambda+1}}e^{-\frac{\lambda}{\beta}\left(\frac{G(x;\eta)^{\tau}}{1-G(x;\eta)^{\tau}}\right)^2}}{1-\gamma_{*}\left\{\lambda,\frac{\lambda}{\beta}\left[\frac{G\left(x;\eta\right)^{\tau}}{\left(1-G\left(x;\eta\right)^{\tau}\right)}\right]^2\right\}} \tag{5}$$

3. THE GENERALIZED ODD NAKAGAMI- FRECHET (GONak-Fr)

In this section, we study generalized odd Nakagami Frechet (GONakFr) distributions. Consider the Frechet distribution with cdf and pdf given by:

$$G\left(x;\rho,\nu\right)=e^{-\left(\frac{\rho}{x}\right)^{\nu}} \tag{6}$$

and

$$g\left(x;\rho,\nu\right)=\frac{\rho^{\nu}\nu}{x^{\nu+1}}e^{-\left(\frac{\rho}{x}\right)^{\nu}} \tag{7}$$

Then the pdf of the GONak-Fr distribution is given by

$$f\left(x;\lambda,\beta,\tau,\eta\right)=\frac{2\lambda^{\lambda}\tau\rho^{\nu}\nu e^{-2\lambda\tau\left(\frac{\rho}{x}\right)^{\nu}}}{x^{\nu+1}\Gamma\left(\lambda\right)\beta^{\lambda}\left(1-e^{-\tau\left(\frac{\rho}{x}\right)^{\nu}}\right)^{2\lambda+1}}e^{-\frac{\lambda}{\beta}\left(e^{\tau\left(\frac{\rho}{x}\right)^{\nu}}-1\right)^{-2}} \tag{8}$$

3.1 Investigation of the Proposed GONak-Fr Distribution

To show that the proposed GONak-Fr distribution is a pdf, we proceed as follows:

$$\int_{0}^{\infty}\frac{2\lambda^{\lambda}\tau\rho^{\nu}\nu e^{-2\lambda\tau\left(\frac{\rho}{x}\right)^{\nu}}}{x^{\nu+1}\Gamma\left(\lambda\right)\beta^{\lambda}\left(1-e^{-\tau\left(\frac{\rho}{x}\right)^{\nu}}\right)^{2\lambda+1}}e^{-\frac{\lambda}{\beta}\left(e^{\tau\left(\frac{\rho}{x}\right)^{\nu}}-1\right)^{-2}}\partial x \tag{9}$$

Let $u=\frac{\lambda}{\beta}\left(e^{\tau\left(\frac{\rho}{x}\right)^{\nu}}-1\right)^{-2}$

$$\partial x=\frac{\beta\left(e^{\tau\left(\frac{\rho}{x}\right)^{\nu}}-1\right)^{3}x}{2\lambda\tau\nu\left(\frac{\rho}{x}\right)^{\nu}e^{\tau\left(\frac{\rho}{x}\right)^{\nu}}}\partial u$$

Eq. (9) becomes

$$\frac{\lambda^{\lambda-1}}{\Gamma\left(\lambda\right)\beta^{\lambda-1}}\int_{0}^{\infty}\left(\frac{\beta u}{\lambda}\right)^{\lambda-1}e^{-u}\partial u \tag{10}$$

then integral in Eq. (10) becomes

$$\frac{1}{\Gamma\left(\lambda\right)}\int_{0}^{\infty}u^{\lambda-1}e^{-u}\partial u=\frac{1}{\Gamma\left(\lambda\right)}\Gamma\left(\lambda\right)=1$$

Hence Generalized Odd Nakagami-Frechet Distribution is pdf.

Various forms of shapes are observed, showing the great flexibility of GONak-Fr distribution.

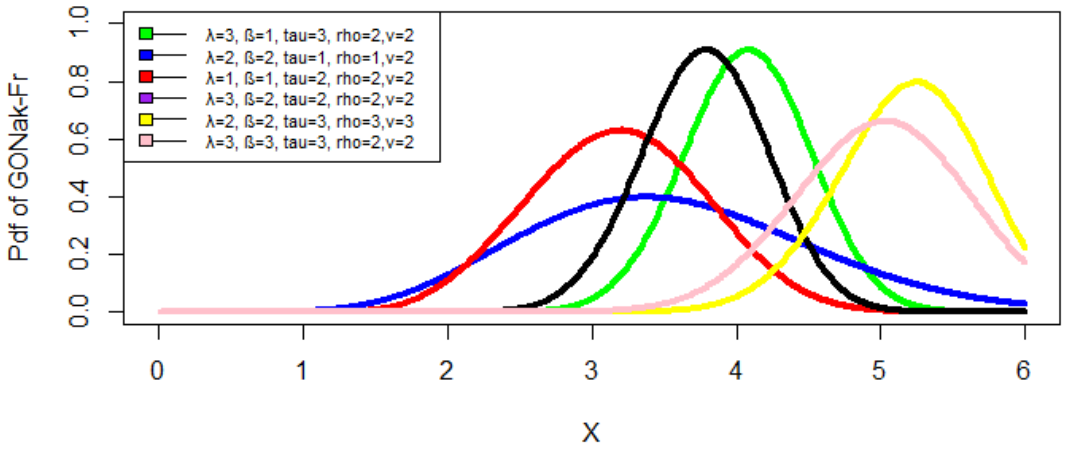

Figure 1. GONak-Fr density function

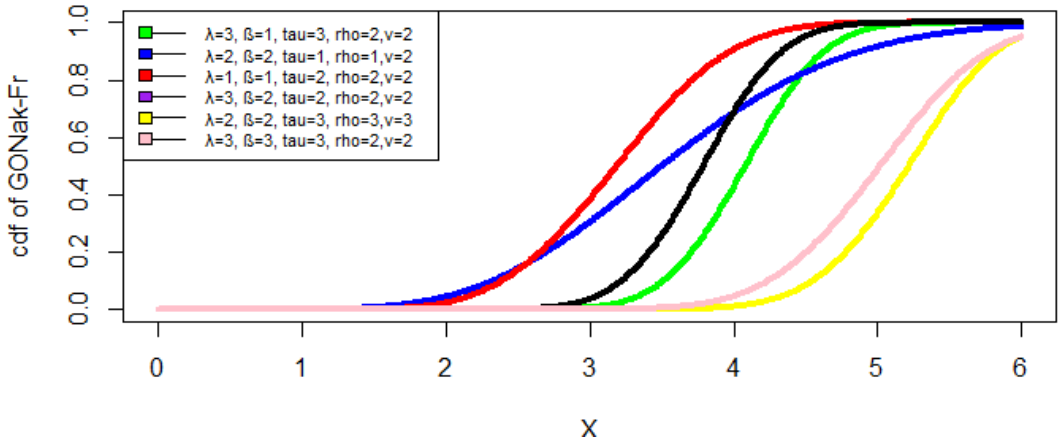

Figure 2. GONak-Fr distribution function

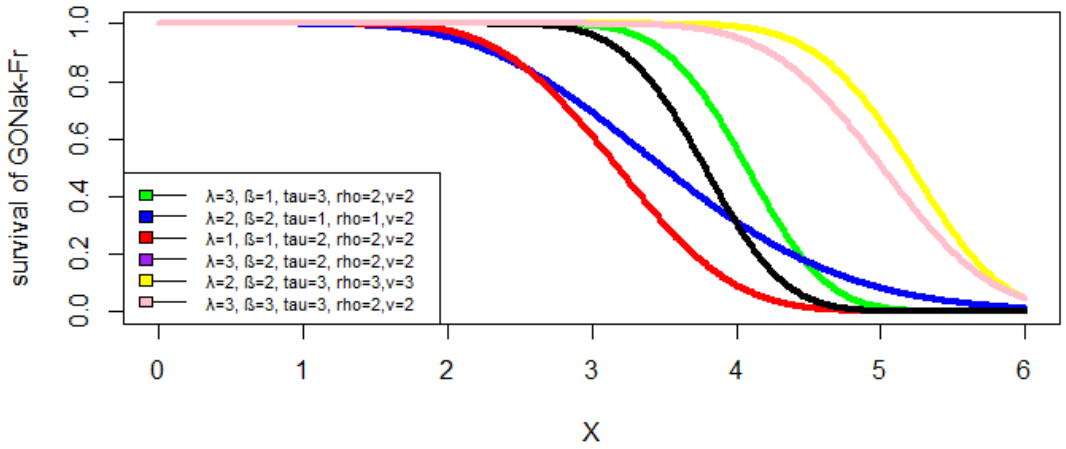

Figure 3. GONak-Fr survival function

3.2 Shape of the Crucial Functions

The shapes of the pdf of the GONak-G family can be defined analytically. The critical points of the GONak-G are given by Eq. (3) are the roots of the resulting equation:

$$\frac{g(x;\eta)'}{g(x;\eta)}+(2\lambda\tau-1)\frac{g(x;\eta)}{G(x;\eta)}+(2\lambda-1)\frac{\tau g(x;\eta)G(x;\eta)}{\left(1-G(x;\eta)^{\tau}\right)}-\frac{2\lambda\tau g(x;\eta)G(x;\eta)^{2\tau-1}}{\beta\left(1-G(x;\eta)^{\tau}\right)^{3}}=0 \qquad (11)$$

3.3 Linear Representation

In this subsection, we provide a very useful linear representation for the GONak-G density function.
We obtain an expansion for density function defined in Eq. (3) as follows: using Taylor expansion the GONak-G *pdf* becomes

$$f(x;\lambda,\beta,\tau,\eta)=\frac{2\lambda^{\lambda}\tau g(x)G(x)^{2\lambda\tau-1}}{\Gamma(\lambda)\beta^{\lambda}\left(1-G(x)^{\tau}\right)^{2\lambda+1}}\sum_{i=0}^{\infty}\frac{(-1)^{i}}{i!}\left(\frac{\lambda}{\beta}\right)^{i}\left[\frac{G(x)^{\tau}}{1-G(x)^{\tau}}\right]^{2i} \qquad (12)$$

Using generalized binomial series we obtain

$$\left(1-G(x)^{\tau}\right)^{-[2(\lambda+i)+1]}=\sum_{j=0}^{\infty}\binom{2(\lambda+i)+j}{j}G(x)^{j\tau} \qquad (13)$$

therefore, inserting Eq. (13) in Eq. (12) the GONak-G pd f will take the following form

$$f(x;\lambda,\beta,\tau,\eta)=\frac{2\tau}{\Gamma(\lambda)}\sum_{i,j=0}^{\infty}\frac{(-1)^{i}}{i!}\left(\frac{\lambda}{\beta}\right)^{\lambda+i}\binom{2(\lambda+i)+j}{j}g(x)G(x)^{2\tau(i+\lambda)+j\tau-1} \qquad (14)$$

this can be written as

$$f(x;\lambda,\beta,\tau,\eta)=\frac{2\tau}{\Gamma(\lambda)}\sum_{i,j=0}^{\infty}\pi_{i,j}g(x)G(x)^{2\tau(i+\lambda)+j\tau-1} \qquad (15)$$

$$\pi_{i,j}=\frac{2\tau}{\Gamma(\lambda)}\frac{(-1)^{i}}{i!}\left(\frac{\lambda}{\beta}\right)^{\lambda+i}\binom{2(\lambda+i)+j}{j} \qquad (16)$$

then,

$$f\left(x;\lambda,\beta,\tau,\eta\right)=\sum_{i,j=0}^{\infty}\omega_{i,j}\ell_{2\tau(i+\lambda)+j\tau}\left(x\right) \tag{17}$$

where

$$\omega_{i,j}=\frac{\pi_{i,j}}{2\tau\left(i+\lambda\right)+j\tau},$$
$$\ell_{2\tau(i+\lambda)+j\tau}\left(x\right)=\left[2\tau\left(i+\lambda\right)+j\tau\right]g\left(x;\eta\right)G\left(x;\eta\right)^{2\tau(i+\lambda)+j\tau-1}$$

Eq. (17) is the infinite linear representation of the GONak-G *pdf* in terms of the exponentiated generated distribution. Similarly, the *cdf* of the GONak-G family can also be expressed as a linear combination of exponentiated generated *cdf* given by

$$F\left(x;\lambda,\beta,\tau,\eta\right)=\sum_{i,j=0}^{\infty}\pi_{i,j}L_{2\tau(i+\lambda)+j\tau}\left(x\right) \tag{18}$$

where,
$L_{2\tau(i+\lambda)+j\tau}\left(x\right)=G\left(x;\eta\right)^{2\tau(i+\lambda)+j\tau}$ is the *cdf* of the exponentiated generated family with the power parameter $2\tau\left(i+\lambda\right)+j\tau.$

4. MATHEMATICAL AND STATISTICAL PROPERTIES

In this section, we provide some mathematical properties of the GONak-G distribution.

4.1. Moments

The r^{th} moment of GONak-G family can be obtained from *pdf* in Eq. (17) as follows

$$\mu_r'=\omega_{i,j}\sum_{i,j=0}^{\infty}\int_0^{\infty}x^r\ell_{2\tau(i+\lambda)+j\tau}\left(x\right)\partial x \tag{19}$$

that is,

$$\mu_r'=\omega_{i,j}I_{r,2\tau(i+\lambda)+j\tau,}\quad r=1,2,3,\ldots \tag{20}$$

where

$$I_{r,2\tau(i+\lambda)+j\tau}=\sum_{i,j=0}^{\infty}\int_0^{\infty}x^r\ell_{2\tau(i+\lambda)+j\tau}\left(x\right)\partial x$$

Finally, the mean and variance of the GONak-G family is given by

$$E\left(X\right)=\omega_{i,j}I_{1,2\tau(i+\lambda)+j\tau,} \tag{21}$$

and

$$Var\left(X\right)=\omega_{i,j}I_{2,2\tau(i+\lambda)+j\tau}-\left[\omega_{i,j}I_{1,2\tau(i+\lambda)+j\tau,}\right]^{2} \tag{22}$$

4.2. Moment Generating Function

The moment generating function of GONak-G family can be obtained from Eq. (20) as follows:

$$M_{(X)}\left(t\right)=\sum_{r=0}^{\infty}\frac{t^{r}\mu_{r}'}{r!}=\sum_{r=0}^{\infty}\frac{t^{r}\omega_{i,j}I_{r,2\tau(i+\lambda)+j\tau}}{r!} \tag{23}$$

4.3. Probability Weighted Moments

[15] stated that for a random variable *X*, the probability weighted moments *(pwm)* is given by:

$$\xi_{s,r}=E\left[X^{s}F\left(x\right)^{r}\right]=\int_{-\infty}^{\infty}x^{s}F\left(x\right)^{r}\ f\left(x\right)\partial x \tag{24}$$

The PWM of GONak-G is obtained by substituting (2) and (17) into (24)

$$\xi_{s,r}=\int_{0}^{\infty}x^{s}\gamma_{*}\left\{\lambda,\frac{\lambda}{\beta}\left[\frac{G\left(x;\eta\right)^{\tau}}{\left(1-G\left(x;\eta\right)^{\tau}\right)}\right]^{2}\right\}^{r}\sum_{i,j=0}^{\infty}\omega_{i,j}\ell_{2\tau(i+\lambda)+j\tau}\left(x\right)\partial x \tag{25}$$

using an expansion of incomplete gamma ratio function leads to

$$\gamma_{*}\left\{\lambda,\frac{\lambda}{\beta}\left[\frac{G\left(x;\eta\right)^{\tau}}{\left(1-G\left(x;\eta\right)^{\tau}\right)}\right]^{2}\right\}^{r}=\frac{\left[\frac{\lambda}{\beta}\left(\frac{G\left(x;\eta\right)^{\tau}}{\left(1-G\left(x;\eta\right)^{\tau}\right)}\right)^{2}\right]^{\lambda r+k}}{\Gamma\left(\lambda\right)^{r}}\sum_{k=0}^{\infty}c_{r,k} \tag{26}$$

using generalized binomial one can obtain

$$\left(1-G\left(x;\eta\right)^{\tau}\right)^{-2(\lambda r+k)}=\sum_{n=0}^{\infty}\binom{2(\lambda r+k)+n-1}{n}G\left(x;\eta\right)^{n\tau} \tag{27}$$

substituting Eq. (27) into Eq. (26) leads to

$$=\frac{\lambda^{\lambda r+k}}{\Gamma\left(\lambda\right)^{r}\beta^{\lambda r+k}}\sum_{k,n=0}^{\infty}\binom{2(\lambda r+k)+n-1}{n}c_{r,k}G\left(x;\eta\right)^{\tau\left[2(\lambda r+k)+n\right]} \tag{28}$$

using generalized binomial one can obtain

$$G\left(x;\eta\right)^{\tau\left[2(\lambda r+k)+n\right]}=\sum_{l=0}^{\infty}\sum_{q=0}^{l}(-1)^{l+q}\binom{\tau\left[2(\lambda r+k)+n\right]-1}{l}\binom{l}{q}G\left(x;\eta\right)^{q} \tag{29}$$

substituting Eq. (29) into Eq. (28) leads to

$$=\frac{\lambda^{\lambda r+k}}{\left[\Gamma\left(\lambda\right)\right]^{r}\beta^{\lambda r+k}}\sum_{k,n=0}^{\infty}\sum_{l=0}^{\infty}\sum_{q=0}^{l}(-1)^{l+q}\binom{2(\lambda r+k)+n-1}{n}\binom{\tau\left[2(\lambda r+k)+n\right]}{l}\binom{l}{q}c_{r,k}G\left(x;\eta\right)^{q} \tag{30}$$

replacing $\sum_{l=0}^{\infty}\sum_{q=0}^{l}$ and $\sum_{l=q}^{\infty}\sum_{q=0}^{\infty}$ one can obtain

$$=\frac{\lambda^{\lambda r+k}}{\left[\Gamma\left(\lambda\right)\right]^{r}\beta^{\lambda r+k}}\sum_{k,n=0}^{\infty}\sum_{l=q}^{\infty}\sum_{q=0}^{\infty}(-1)^{l+q}\binom{2(\lambda r+k)+n-1}{n}\binom{\tau\left[2(\lambda r+k)+n\right]}{l}\binom{l}{q}c_{r,k}G\left(x;\eta\right)^{q} \tag{31}$$

$$F\left(x\right)^{r}=\sum_{q=0}^{\infty}\Lambda_{q}G\left(x;\eta\right)^{q} \tag{32}$$

where,

$$\Lambda_{q}=\frac{\lambda^{\lambda r+k}}{\left[\Gamma\left(\lambda\right)\right]^{r}\beta^{\lambda r+k}}\sum_{k,n=0}^{\infty}\sum_{l=q}^{\infty}(-1)^{l+q}\binom{2(\lambda r+k)+n-1}{n}\binom{\tau\left[2(\lambda r+k)+n\right]}{l}\binom{l}{q}c_{r,k}$$

Finally, the *PWM* of GONak-G is obtained by

$$\zeta_{s,r} = \sum_{i,j,q=0}^{\infty} \Lambda_q \omega_{i.j} \ell_{s,q+2\tau(i+\lambda)+j\tau}(x) \tag{33}$$

4.4. Entropies

In this subsection, Renyi entropy will be mentioned as an important measure of uncertainty. The Rényi entropy of a random variable *X* is defined mathematically as follows:

$$I_R(\delta) = \frac{1}{1-\delta}\log\left(\int_0^{\infty} f^{\delta}(x)\partial x\right) \tag{34}$$

By applying the binomial theory and exponential expansion in the *pdf* (3), then the *pdf* $f^{\delta}(x)$ can be expressed as follows

$$f^{\delta}(x) = \sum_{p,k=0}^{\infty} t_{p,k} g(x)^{\delta} G(x)^{2\tau(\lambda\delta+p)-\delta+\tau k} \tag{35}$$

where,

$$t_{p,k} = \left(\frac{2\tau}{\Gamma(\lambda)}\right)^{\delta} \frac{(-1)^p}{p!} \delta^p \left(\frac{\lambda}{\beta}\right)^{\lambda\delta+p} \binom{\delta(2\lambda+1)+2p+k-k}{k}.$$

Therefore, the Rényi entropy of GONak-G family is obtained by using (34) as follows

$$I_R(\delta) = \frac{1}{1-\delta}\log\left\{\sum_{p,k=0}^{\infty} t_{p,k}\int_0^{\infty} g(x)^{\delta} G(x)^{2\tau(\lambda\delta+p)-\delta+\tau k}\partial x\right\} \tag{36}$$

The δ -entropy is defined by

$$H_{\delta}(X) = \frac{1}{1-\delta}\log\left\{1-\int_0^{\infty} f^{\delta}(x)\partial x\right\} \tag{37}$$

Therefore, the δ -entropy of GONak-G family is obtained by using (37) as follows

$$H_{\delta}(X) = \frac{1}{1-\delta}\log\left\{1-\sum_{p,k=0}^{\infty} t_{p,k}\int_0^{\infty} g(x)^{\delta} G(x)^{2\tau(\lambda\delta+p)-\delta+\tau k}\partial x\right\} \tag{38}$$

4.5. Order Statistics

Let $x_1, x_2, \ldots, x_n$ be an independent random sample from a distribution function, *F(x)*, with an associated probability density function, *f (x)*. Then, the probability density function of the ith order statistics, $x_{(i)}$, is given by:

$$f_{X_{(j)}}(x) = \frac{n!}{(j-1)!(n-j)!}\sum_{z=0}^{n-j}(-1)^z \binom{n-j}{z} f_X(x)\left[F_X(x)\right]^{z+j-1} \tag{39}$$

The pd f of r^{th} order statistic from GONak-G distribution is obtained by substituting equation (2) and (3) into (39)

$$f_{X_{(j)}}(x) = \frac{n!}{(j-1)!(n-j)!}\sum_{z=0}^{n-j}(-1)^z \binom{n-j}{z} \frac{2\lambda^{\lambda}\tau g(x)G(x)^{2\lambda\tau-1}}{\Gamma(\lambda)\beta^{\lambda}\left(1-G(x)^{\tau}\right)^{2\lambda+1}} e^{-\frac{\lambda^2}{\beta}\left(\frac{G(x;\eta)^{\tau}}{1-G(x;\eta)^{\tau}}\right)^2}$$
$$\gamma_*\left\{\lambda, \frac{\lambda}{\beta}\left[\frac{G(x;\eta)^{\tau}}{\left(1-G(x;\eta)^{\tau}\right)}\right]^2\right\}^{z+j-1} \tag{40}$$

We now use the series expansion for the incomplete gamma ratio function and substituting into Eq. (40) lead to

$$f_{X_{(j)}}(x) = \frac{n!}{(j-1)!(n-j)!}\left(\frac{\lambda}{\beta}\right)^{2\lambda+\nu}\sum_{z=0}^{n-j}\sum_{s=0}^{\infty}\sum_{i=s}^{\infty}\sum_{\nu=0}^{\infty}\frac{(-1)^{z+i+s+\nu}}{(\lambda+\nu)\nu!\Gamma(\lambda)}\binom{n-j}{z}\binom{z+j-1}{i}\binom{i}{s}$$
$$\frac{2\tau g(x)G(x)^{4\lambda\tau+\nu-1}}{\Gamma(\lambda)\left(1-G(x)^{\tau}\right)^{4\lambda+\nu+1}} e^{-\frac{\lambda}{\beta}\left(\frac{G(x;\eta)^{\tau}}{1-G(x;\eta)^{\tau}}\right)^2} \tag{41}$$

4.6. Quantile Function

By considering (2) quantile function (qf) *X* is obtained as follows:

$$u = \gamma_*\left\{\lambda, \frac{\lambda}{\beta}\left[\frac{G(x;\eta)^{\tau}}{\left(1-G(x;\eta)^{\tau}\right)}\right]^2\right\}$$

$$u\Gamma(\lambda) = \gamma\left\{\lambda, \frac{\lambda}{\beta}\left[\frac{G(x;\eta)^{\tau}}{\left(1-G(x;\eta)^{\tau}\right)}\right]^2\right\}$$

$$G(x;\eta)=\left\{\frac{\left[\frac{\lambda}{\beta}\gamma^{-1}\left(\lambda,u\Gamma(\lambda)\right)\right]^{\frac{1}{2}}}{1+\left[\frac{\lambda}{\beta}\gamma^{-1}\left(\lambda,u\Gamma(\lambda)\right)\right]^{\frac{1}{2}}}\right\}^{\frac{1}{\tau}} \tag{42}$$

The quantile function of GONak-Fr distribution is given by:

$$x=\left\langle \frac{-1}{\rho^{v}}\ln\left\{\frac{\left[\frac{\lambda}{\beta}\gamma^{-1}\left(\lambda,u\Gamma(\lambda)\right)\right]^{\frac{1}{2}}}{1+\left[\frac{\lambda}{\beta}\gamma^{-1}\left(\lambda,u\Gamma(\lambda)\right)\right]^{\frac{1}{2}}}\right\}^{\frac{1}{\tau}}\right\rangle^{\frac{-1}{v}} \tag{43}$$

4.6. Estimation of GONak-G Family

This subsection deals with the maximum likelihood estimators of the unknown parameters for the GONak-G family of distributions based on complete samples of size n. Let $X_1, X_2,\ldots, X_n$ be observed values from the GONak-G family with a set of parameter $\Theta=(\lambda,\beta,\tau,\eta)'$. The log-likelihood function for parameter vector $\Theta=(\lambda,\beta,\tau,\eta)'$. is obtained from equation (3) as follows

$$\begin{aligned}\ell(\Theta)&=n\ln 2+n\lambda\ln\lambda-n\ln\tau-n\ln\Gamma(\lambda)-n\lambda\ln\beta+\sum_{i=0}^{n}\ln g(x;\eta)+(2\lambda-1)\\&\sum_{i=0}^{n}\ln G(x;\eta)-(2\lambda+1)\sum_{i=0}^{n}\ln\left[1-G(x;\eta)^{\tau}\right]-\frac{\lambda}{\beta}\sum_{i=0}^{n}\left[W(x;\eta)\right]^{2}\end{aligned} \tag{44}$$

where $W(x;\eta)=\dfrac{G(x;\eta)^{\tau}}{1-G(x;\eta)^{\tau}}$

The components of the score function $U(\Theta)=\left(U_{\lambda},U_{\beta},U_{\tau},U_{\eta}\right)$ are given by

$$U_{\lambda}=n\ln\lambda-n-n\Psi\left(\lambda\right)-n\ln\beta+2\tau\sum_{i=0}^{n}\ln G\left(x;\eta\right)-2\sum_{i=0}^{n}\ln\left[1-G\left(x;\eta\right)^{\tau}\right]-\frac{\sum_{i=0}^{n}\left[W\left(x;\eta\right)\right]^{2}}{\beta} \tag{45}$$

$$U_{\beta}=-\frac{n\lambda}{\beta}+\frac{\lambda\sum_{i=0}^{n}\left[G\left(x;\eta\right)\right]^{2}}{\beta^{2}}=0 \tag{46}$$

$$U_{\tau}=\frac{u}{\tau}+2\lambda\sum_{i=0}^{n}\ln G\left(x;\eta\right)+\frac{\left(2\lambda+1\right)\sum_{i=0}^{n}G\left(x;\eta\right)^{\tau}\ln G\left(x;\eta\right)}{\left[1-G\left(x;\eta\right)^{\tau}\right]}-\frac{\lambda}{\beta}\sum_{i=0}^{n}\frac{G\left(x;\eta\right)^{\tau}\ln G\left(x;\eta\right)}{\left[1-G\left(x;\eta\right)^{\tau}\right]^{2}}=0 \tag{47}$$

$$U_{\eta}=\sum_{i=0}^{n}\frac{g^{\eta}}{g\left(x;\eta\right)}+\left(2\lambda-1\right)\sum_{i=0}^{n}\frac{G^{\eta}}{G\left(x;\eta\right)}+\left(2\lambda+1\right)\sum_{i=0}^{n}\frac{G^{\eta}G\left(x;\eta\right)^{\tau-1}\tau}{1-G\left(x;\eta\right)^{\tau}}-\frac{\lambda}{\beta}\sum_{i=0}^{n}\frac{G^{\eta}G\left(x;\eta\right)^{\tau-1}\tau}{\left[1-G\left(x;\eta\right)^{\tau}\right]^{2}}=0 \tag{48}$$

where $g^{\eta}=\frac{\partial g\left(x;\eta\right)}{\partial\eta}$ and $G^{\eta}=\frac{\partial G\left(x;\eta\right)}{\partial\eta}$.

Setting $U_{\lambda},U_{\beta},U_{\tau},U_{\eta}$ equate to zero and solving the equations simultaneously result in the ML estimates $\hat{\Theta}=\left(\hat{\lambda},\hat{\beta},\hat{\tau},\hat{\eta}\right)$. These estimates cannot be solved algebraically and statistical software can be used to solve them numerically via iterative technique.

5. RESULTS AND DISCUSSION

In this section, the fitting of GONakG and some generated families of distribution. We present two applications to real life data set to illustrate the potentiality of the GONak-G family of distribution. To compare its performance, we consider Generalize Odd Nakagami Frechet (GONakFr) to other generated models. The Akaike information criterion (AIC), Consistent Akaikes Information Criterion (CAIC), Bayesian information criterion (BIC), Anderson-Darling (A), Kolmogorov Smirnov test (K.S), and the P-Value of K.S test, have been chosen for the comparison of the models.

The first data set which contains 76 observation and is recently used by [16], [17], and [18] it represents the life of fatigue fracture of Kevlar 373/epoxy subjected to constant pressure at 90 percent stress level until all had failed. The data is as follows: 0.0251, 0.0886, 0.0891, 0.2501, 0.3113, 0.3451, 0.4763, 0.5650, 0.5671, 0.6566, 0.6748,0.6751, 0.6753, 0.7696, 0.8375,

0.8391, 0.8425, 0.8645, 0.8851, 0.9113, 0.9120, 0.9836, 1.0483, 1.0596, 1.0773, 1.1733, 1.2570, 1.2766, 1.2985, 1.3211, 1.3503, 1.3551, 1.4595, 1.4880, 1.5728, 1.5733, 1.7083, 1.7263, 1.7460, 1.7630, 1.7746, 1.8275, 1.8375, 1.8503, 1.8808, 1.8878, 1.8881, 1.9316, 1.9558, 2.0048, 2.0408, 2.0903, 2.1093, 2.1330, 2.2100, 2.2460, 2.2878, 2.3203, 2.3470, 2.3513, 2.4951, 2.5260, 2.9911, 3.0256, 3.2678, 3.4045, 3.4846, 3.7433, 3.7455, 3.9143, 4.8073, 5.4005, 5.4435, 5.5295, 6.5541, 9.0960.

The second set which contains 30 observation and is recently used by [19] and [20] it represents successive values of March precipitation (in inches) in Minneapolis/St Paul. The data are as follows: 0.77, 1.74, 0.81, 1.20, 1.95, 1.20, 0.47, 1.43, 3.37, 2.20, 3.00, 3.09, 1.51, 2.10, 0.52, 1.62, 1.31, 0.32, 0.59, 0.81, 2.81, 1.87, 1.18, 1.35, 4.75, 2.48, 0.96, 1.89, 0.90, 2.05.

Tables 1 and 2 display a summary of the MLEs and values of goodness-of-fit measures for the GONak-Fr model and other different models, respectively. As you see, the GONak-Fr is selected as the best model with all the criteria among all the fitted models.

Table 1. MLEs and Goodness-of-fit measures for the first data set

Models	MLE	$-\ell$	AIC	CAIC	BIC	A	K.S	P Value
GONakFr	0.8940793 0.2295717 1.8947034 0.5202491 0.3507287	119.7429	249.4857	250.34281	261.1394	1.739569	0.49246	2.22e-16
EWW	1.8638979 1.5739533 0.7065971 0.3125043 0.9306594	124.915	259.83	260.6872	271.4837	1.092538	0.14126	0.08724
OGGFr	1.6021457 1.5297831 0.5340209 0.4477832	125.614	259.228	259.7914	268.5509	1.183529	0.093698	0.488
OGGW	1.2061588 1.3700706 0.5225529 0.6039366	124.733	257.466	258.0294	266.7889	1.115889	0.13597	0.1095

Table 2. MLEs and Goodness-of-fit measures for the second data set

Models	MLE	$-\ell$	AIC	CAIC	BIC	A	K.S	P Value
GONakFr	0.3309079 0.8366780 1.9417631 0.7704069 1.1089862	34.56199	79.12398	81.62398	86.12997	0.6313438	0.22	0.1096
EWW	1.5264454 0.6836198 1.3895067 0.6091976 0.6701214	39.20578	88.41156	90.91156	95.41754	0.2347084	0.10255	0.9106
OGGFr	1.6076918 0.8512776 1.3064885 0.8217882	37.89086	83.78171	85.38171	89.3865	0.1032816	0.060615	0.9999
OGGW	0.5533399 1.7371373 1.3685022 0.9848482	37.98979	83.97959	85.57959	89.58438	0.1259235	0.089259	0.9706

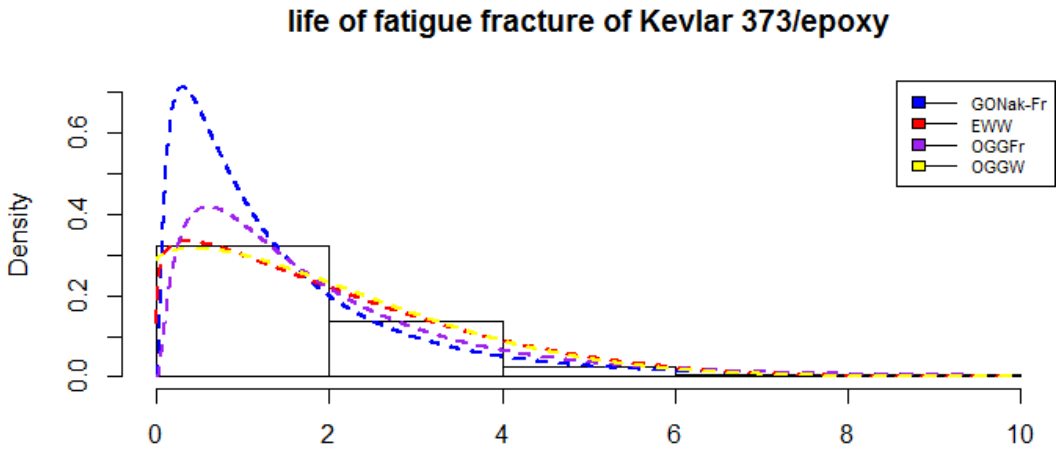

Figure 4. Histogram and estimated pdf for the life of fatigue fracture

6. CONCLUSIONS

In this article, we proposed a new Generalized Odd Nakagami (GONak-G) family of distributions, with a special focus on the Frechet distribution as parent distribution. The distribution is named Generalized Odd Nakagami Frechet distribution. The pdf, cdf, survival and hazard function was derived. Additionally, some of the mathematical properties of the new class including quantile, moments, probability weighted moment, order statistics and entropies were also derived. The model parameters were estimated using the maximum likelihood estimation method. Finally, two applications on real life data set are presented to illustrate the potentiality of the proposed model. The new distribution was found to provide a better fit than its competitors.

REFERENCES

[1] Eugene, N., Lee, C. and Famoye, F. (2002). Beta-normal distribution and its applications. *Communication in Statistics-Theory and Methods*, 31: 497–512.

[2] Cordeiro, G.M. and De Castro, M. (2011). A new family of generalized distributions. *Journal of Statistical Computation and Simulation*, 81: 883-893.

[3] Olanrewaju, I., Shittu, O.I. and Adepoju K.A. (2013). On the beta-nakagami distribution. *Progress in Applied Mathematics*, 5(1):49–58.

[4] Bourguignon, M., Silva, R.B. and Cordeiro, G.M. (2014). The Weibull-G family of probability distributions. *Journal of Data Science*, 12(1): 53-68.

[5] Hassan, A.S. and Hemeda, S.E. (2016). The additive Weibull-g family of probability distributions. *International Journals of Mathematics and its Applications*, 4: 151-164.

[6] Pescim, R. R., Gauss, M., Cordeiro, G.M., Demetrio, C.G.B., Ortega, E.M.M. and Nadarajah, S. (2012). The new class of Kummer beta generalized distributions. *SORT-Statistics and Operations Research Transactions*, 36(2):153–180.

[7] Cordeiro, G.M., Ortega, M.M.E. and Da Cunha, C.C.D. (2013). The exponentiated generalized class of distributions. *Journal of Data Science*, 11(1):1–27.

[8] Zografos, K. and Balakrishnan, N. (2009). On families of beta- and generalized gamma-generated distributions and associated inference. *Statistical Methodology*, 6: 344–362.

[9] Ristic, M.M. and Balakrishnan, N. (2012). The gamma-exponentiated exponential distribution. *Journal of Statistical Computation and Simulation*, 82:1191–1206.

[10] Alexander, C., Cordeiro, G.M., Ortega, E.M.M. and Sarabia, J.M. (2012). Generalized beta-generated distributions. *Computational Statistics & Data Analysis*, 56(6):1880–1897.

[11] Amini, M., Mostafaee, M.S. and Ahmadi, J. (2014). Log-gamma-generated families of distributions. *Statistics*, 48(4):913–932.

[12] Handique, L. and Chakraborty, S. (2017). A new beta generated Kumaraswamy marshall-olkin-g family of distributions with applications. *MJS*, 36(3):157–174.

[13] Alizadeh, M., Cordeiro, G.M., De Brito, E. and Demetrio, C.G.B. (2015). The beta marshall-olkin family of distributions. *Journal of Statistical Distributions and Applications*, 2(1):4

[14] Hamzeh Torabi, H. and Montazeri, N.H. (2014). The logistic-uniform distribution and its applications. *Communications in Statistics-Simulation and Computation*, 43(10):2551–2569.

[15] Oguntunde, P. E., Adejumo, A. O. and Owoloko, E. A. (2017). On the exponentiated generalized inverse exponential distribution. *Proceedings of the World Congress on Engineering*, Vol. I

[16] Barlow, R.E., Toland, R.H. and Freeman, T. (1984). A Bayesian analysis of stress-rupture life of kevlar 49/epoxy spherical pressure vessels. *In Proc. Conference on Applications of Statistics Ao, Marcel Dekker, New York.*

[17] Gomez, M. Y., Bolfarine, H., and Gomez, W.H. (2014). A new extension of the exponential distribution. *Revista Colombiana de Estadıstica*, 37(1):25–34.

[18] Greenwood, J.A., Landwehr, J.M. and Matalas, N.C. (1979). Probability weighted moments: definitions and relations of parameters of several distributions expressible in inverse form. *Water Resources Research*, 15: 1049-1054.

[19] Hinkley, D. (1977). On quick choice of power transformations. *Journal of the Royal Statistical Society, Series (c), Applied Statistics*, 26:67–69.

[20] Elgrahy, M. and Hassan, A. (2019). Exponentiated weibull weibull distribution. Statistical properties and applications. *Gazi University Journal of Science*, 32(2):616–635.

NATURENGS
MTU Journal of Engineering and Natural Sciences
https://dergipark.org.tr/tr/pub/naturengs
DOI: 10.46572/nat.2020.13

Influence of a Clay Subgrade Stabilized with Blast Furnace Slag on Flexible Road Pavement Thickness and Cost

Tacettin GEÇKİL[1], Mehmet Mahmut TANYILDIZI[2*], Ceren Beyza İNCE[3], Ekrem Serdar YILDIRAN[4]

[1,3]Department of Civil Engineering, İnönü University, Malatya, Turkey.
[2]Second Army Command, Malatya, Turkey.
[4]Togi Metal Construction, Malatya, Turkey.

(**Received:** 03.08.2020; **Accepted:** 06.10.2020)

ABSTRACT: It has become a necessity in Highway Engineering, due to today's heavy vehicle traffic loads, that subgrade with poor bearing capacity on which the road will rest be improved with various methods and additives. In this study, it has been aimed to improve clay soil with poor bearing strength with the contribution of waste blast furnace slag (BFS) and to investigate its effect on the thickness and cost of flexible road pavement. This study aims to improve clay soil with poor bearing strength with the contribution of waste BFS. Moreover, it tries to investigate the effects of BFS on the thickness and cost of flexible road pavement. For this purpose, in the study, stabilized mixture samples were prepared by adding 5, 10, 15, 20% by weight of BFS to the clay soil. After these prepared samples have been mixed homogeneously, standard proctor, unconfined compression and California Bearing Ratio (CBR) tests were applied to the samples. As a result of experimental studies, it was observed that the increase in BFS resulted in a decrease in the maximum dry density of the samples and an increase in the optimum moisture content. Also, the highest unconfined compression strength was obtained from 20% of BFS added samples. CBR values of the samples tested at this rate increased by 8.71 times compared to pure clay soil. Using these experimental data, the flexible road pavement layer thicknesses to be constructed with the AASHTO 1993 method on the BFS added ground were calculated, and pavement cost analyzes were made considering current prices. As a result of the calculations, the design calculation was made according to the layer thicknesses determined for both soils. it was determined that adding 20% BFS to the soil decreased the road pavement layer thickness by 29.41% compared to the pure clay soil. The cost calculation results show that compared to the pure clay soil, there is about a 5.65% decrease in the pavement cost for clayey soils with 20% BFS. According to these results, when the subgrade of a 1000 m in length and 20 m in width road is improved with 20% BFS, 8.400,00 TL saving will be provided in the cost of flexible pavement.

Keywords: Clay soil, Blast furnace slag, Stabilization, Flexible pavement, AASHTO method.

1. INTRODUCTION

Nowadays, the problems encountered in the disposal of the wastes arising as a result of developing industry and technology, increasing population, and growing cities have reached day by day unignorable levels. For this reason, the disposal of industrial and industrial wastes has become very important. For this purpose, the use of various waste materials has become quite common in different civil engineering applications such as ground stabilization and filling formation [1, 2]. Ground stabilization is generally the process to improve the strength of the soils by adding various additives to the soils with poor bearing capacity.

*Corresponding Author: mmtanyildizi@hotmail.com
ORCID number of authors: [1] 0000-0001-8070-6836, [2] 0000-0001-5992-2665, [3] 0000-0002-6385-0964, [4] 0000-0002-8678-5544

Ground stabilization is generally the process to improve the strength of the grounds by adding various additives to the subgrade with poor bearing capacity. For this purpose, lime, blast furnace slag, fly ash, cement, etc. are used to remove the negative properties of the ground. It is tried to increase the strength of the grounds by adding chemical additives [3]. It has been observed that the properties of the soils can be improved in their properties such as volumetric stability, strength, permeability, compressibility, durability by using these additives.

Furthermore, the cost efficiency and easy availability of these additives have made them preferable for their use in the improvement or stabilization of the ground [4-6].

Clay soils with poor bearing capacity, high shrinkage, swelling, permeability and liquefaction potential, low shear strength, which are undesirable to be found in road construction work, are generally called weak grounds. Therefore, in road construction works encountered with this type of ground, soils with high bearing capacity and no swelling potential (better geotechnical properties) are obtained by using additives [7].

In this study, the effect of waste BFS on the strength of a clay road subgrade with poor bearing capacity was investigated and, this situation was evaluated in terms of road flexible road pavement cost in the light of the findings obtained as a result of experimental research.

Emerging as a byproduct during iron and steel production, BFS is used in various engineering applications such as road pavements and filling material in road engineering. The structure of BFS consists of 95% elements such as silica, calcium, aluminum, magnesium and oxygen [7-10]. It is thought that using BFS, which is obtained as a byproduct with these features, to increase the strength of weak soils will be beneficial both in terms of bearing capacity of the soil, waste disposal and economic gain [10].

In many countries, positive results have been obtained in soil improvement studies carried out using BFS. Studies have shown that BFS is not affected by groundwater and is suitable for use in the land and that BFS can be used as an additive in road stabilization [11, 12].

Sivrikaya et al. [13] have investigated the usability of BFS to increase the strength of clay soils. For this purpose, 5%, 10, 20, 30 and 50% of BFS were added to two different clay soils, and the properties of the samples were examined. It was determined for both pure clay soils that as the BFS ratio increased, the bulk density also increased. Similarly, while the plastic limit (PL) values of clay soils increased, liquid limit (LL) values decreased. When these results were evaluated, it was found that the plasticity indexes (PI) of the clays decreased in the range of 92-180%. The decrease in PI values with BFS contribution has resulted in reduced sensitivity of clay soils to water.

Bilgen et al. [14] have investigated the usability of BFS and lime in improving the strength of clayey soils. Within the scope of the study, mixed samples have been prepared between 0% and 7.5% for BFS and 0% and 5% for lime, and the properties of these samples have been determined. According to the results of the experiment, it has been determined that BFS has no effect on plasticity alone, but plasticity has decreased from 28 to 9 in 5% lime and 3.33% BFS mixture. BFS did not cause a significant change in the optimum moisture content when used alone or in combination with lime. When BFS is used alone, it increases the unconfined compressive strength by approximately two times, and when the mixture of 5% lime and 3.33% BFS is used together, the unconfined compressive strength increases 11 times.

Cokca et al. [15] investigated the effects of the BFS and BFS-cement mixture on the strength of the soils with swelling properties. Within the scope of the study, a 5% to 25% BFS and BFS-cement mixture has been added to the soil samples. The effects of these additives on grain size distribution, Atterberg limits, rate of swelling have been investigated. As a result of the experimental studies, it was determined that as the amount of additive increased, the plasticity index (PI) and swelling percentage of the soils decreased, while its specific gravity increased. As a result of the study, it was concluded that a 15% BFS - 5% cement mixture is the most optimum option considering both environmental effects and swelling percentage.

Bilici et al. [16] The ground was mixed in different proportions with the waste material, BFS and fly ash (FA). In the series with additives, lime is kept constant at 3% in order to ensure the pozzolanic reaction, in the first stage 3%, 6%, 9%, 12%, 15% FA and in the second stage 3%, 6%, 9%, 12% BFS additive series Uncured (early period), 7 days and 28 days unconfined compression tests were applied to the prepared samples. In this context, by reducing the soil sample in work with additives, lime, FA and BFS were added as much as it was reduced, thus keeping the dry mass of the total mixture constant. It has been determined that the highest strength occurs at 3% lime + 12% FA and 3% lime + 9% BFS additives.

Geçkil et al. [17] The effect of adding lime to clay soil on strength was investigated. For the study, lime, which is used as an additive, was added to the clay soil in different percentages by weight. In the prepared mixtures, lime was added in 2.5%, 5%, 7.5%, 10%, 15% and 20% of the weight of clay. The samples prepared in different proportions were homogeneously mixed, and then compaction, unconfined compression and CBR tests were performed. As a result of experimental studies, as the lime content in the mixture increased, the plasticity index and maximum dry density decreased while the optimum moisture content increased. In addition, the highest unconfined compressive strength value of the samples cured for 7 and 28 days was obtained at the rate of 5% lime. For this additive ratio, the CBR values of the samples cured at the same time were 1.37 and 2.08 times higher than the additive-pure clay soil, respectively.

In this study, unlike other studies conducted in the literature [16, 17], the effect of a clayey road subgrade with improved bearing capacity with BFS on flexible road pavement layer thicknesses and costs have been investigated. For this purpose, compression, unconfined compression, CBR tests were carried out on soil samples with increased strength, and with the help of the AASHTO 1993 design method, flexible pavement layer thicknesses have been determined on the soil with pure clay and BFS, and their current costs have been calculated. In a study in the literature [18] a clay soil stabilized with BFS, the samples prepared by adding 5, 10, 15, 20% BFS to the clay soil by weight, Standard Proctor, unconfined compression and CBR tests. As a result of the experiment, it was determined that the highest strength was obtained from mixtures containing 20% BFS. In the design calculations made according to the layer thicknesses determined for both ground with the AASHTO 1993 method, it was determined that adding 20% BFS to the ground reduced the thickness of the road pavement layer by 26.67% compared to the pure clay soil. In this study, it was determined that the highest strength was obtained with 20% BFS as a result of 7 days of curing under the same test conditions, but the thickness of the road pavement layer was decreased by 29.41%.

2. MATERIAL AND EXPERIMENTAL STUDIES

Within the scope of experimental studies, clay material was used as a road subgrade provided from the Malatya Kiltepe region. The engineering properties of the clay material are determined according to the TS 1900-1 standard and are shown in Table 1.

Table 1. Physical properties of clay soil

Parameter	Unit	Value
Density of particles (γ_s)	g/cm^3	2.680
Maximum dry density (g_{kmax})	g/cm^3	1.450
Optimum moisture content (w_{opt})	%	27
Liquid limit (LL)	%	61
Plastic limit (PL)	%	29
Plasticity index (PI)	-	32
Unified soil classification system (USCS)	-	CH
AASHTO classification system		A-7-6

By the Highways Technical Specifications (HTS) data, stabilization-improvement is envisaged for the soils classified as A5, A6, A7, A-2-6, A-2-7 in AASHTO classification system [19]. While the class of soil provided in the study is determined as high plasticity clay (CH) according to the unified soil classification system (USCS) data, it is determined as A-7-6 (poorest soil) according to AASHTO classification system data. Besides, since clay soil is PI 32 ≥10, the strength of clay soil with a poor bearing capacity was increased by stabilization following HTS.

BFS having a specific weight of 2.750 g/cm^3 and used to improve the strength of the clay soil was provided from Karçimsa cement factory in Karabük province, and its chemical properties are shown in Table 2.

Table 2. Chemical properties of blast furnace slag (BFS)

Chemical Component	SiO_2	Al_2O_3	Fe_2O_3	CaO	MgO	SO_3	S	Na_2O	K_2O	TiO_2	Mn_2O_3	Cl
Content by Weight (%)	32.47	9.94	1.25	32.45	9.31	0.82	0.33	0.31	0.85	1.16	3.51	0.015

Within the scope of the study, before the clay-BFS mixture samples have been prepared, both materials have been dried in an oven of 105 ± 5 °C for 24 hours. Then, taking into consideration the previous studies [12-14] in the literature, clay stabilized mixtures have been prepared by adding 5, 10, 15 and 20% BFS by weight.

In the whole study, pure clay and stabilized mixtures have been named clay, 5% BFS, 10% BFS, 15% BFS and 20% BFS respectively.

In the study, three samples of pure clay and stabilized mixture samples were prepared, and the Standard Proctor experiment has been carried out on the samples following TS 1900-1. While stabilized samples have been tested for optimum moisture content ratio determination, Sodium

Hydroxide (NaOH) solution instead of water has been added [20] to increase the pozzolanic reactivity of the BFS and provide good adherence with the soil.

As a result of the compression studies, the dry density-moisture content graphs obtained as a result of the standard proctor experiments of the samples are shown in Figure 1.

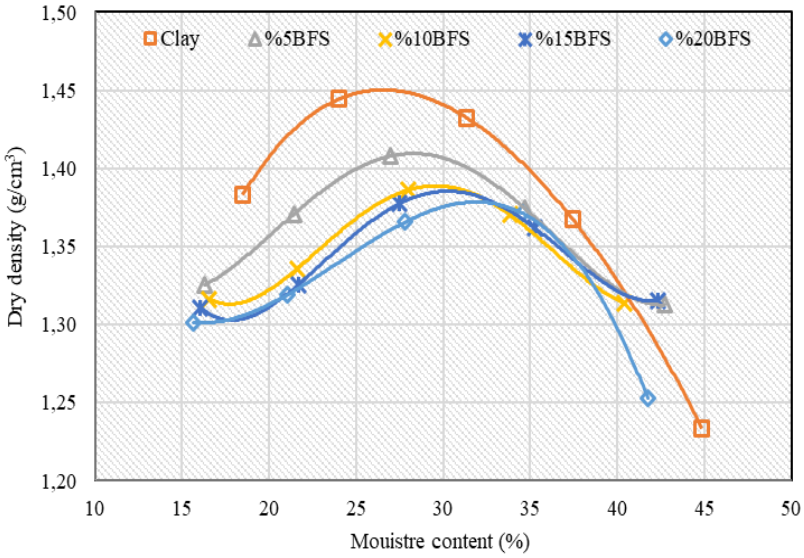

Figure 1. Dry density (g_k) – moisture content (%) graphic of samples

When Figure 1 is taken into consideration, it is observed that there is a decrease in the maximum dry densities of the samples and an increase in the optimum moisture content in proportion to the rise in the amount of BFS. It is thought that the increase in moisture content and the decrease in dry density are due to the high water absorption potential of BFS and its fine grain [20].

The unconfined compression test is an experiment that is generally used to determine the slip resistance in water-saturated normal consolidated clayey soils, and the soil resistance can be calculated from the Mohr circle obtained as a result of the test. In the experiment, cylindrical cohesion soil samples, preferably 38 mm in diameter and 76 mm in length, are used. This experiment is carried out in two ways: stress-controlled and deformation-controlled, but the one with unit length shortening control is commonly preferred. Since the experiment may cause changes in the moisture content of the sample during the experiment, it should be completed within 5-10 minutes, and the unit height shortening should be 0.5/min-2%/min. The experiment can be completed when the load carried by the sample starts to decrease or after the length shortening reaches 20%. In this experiment, the greatest value of axial stress gives the unconfined compressive strength (q_u). The undrained shear strength is obtained by $\tau = c_u = q_u / 2$ relation [21].

Within the scope of the experimental studies, mixture samples were prepared to subject them to unconfined compression and CBR tests, taking into account the optimum moisture content found as a result of the Standard Proctor experiment. First, all prepared samples were subjected to a 7-day curing period and were subjected to an unconfined compression experiment at the end of this period. Stress-Strain graphics obtained by mixed pure samples as a result of the 7-day curing period are given in Figure 2.

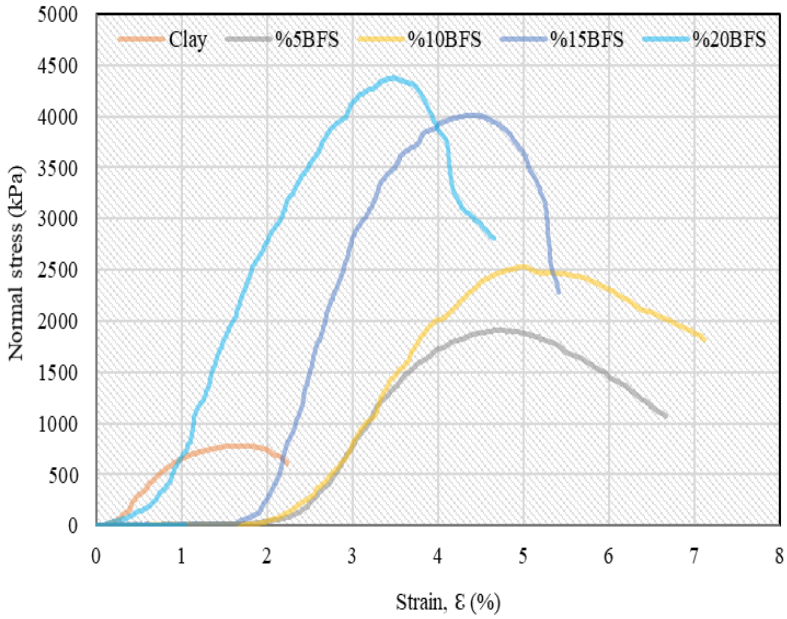

Figure 2. Unconfined compression test results of pure and BFS additive samples

As seen in Figure 2, it was determined that the maximum unconfined compression resistance among the prepared mixtures belongs to clay samples with 20% BFS additive. At the end of the 7-day curing period, a significant increase in unconfined compression resistance of the stabilized clay has been observed with a 20% BFS additive. This situation is considered to be caused by the BFS being a pozzolanic material and the late strength of the pozzolanic materials. However, considering the previous studies using BFS, it is seen that the rates giving maximum strength differ from each other [12-14]. As a result of the researches, it is considered that this difference is probably due to the structural differences of the clays and BFS used and the type and amount of the solutions used to increase the pozzolanic reaction, as stated in a similar study by Arulrajah [20]. Also, Bilici et al. [16] prepared mixture samples using different amounts of waste BFS and FA in their study. Samples of 3%, 6%, 9%, 12%, 15% FA in the first stage and 3%, 6%, 9%, 12% BFS samples in the second stage were tested for 7 days 28 days unconfined compression test. They found that the highest strength occurred in samples with 3% lime + 12% FA and 3% lime + 9% BFS. They evaluated the reason for this situation because BFS has higher pozzolanic property.

However, considering the previous studies using BFS, it is seen that the rates giving maximum strength may differ from each other [12-14]. As a result of the examinations made, it has been observed that this difference may result from structural differences of the clays and BFS used and the type and amount of the solutions used to increase the pozzolanic reaction.

Pure and stabilized mixture samples have been subjected to CBR test after the most effective additive rate was obtained as 20% as a result of the unconfined compression tests. For this purpose, mixture samples containing pure clay and 20% BFS have been prepared and, these samples were subjected to a curing period of 7 days. In the study, two samples were prepared for each experiment in parallel with the studies in the literature [13, 14]. CBR test results of pure clay and 20% BFS added mixture samples are shown in Table 3.

Table 3. CBR values of pure clay and 20% BFS added mixture samples

Sample	Curing Period	CBR (2.5 mm), (%)	CBR (5 mm), (%)
Pure clay	7 days	31.2	25.6
Pure clay+%20 BFS		179.7	222.9

As shown in Table 3, CBR values of 2.5 and 5 mm displacements of the Pure Clay subjected to a 7-day curing period were determined as 31.2% and 25.6%, respectively, and CBR values of 20% BFS-added clay soils corresponding to the same displacements were determined as 179.7% and 222.9% respectively as a result of experiments. Accordingly, CBR values of samples containing 20% BFS compared to pure clay soil increased by 5.76 and 8.71 times, respectively. These results show that BFS has a very positive effect on the clay soil's resistance to swelling deformations. In a study conducted in the literature [22] The change in swelling pressure and swelling percentages was investigated by adding slaked lime in different proportions (1%, 3%, 5%, 7%, 9%) by weight to "CH" clays, which may pose a risk for light structures and have high swelling potential. For all experimental samples, it was determined that as the lime additive ratio by weight increased, the CBR values increased and when it was 5%, the swelling percentage and swelling pressure decreased on average 91%, respectively.

3. RESULTS AND DISCUSSION

3.1. Analytical Investigation of Bearing Capacity in Flexible Pavement by AASHTO Method

Highway pavements are generally designed in two ways: flexible and rigid road pavements. Flexible road pavements where asphalt cement is used as binder material by and large consists of asphalt concrete coating, foundation and subbase layers. Pavements consisting of a coating layer constructed using portland cement are called rigid road pavements and these structures are conventionally composed of foundation and concrete slab coating [25]. A typical flexible road pavement section is given in Figure 3 below.

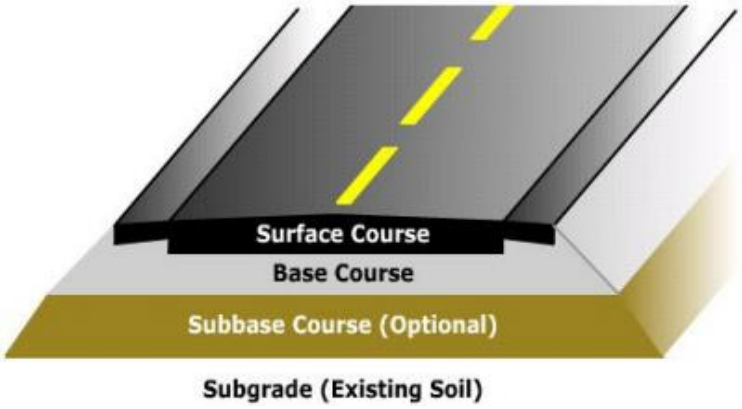

Figure 3. A typical flexible pavement section view [23]

In highway flexible pavement design, the aim is to determine the thickness of the pavement layers that can safely carry the traffic that will recur during the design life of the projected road

and to determine the properties of the materials that will form the pavement layers. In this context, the empirical equation given in Equation 1 is used in the calculation of AASHTO 1993 pavement layer thicknesses. Using this equation, the Number of Pavement (SN) value is calculated for flexible pavement design [24].

$$\mathrm{Log}T_{8,2}=Z_R\times S_0+9{,}36\times\log_{10}(SN+1)-0{,}20+\frac{\log(\Delta PSI/(4{,}2-1{,}5))}{0{,}40+[1094/(SN+1)^{5{,}19}]}+2{,}32\times\mathrm{Log}_{10}(M_R)-8{,}07 \quad (1)$$

In this place;
$T_{8.2}$: The number of standard axles (8.2 tons) that will repeat during service life
M_R: Subgrade resilient modulus, psi (6.8950×10^3 Pa)
S_0: Total standard deviation
Z_R: Standard normal deviate
SN: Structural number (inches)
P_0: İnitial design serviceability index
P_t: Design terminal serviceability index
ΔPSI: Difference between the initial design serviceability index, P_o, and the design terminal serviceability index, P_t (P_0-P_t)

After the SN value is calculated with Equation 1, the required, flexible pavement layer thicknesses are calculated with Equation 2, considering the layer coefficients given in Table 4 [23].

$$SN = a_1 \times D_1 + a_2 \times D_2 \times M_2 + a_3 \times D_3 \times M_3 \ldots\ldots\ldots\ldots .a_i \times D_i \quad (2)$$

In this equation; a_1, a_2, a_3 respectively are the structural layer coefficients of the coating, base and subbase layers, D_1, D_2, D_3 are layer thicknesses of coating, base, subbase, M_2, M_3 are the drainage coefficients of base and subbase layers.

In this study, the drainage coefficients are considered as 1.00 in the calculation of flexible road pavement layer thicknesses.

Table 4. AASHTO layer coefficients [24]

Layer type	Marshall Stability (kg)	CBR (%)	Relative Strength Coefficient (a)
Surface course			
Wearing course	≥900	-	0.42
Binder course	≥750	-	0.40
Bituminous base course	≥600	-	0.36
Base course			
Granular base	-	≥100	0.14
Plant mix base	-	≥120	0.15
Subbase			
Sand-gravel subbase	-	≥30	0.11
Crushed-stone subbase	-	≥50	0.13

After determining the flexible pavement layer thicknesses, SN* values given in Figure 4 were calculated, and the control of the layer thicknesses has been made.

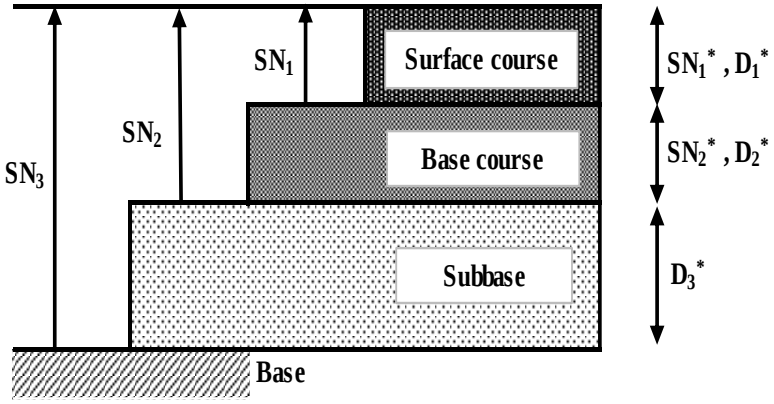

Figure 4. Pavement numbers in flexible pavement

SN_1: SN required on the base layer
SN_2: SN required on subbase layer
SN_3: Required SN on base soil
*: It shows the current values according to the material used.

In the study, to determine the effects of BFS on the flexible road pavement, flexible pavement design was made with the AASHTO 1993 method, taking into account the optimum strength and 7-day curing time.

3.2. Analytical Investigation of Base Soil Bearing Capacity of Pure and 20% BFS Additive Clay Soil in Flexible Pavement with AASHTO Method

In the 20-year project life, roads with an equivalent standard axle load repetition number of more than 60-75x10^6 were recommended to be made rigid. It is foreseen that the roads with an equivalent standard axle load repetition number lower than this value will be made flexible road pavement [25].

For flexible pavement design, CBR values of 20% BFS added clay soil at the end of the 7-day curing period have been taken as a basis. Calculations were made using the CBR values of %31.2 ve %222.9 which have been obtained from pure and 20% BFS added clay soils, respectively.

For this, first of all, it is necessary to calculate the modulus of elasticity (M_R) of the soil of the road whose pavement will be designed with the AASHTO method.

M_R=1500×CBR connection is available between the M_R and CBR values of the soil, and if the CBR value of the soil is known, the M_R value can be approximately calculated [26].

Accordingly, M_R values for pure and 20% BFS added clay soil were determined as 46.800 psi (322674641,32 Pa) for clay soil and 334.350 psi (2305262101 Pa) for 20% BFS added clay soil, respectively. Using the data in Table 5, the SN_3 (SN) required on the base for pure and 20% BFS added clay soils were calculated with the help of Equation 1 as 6.16 inches (15.65 cm) and 3.11 inches (7.90 cm), respectively.

Table 5. Parameters used in flexible pavement design [25]

Parameter	Selected Values
Equivalent standard axle load repetition number, $T_{8,2}$	50.000.000
Standard normal deviate, Z_R (State road R=%85)	-1.037
The first serviceability of the road, P_0	4.20
The last serviceability of the road, P_t (For motorways, state roads 2.5)	2.50
Service capability index, ΔPSI	1.70
Total standard deviation, S_0	0.45

3.3. Determination of Flexible Pavement Layer Thicknesses for Pure and 20% BFS Additive Soil and Control of These Thicknesses

With Equation 1, the SN_3 values for pure clay ground are calculated as 6.16 inches (15.65 cm) and 3.11 inches (7.90 cm) for the 20% BFS-added soil. The selected flexible road pavement layer thicknesses are given in Table 6, and layer thicknesses selected for 20% BFS added soil are shown in Table 7.

Table 6. Recommended layer thicknesses for pure clay soil

Layer Name	Recommended Thickness (D_i), (cm)	Layer Coefficient (a_i)
Wearing Course	5	0.42
Binder Course	10	0.40
Bituminous Base Course	11	0.36
Plant Mix Base	25	0.15
Crushed-Stone Subbase	15	0.13

Table 7. Recommended layer thickness for soil with 20% BFS additive

Layer Name	Recommended Thickness (D_i), (cm)	Layer Coefficient (a_i)
Wearing Course	5	0.42
Binder Course	10	0.40
Bituminous Base Course	11	0.36
Plant Mix Base	25	0.15
Crushed-Stone Subbase	-	-

Total pavement layer thicknesses determined for pure and 20% BFS added clay soil was determined as 66 cm and 51 cm, respectively. For clayey soils containing 20% BFS, it was determined that the layer thickness decreased by 29.41% compared to the pure soil.

To control the selected layer thicknesses, the plant mix base is selected from Table 4 as CBR = 120, and the crushed stone subbase is CBR = 50 and the plant mix base is calculated as M_R = 180.000 psi and the crushed stone subbase is calculated as M_R = 75.000 psi. After calculating the M_R value, the required SN values on these layers were calculated as SN_1 = 3.93 inches (9.98 cm) for the plant mix base with the help of Equation 1 and SN_2 = 5.32 inches (13.51 cm) for the crushed stone subbase.

Flexible road pavement layer thickness control calculated for pure clay soil is given in Table 8, and 20% BFS is added to soil in Table 9.

In the calculations in Table 8 and Table 9, the relative strength coefficients of wearing, binder, bituminous base course, base and subbase layers, D_1, D_2, D_3, D_4, D_5 show wearing, binder, bituminous base course, base and subbase layer thicknesses.

Table 8. Control of flexible pavement layer thicknesses for pure clay soil

D_1 (cm)	**a_1**	**D_2 (cm)**	**a_2**	**D_3 (cm)**	**a_3**	**D_4 (cm)**	**A_4**	**D_5 (cm)**	**A_5**	**$SN^* = a_i \times D_i$**	**Definitions**
5	0.42	10	0.40	11	0.36	-	-	-	-	SN_1^* =10.06	For plentmix crushed stone base $SN_1^* > SN_1$ (10.06>9.98) appropriate.
$D_4^*=(SN_2-SN_1^*)/a_4$ = (13.51-10.06)/0.15=23 cm, Selected D_4=25 cm $SN_2^*=25\times0.15=3.75$ $SN_1^* + SN_2^*=10.06+3.75=13.81\geq13.51$ (SN_2)											
For pure clay soil; $D_5^* \geq (SN_3-(SN1^*+SN2^*))/a_5$ $D_5^* \geq (15.65-(10.06+3.75))/0.13$ $D_5^* \geq 14.15$ selected D_5=15 cm $(SN_1^* + SN_2^*)+(15\times0.13)=13.81+1.95=15.76\geq15.65$											

Table 9. Flexible pavement layer thickness control for 20% BFS additive soil

D_1 (cm)	**a_1**	**D_2 (cm)**	**a_2**	**D_3 (cm)**	**a_3**	**D_4 (cm)**	**A_4**	**D_5 (cm)**	**A_5**	**$SN^* = a_i \times D_i$**	**Definitions**
5	0.42	10	0.40	11	0.36	-	-	-	-	SN_1^* =10.06	For plentmix crushed stone base $SN_1^* > SN_1$ (10.06>9.98)
$D_4^*=(SN_2-SN_1^*)/a_4$ = (13.51-10.06)/0.15=23 cm, Selected D_4=25 cm $SN_2^*=25\times0.15=3.75$ $SN_1^* + SN_2^*=10.06+3.75=13.81\geq13.51$ (SN_2)											
20% BFS added soil for clay soil; $D_5^* \geq (SN_3-(SN_1^*+SN_2^*))/a_5$ $D_5^* \geq 0$, D_5=0 (subbase will not be made) $(SN_1^* + SN_2^*)+(0\times0.13)=13.81+0=13.81\geq7.90$ (SN_3)											

3.4. Economic Analysis for Pure and 20% BFS Added Clay Soils

In the study, the impact of BFS-improved clay soil on highway flexible pavement costs was evaluated based on the data of the General Directorate of Highways (GDH).

In unit price charts published by GDH, unit weight (ton) and unit volume (m^3) costs for subbase and base layers; Unit area (m^2) costs have been published for the bituminous base course, binder and wear layers. In the study, the 2019 GDH unit price item number was used for the economic analysis of highway pavements. In this context, the unit costs to be used within the scope of analysis for pure clay soil are given in Table 10 [27].

Table 10. Unit costs for pure clay soil according to layer types

Item Number	Definition and Unit	Unit Price (TL)	Cost of m^2/cm (TL)
GDH/6405/S-M	Making 1 m^2 asphalt concrete wear layer in 5 cm compacted thickness, (m^2)	13.06	2.61
GDH/6320	Making asphalt concrete binder layer (with crushed and screened quarry stone), (ton) Note: Coating density 2.40 g/cm^3	83.78	2.02
GDH/6211-A	Making 1 m^2 asphalt concrete Bituminous base course layer in 11 cm compacted thickness, (m^2)	20.11	1.83
GDH/6100/3	Making plant mix base (with broken and sieved quarry stone), (ton) Note: Coating density 2.40 g/cm^3	40.49	0.97
GDH/6000	Making the subbase with crushed and screened material from quarry stone, (m^3)	41.68	0.42

In the calculation of the unit cost according to the layer types for the pure clay soil, the crushed stone subbase layer is 15 cm, the plant mix base layer is 25 cm, the bituminous base course layer is 11 cm, the binder layer (asphalt concrete) is 10 cm and the wear layer (asphalt concrete) is 5 cm as shown in Table 6.

In the cost calculation of flexible road pavement, the cost of each layer was calculated by dividing the unit prices given in Table 10 by the thickness of the layer in terms of "m^2 /cm", and the total and pavement unit cost has been determined. According to these calculations, the unit cost of the flexible road pavement thickness in m^2/cm was obtained as 7.85 TL.

Similarly, in calculating the unit cost according to the layer types for clay soil with 20% BFS additive, the plant mix base layer was calculated as 25 cm, bituminous base course layer 11 cm, binder layer 10 cm and wearing layer (asphalt concrete) as 5 cm as also shown in Table 8.

Table 11 shows the unit costs to be used within the scope of the analysis of 20% BFS added clay soil [27].

Table 11. Unit costs by layer types for 20% BFS added clay soil

Item Number	Definition and Unit	Unit Price (TL)	Cost of m^2/cm (TL)
GDH/6405/S-M	Making 1 m^2 asphalt concrete wear layer in 5 cm compacted thickness, (m^2)	13.06	2.61
GDH/6320	Making asphalt concrete binder layer (with crushed and screened quarry stone), (ton) Note: Coating density 2.40 g/cm^3	83.78	2.02
GDH/6211-A	Making 1 m^2 asphalt concrete Bituminous base course layer in 11 cm compacted thickness, (m^2)	20.11	1.83
GDH/6100/3	Making plant mix base (with broken and sieved quarry stone), (ton) Note: Coating density 2.40 g/cm^3	40.49	0.97

According to these calculations, the unit cost of the flexible road pavement thickness in m^2/cm for 20% BFS added clay soil was obtained as 7.43 TL.

According to these calculations, 20% BFS added clay soil reduces the unit cost by approximately 5.65% compared to pure clay soil in determining layer thicknesses. If the road soil is improved with 20% BFS on a divided road of 1000 m in length and 20 m in width, 8,400.00 TL will be saved. Within the scope of similar studies conducted with waste material in the literature; In determining the thickness of the flexible road pavement layer, if the soil with 10% fly ash (FA) added clay soil and 10% FA on the 1000 m in length and 20 m in width divided road, the road soil is improved, 81,840.00 TL will be saved [28].

4. CONCLUSIONS

In this study, the effects of a clay subgrade soil, whose strength is increased by adding BFS, to highway flexible road pavement layer thicknesses and costs were obtained;

- ✓ Due to the increase in the amount of BFS in the content of the clay soil, the optimum moisture content of the mixes increased and the maximum dry density values decreased. This is thought to be due to the high water absorption potential of the BFS and its fine grain structure.

- ✓ According to the results of the unconfined compression test, the unconfined compression strength of the pure soil increased with the addition of BFS and the highest strength was obtained from mixtures containing 20% BFS. This result shows that BFS has a healing effect on the shear strength and cohesion ability of the clay soil.

- ✓ According to CBR test results, 7 days of 20% BFS additives increased the CBR value of 7 days of pure clay soil approximately by 8.71 times. This significant increase shows that BFS has a very positive effect on the permanent deformation resistance of the clay soil.

- ✓ According to layer thicknesses calculated for pure and additive soils, layer thickness for clayey soils containing 20% BFS showed a great decrease by 29.41% compared to pure soil.

- ✓ According to the cost calculation results, the cost of the pavement for clayey soils containing 20% BFS decreased by approximately 5.65% compared to the pure clay soil. due to the decrease in layer thicknesses.

- ✓ Considering the unit costs for highway pavement layers, when the subgrade of a divided road of 1000 m in length and 20 m in width is improved with 20% BFS, 8,400.00 TL saving will be achieved in the cost of flexible road pavement compared to pure soil.

As a result, it was found that with the addition of BFS to a clayey subgrade, the strength of the subgrade increased significantly, and the flexible road pavement layer thicknesses and construction costs were reduced significantly. For this reason, it is thought that if the subgrades are improved with BFS, it will be very beneficial in terms of decreasing the road pavement cost and any possible damages to the environment. Additionally, operations such as storage and transportation of artificial pozzolanic materials such as BFS formed as a result of industrial activities lead to the occupation of fertile agricultural lands and serious damage to the environment. In this context, the use of waste materials such as BFS as road infrastructure filling material to form soil improvement; is of great importance in reducing environmental pollution, decreasing high costs due to stabilization of soils with poor bearing capacity and reusing waste materials [29].

Acknowledgments

This study has been supported by Inonu University Scientific Research Projects (SRP) Coordination Unit, project number FDK-2018-957.

REFERENCES

[1] Kozak, M. (2010). Investigation of the usage areas of textile wastes as building materials. *Electronic Journal of Building Technologies*, 6(1): 62-70.

[2] Aruntaş, H.Y. (2006). Potential use of fly ash in the construction industry. *Journal of Gazi University Faculty of Engineering and Architecture*, 21(1): 193-203.

[3] Tunç, A. (2002). *Geotechnics and applications in road engineering*. Atlas Publishing, Istanbul.

[4] Çakılcıoğlu, İ. (2007). *Stabilization of high plasticity clays*. Master Thesis, Sakarya University Institute of Science, Sakarya.

[5] Hausman, M.R. (1990). *Engineering principles of ground modification*. International Edition, 321-335.

[6] Kılıç, G. (2008). *Ground stabilization with cement.* Master Thesis, Yıldız Technical University Institute of Science, Istanbul.

[7] Emery, J.J, Kim, C.S, and Cotsworth, R.P. (1976). Base stabilization using pelletized blast furnace slag, 4(1):94-100.

[8] Öner, A, and Yıldırım, T. (2005). Effect of crushed stone sand content on concrete properties in concretes with and without ground blast furnace slag. *Earthquake Symposium*, Kocaeli.

[9] Tokyay, M. and Erdoğdu, K. (2002). *Slags and slag cements*. Cement Manufacturers Association of Turkey, Ankara.

[10] ACI 233.R-95, (2005). Ground granulated blast-furnace slag as a cementitious constituent in concrete. Reported by Acı Committee 233, American Concrete Institute, Detroit, Michigan.

[11] Bilgen, G., Kavak, A., Yıldırım, S.T. and Çapar, Ö.F. (2010). The place and importance of blast furnace slag in the construction industry. *Proceedings of the 2nd National Solid Waste Management Congress*, Volume 1: 506-513, Mersin.

[12] Bilgen, G. (2007). *Ground stabilization with blast furnace slag*. Master Thesis, Institute of Science, Kocaeli.

[13] Sivrikaya, O., Yavascan, S. and Cecen, E. (2014). Effects of ground granulated blast-furnace slag on the index and compaction parameters of clayey soils. *Acta Geotechnica*, 19-27.

[14] Bilgen, G., Kavak, A. and Çapar, Ö.F. (2012). The use of steel shop slag as an additive to a low-plasticity clay and its interaction with lime. *Karaelmas Science and Engineering Journal*, 2(2):30-38.

[15] Cokca, E., Yazici, V. and Ozaydin, V. (2009). Stabilization of expansive clays using granulated blast furnace slag (GBFS) and GBFS-cement. *Geotechnical and Geological Engineering*, 27: 489-499.

[16] Bilici, H., Okur, D.V., Türköz, M. and Savaş H. (2020). Fly Ash and Blast Furnace Slag on the Strength of Clay Soil Impact and Comparative Analysis of Contributions. *BEU Journal of Science*, 9 (2), 910-919.

[17] Geçkil, T., Sarıcı T. and Yıldıran E.S. (2019). Improving the Strength of a Clay Soil with Lime Additive. *Çukurova University Journal of the Faculty of Engineering and Architecture*, 34(4), pp. 171-179.

[18] Geçkil, T., Tanyıldızı, M.M. and Yıldıran E.S. (2020). Effects of a Clay Soil Stabilized by Blast Furnace Slag on Road Flexible Pavement Layer Thickness and Cost. *Fırat University Journal of Engineering Sciences*, 32(2), 509-520.

[19] HTS (2013), Highways Technical Specifications Project Guide, Technical Research Department, Ankara.

[20] Arulrajah, A., Mohammadinia, A., Horpibulsuk, S. and Samingthong, W. (2016). Influence of class f fly ash and curing temperature on strength development of fly ash recycled concrete aggregate blends. *Construction and Building Materials*, 127:743-750.

[21] Gençdal, H., Berilgen, S. and Kılıç, H. (2020). Investigation of volume change behavior on compacted high plasticity clay ground for different initial conditions. *Gazi University Journal of Engineering and Architecture Faculty*. 35(3): 1421-1436.

[22] Öztürk, Y.Z., Ünsal, N and Akbaş, S.O (2015). Assessment of The Swellıng and Lıme Stabılızatıon Potentıal of Gölbaşı (Ankara) Resıdentıal Area Clays. *Journal of the Faculty of Engineering and Architecture of Gazi University*, 30(2): 309-318.

[23] Gökalp, İ., Uz, V.E., Saltan, M. and Tutumluer, E. (2018). Technical and environmental evaluation of metallurgical slags as aggregate for sustainable pavement layer applications. *Transportation Geotechnics*, 14: 61-69.

[24] American Association of State Highway and Transportation Officials, AASHTO Guide for Design of Pavement Structures. Washington, D.C.:1993.

[25] Highways Flexible Pavement Project Design Guide (2008), Technical Research Department, Ankara.

[26] Kök, B.V., Yılmaz, M. and Geçkil A. (2012). The effect of cement stabilized soil on flexible pavement cost. *Pamukkale University Journal of Engineering Sciences*, Volume 18, Number 3, Pages 165-172.

[27] http://www.birimfiyat.net, 2019.

[28] Geçkil, T., Tanyıldızı, M.M. and Yıldıran E.S. (2019). The Effects of a clay floor ıncreased wıth fly ash on road pavement. *I. Internatıonal Scıence and Innovatıon Congress*, 407-413.

[29] Uysal, F.F. and Selin Bahar, S. (2018). Slag Types and Utılızatıon Areas. *Trakya University Journal of Engineering Sciences*, 19(1): 37-52.

NATURENGS
MTU Journal of Engineering and Natural Sciences
https://dergipark.org.tr/tr/pub/naturengs
DOI: 10.46572/nat.2020.14

Low Cost Activated Carbon Synthesis, Characterization and Adsorption Applications

İlhan KÜÇÜK[1*], Yunus ÖNAL[2]

[1]Muş Alparslan University, Muş, Turkey.
[2]Department of Chemical Engineering, Faculty of Engineering, İnönü University, Malatya, Turkey.

(**Received:** 19.11.2020; **Accepted:** 06.12.2020)

ABSTRACT: In this study, activated carbon was synthesis from peach kernel shells, which is agricultural waste. The synthesized activated carbons were characterized and their adsorption properties were examined. Activated carbons were synthesized by the physical activation method and CO_2 was used as the activation gas. The synthesis was carried out in two steps. In the first step, it was subjected to the carbonization process at 4 different temperatures. During the carbonization process, two different gas flows were used. In the activation process, a temperature of 800°C was used. The surface area and morphological properties of the obtained activated carbons were studied by BET, XRD, FTIR and elemental analyzes. Methylene blue was used during adsorption. The adsorption capacities of the samples were calculated.

Keywords: Activated carbon, Biomass, Physical activation, Adsorption.

1. INTRODUCTION

With the increasing world population, environmental pollution has increased and this has started to affect human health negatively. Increasing pollution has especially polluted our rivers and caused great problems for both human and living life. Especially the drinking water shortage is increasing day by day and urgent measures should be taken. It is important to remove the increasing pollution from nature. Both the efficient materials to be made with these impurities and the use of these materials are important [1,2].

Especially the increasing need for materials used in the adsorption process is increasing day by day. Activated carbon comes first among these materials. The advantages of activated carbons from other materials are that they can be synthesized from waste materials, high surface areas, strong adsorption properties and easy usage. Due to these properties, activated carbon is widely used in adsorption processes [3]. The properties of activated carbons can be synthesized from waste materials, usually by chemical and physical activation. Chemical activation is carried out in two different ways. First, the chemical substance can be applied to the raw material. This activation can be carried out by directly adding chemicals to the raw material. It can also be carried out by adding pure water to the added chemical. This method is called impregnation. Another way of carrying out chemical activation is in two steps. In the first step, carbonization is carried out. Chemical impregnation is applied to the carbonized product. This event is the other type of chemical activation. In physical activation, activated carbon synthesis is carried

*Corresponding Author: i.kucuk@alparslan.edu.tr
ORCID number of authors: [1]0000-0003-2876-3942 , [2] 0000-0001-6342-6816

out in two steps. The raw material is carbonized. Activation is applied to the carbonized product. CO_2 and water vapor are used for activation. Although the physicochemical activation process has emerged in recent years, it is not a widely used method. What is done in this method is mixing physical and chemical activation [4-6].

Adsorption is the phenomenon of solid, liquid, or gas molecules adhering to a solid surface. This event is to be used excessively, especially in water treatment. The most important pollution in water is the dyestuffs used in textiles, dyeing paper and pulp, plastic, leather, cosmetics, and food industries, and many other areas. Different methods can be used to clean these impurities. Some of these methods are coagulation, reverse osmosis, photodegradation, electrochemical oxidation, ozonation and adsorption. The adsorption method has many advantages compared to other methods. Some of these advantages are low cost, simple installation and ease of application [7, 8].

Methylene blue is the most used basic dye in adsorption studies. Although its use is not very dangerous, it causes vomiting, jaundice, skin diseases and heart diseases in living creatures that are constantly exposed [9].

In this study, activated carbon was synthesis from peach seed shells by physical activation. CO_2 was used as gas in physical activation. The reason for using the peach kernel shell is that it has a high carbon content and is abundant in this waste. The reason for using CO_2 is that its pore distribution is in a narrow area. Carbonization temperatures of 700 °C, 800 °C, 900 °C and 1000 °C were used. 800 °C was applied as the activation temperature.

2. MATERIAL AND METHODS

2.1. Preparation of Activated Carbons

Activated carbons, the peach seed shell was synthesized without any pretreatment. Peach kernel shell is primarily subjected to pyrolysis. During the pyrolysis process, peach kernel shells were kept at 700°C, 800°C, 900°C and 1000°C at 100 ml/min and 500 ml/min gas flow for 1 hour at a maximum temperature of 10°C/min. The solid sample taken from the oven was placed in the oven for physical activation without any pretreatment. The placed sample was activated at 800°C with CO_2. The synthesis is completed by keeping the sample at this temperature for 1 hour at a heating rate of 10°C/min. As a result of the activation, the activated carbons were ground and ready for the analysis phase.

2.2. Analyzes

XRD analysis with Rigaku RadB-DMAX II computer-controlled X-ray diffractometer, SEM images with LECO EVO40 brand device, FTIR analysis with Perkin Elmer 100 device, elemental analysis and percentage values with LECO CHNS 932 elemental analyzer, Surface area of activated carbons 77 K and at relative pressure (P / Po) between 10^{-6}-1 and N_2 adsorption with Brunauer-Emmett-Teller (BET) Tristar 3000 Micromeritics branded Surface Analyzer.

2.3. Adsorption Test

1000 ppm methylene blue stock solution was prepared for the adsorption experiment. The stock solution prepared was diluted 10 times and was prepared for the adsorption process by placing it in 100 ppm and 100 ml. 0.1 grams of activated carbon sample was placed in the prepared

flasks and the adsorption process was started for 24 hours. In this process, the mouths of the erlenmeyer were closed with paraffin. Then the extracted samples were measured with a UV-VIS device and the samples were calculated as in Equation 1.

$$q = \frac{C_0 - C_e}{W} * V \quad (1)$$

q = The amount of methylene blue adsorbed,(mg/g)
C_0= Initial concentration of methylene blue,(mg/L)
C_e= Measured methylene blue concentration, (mg/L)
w = Activated carbon amount,(mg)
V = Solution Volume,(L)

3. RESULTS AND DISCUSSION

BET, FTIR, XRD and Elemental Analysis were performed on activated carbons synthesized from peach kernel shell. Activated carbon was characterized by the analyzes performed. BET analysis results of activated carbons are shown in Table 1.

Table 1. BET analysis results

	Carbonization		**Physical Activation**						
Codes	Temperature °C	Gas Flow Rate	Temperature (°C/100 ml CO_2)	S_{BET} m^2/g	S_{micro} m^2/g	S_{mezo} m^2/g	V_T cm^3/g	V_{micro} cm^3/g	V_{mezo} cm^3/g
AC1	700	100	800	351.34	351.34	-	-	0.18	-
AC2	700	500	800	334.55	334.55	-	-	0.18	-
AC3	800	100	800	333.04	333.04	-	-	0.18	-
AC4	800	500	800	347.51	347.51	-	-	0.18	-
AC5	900	100	800	168.39	168.39	-	-	0.17	-
AC6	900	500	800	205.82	205.82	-	-	0.16	-
AC7	1000	100	800	12.06	12.06	-	-	0.052	-
AC8	1000	500	800	2.08	2.08	-	-	0.05	-

According to the BET analysis results shown in Table 1, the highest surface area belongs to the AC1 sample with 351.34. The lowest surface area belongs to the AC8 sample with 2.08. Increased carbonization temperature harmed the surface area. Also, the increased gas flow caused differences in the surface area. The reason for this can be shown that with the increasing gas flow, more N_2 particles touch the sample and the differences in the structure occur. However, this situation does not cause pore formation in the structure. Because the gas cannot fully form the pores during the carbonization process. The pores formed by the activation gas either expand completely or pores that are not fully formed begin to form. When looking at activated carbons synthesized at 700°C and 800°C, there is not much change in surface areas. However, when the temperature increases, there is a decrease in surface areas. The decreasing surface area can be explained as breaking down the pore walls in activated carbon with increasing temperature. Another explanation is that the pore formation in the material may have decreased with increasing temperature. Since activated carbons are produced by the physical

activation method, CO_2 is used as the activating gas. Activation gas did not show mesopore formation in the samples. All of the pores formed in all samples are microporous.

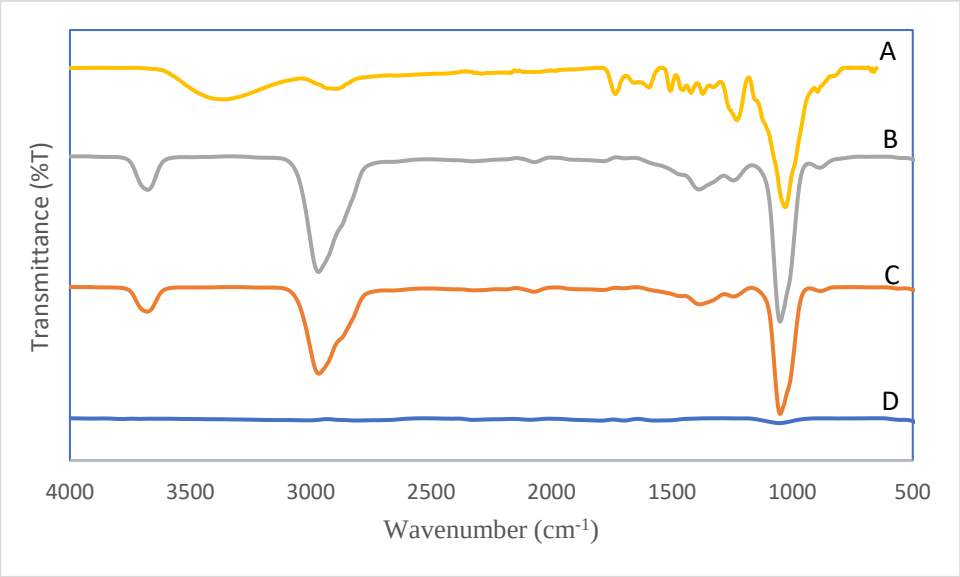

Figure 1. FTIR spectrum A: Raw peach B: AC1 C: AC3 D: AC7

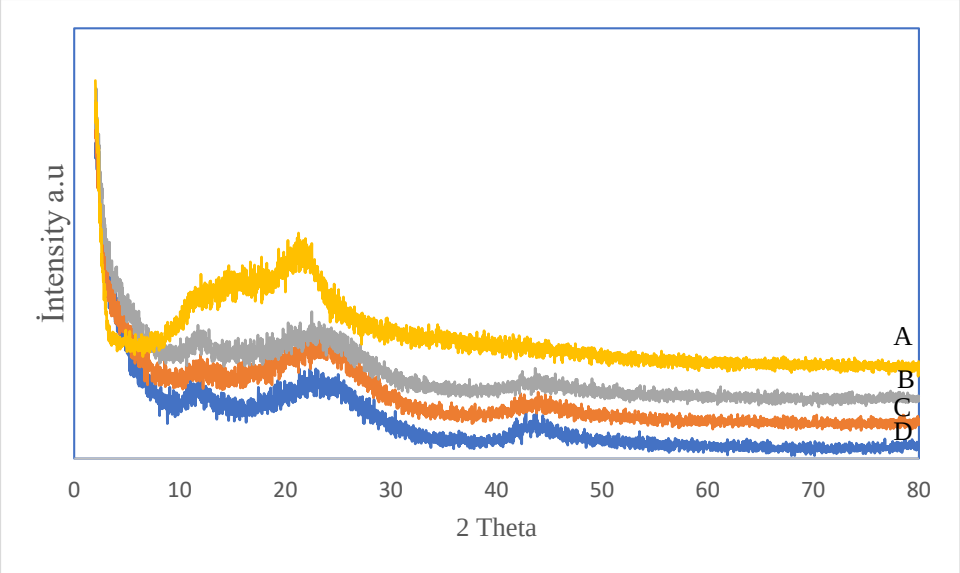

Figure 2. XRD spectrum A: Raw peach B: AC1 C: AC3 D: AC7

FTIR results of some samples are given in Figure 1. According to Figure 1, the peaks existing in the raw peach kernel shell decreased or disappeared in the activated carbon. This phenomenon can be explained by structural changes during carbonization and activation. It is related to the peak-OH stress occurring around 3350 cm^{-1} in the raw peach peel, and it is proof of the presence of hydroxide molecules in the structure. This may mean the presence of a structure such as phenol or alcohol in the hydroxide molecule structure. In addition, this peak occurred in cellulose in the structure. The peak that occurred around 3050 cm^{-1} was formed by

C-H bending in the structure. The peak that occurs at about 1700 cm^{-1} is the peak that occurs from the C=O molecule in the structure. The peak that occurs at about 1100 is from the C-O molecule. Another characteristic analysis for samples is XRD analysis. XRD analysis is shown in Figure 2. According to XRD analysis, no crystallized regions were found in the raw peach skin. There are 3 different semi-crystalline zones in the structure. The structure is generally amorphous. The flat peak around 22 thetas appears as the cellulose peak and is seen in cellulose-containing materials. This peak is considerably reduced in activated carbon samples. This means that the cellulose in the structure is broken down.

Table 2. Elemental analysis of some samples

Sample	%C	%H	%N	%S	%O
Peach Kernel Shell	50.45	5.683	0.072	-	43.795
700°C 100 ml/min N_2 800°C CO_2	51.11	0.874	0.134	-	47.882
800°C 100 ml/min N_2 800°C CO_2	47.45	0.776	0.218	-	51.556
1000°C 100 ml/min N_2 800°C CO_2	80.40	0.699	0.475	-	18.426
1000°C 500 ml/min N_2 800°C CO_2	69.16	0.441	0.663	-	29.736

Some samples were analyzed for elementary analysis. Element analysis results are given in Table 2. According to Table 2, there is approximately 50% carbon content in the raw peach kernel shell. Increasing carbon content in materials is important for active carbon synthesis. This ratio in peach kernel shell is sufficient for activated carbon synthesis. The carbon content of activated carbons is generally higher than the raw peach kernel shell. This result is generally expected. This is because the shell is subjected to pyrolysis and activation processes. In general, there is a noticeable decrease in the amount of hydrogen. There is an increase in the amount of nitrogen. The occurrence of these differences is a show of change in structure. In addition, the increased amount of carbon according to the element analysis results caused some peaks to expand and decrease in FTIR and XRD analyzes. Approximately 1100 cm^{-1} peak increase occurring in FTIR consists of C-O stretch and vibration. The increase in this peak and the increase in the C-H bending peak at approximately 3050 cm^{-1} can be explained by the ratio of C/H and C/O. Also, the change in XRD, especially the decrease in the peak of cellulose, is observed. However, the regular regions seen may come from the increased amount of carbon.

Methylene blue adsorption capacitors of activated carbons were studied. Study results are given in Table 2. The methylene blue adsorption capacity of the activated carbons synthesized according to Table 2 was found to be quite low. The methylene blue molecule is a very large molecule with a molecular structure of $C_{16}H_{18}ClN_3S$. When looking at the synthesized activated carbons, pores are generally micropores. Micropores are a term used for pores formed at 2 nm and below. These pores are too low for methylene blue to enter. Therefore, since the methylene blue molecule cannot pass through the pores, it is quite natural that the methylene blue adsorption capacity is quite low.

Table 3. Methylene Blue adsorption of samples

Carbonization		**Physical Activation**		
Temperature °C	Gas Flow Rate	Temperature (°C/100 ml CO_2)	S_{BET} m^2/g	Adsorption Capacity q_e (mg/g)
700	100	800	351.34	-
700	500	800	334.55	1.66
800	100	800	333.04	1.77
800	500	800	347.51	-
900	100	800	168.39	2.76
900	500	800	205.82	3.67
1000	100	800	12.06	1.66
1000	500	800	2.08	4.44

4. CONCLUSIONS

In this study, activated carbon synthesis was prepared from a peach kernel shell. In the synthesis of activated carbon, the surface area was expanded and these results are given by the measurement of the BET device. In the results given, the structure consists entirely of micropores. This means that the pores seen in this structure are quite small. It is seen in the literature that active carbons synthesized by physical activation generally have lower surface areas than those synthesized by chemical activation. In addition to the fact that the surface areas are very small, the rate of micropore is quite high. Water vapor is used in physical activation, which is another study in the literature. By the information given in the literature, the surface area of activated carbons synthesized by water vapor activation is higher than CO_2. This phenomenon explains that the H_2O molecule is smaller than the CO_2 molecule. Small molecules enter the pore circles and expand the pores. Therefore, more mesopore is observed in studies used H_2O. In this study, the benefit of the CO_2 molecule used in comparison to other activation agents is that it produces a high amount of micropore. In line with these results, if a high amount of micropore is desired in the activated carbon that we will synthesize, CO_2 should be used. However, since these activated carbons have low methylene blue adsorption, other application areas can be examined.

With this study, a new type of activated carbon with narrow pore distribution was added to the literature. A narrower pore distribution can be achieved by further expanding the study. Activated carbons which narrow pore distribution can be used as carbon molecular sieves.

Acknowledgment
This study was supported by the unit of Scientific Researches of Inonu University in Malatya, Turkey; Project no: FDI-2017-680

REFERENCES

[1] Türkyılmaz, A. (2018). Sulu Çözeltilerde Nano Kil(Halosit) Yüzeyine Metilen Mavisi Adsorpsiyonu Ve Kinetiği, *BAUN Fen Bil. Enst. Dergisi*, 20(2): 413-424.

[2] Türkyılmaz, A. ve Işınkaralar, K. (2020). Sulu Çözeltilerden Aktif Karbon Üzerine Adsorpsiyon İle Antibiyotiklerin (Tetrasiklin Ve Penisilin G) Giderimi, *Journal of Engineering Sciences and Design*, 8(3): 943-951.

[3] Uzunoğlu, D., Özer, A. ve Özdemir, Z. (2015). Basıc Red 46 Boyar Maddesinin Montmorillonitli Kireç Taşına Adsorbsiyonu, *Anadolu University Journal of Science and Technology A- Applied Sciences and Engineering*, 16(2): 303-315.

[4] Erdoğan, F.O. and Kopaç, T. (2020). Investigation of acetone adsorption characteristics of activated carbons obtained from Zonguldak-Karadon coal at room temperature, *Journal of the Faculty of Engineering and Architecture of Gazi University*, 35(4): 2211-2224.

[5] Ioannidou, O. and Zabaniotou, A. (2005). Agricultural residues as precursors for activatedcarbon production-A review. *Renewable and Sustainable Energy Reviews* 11: 1966–2005.

[6] Heidarinejad, Z., Dehghani, M.H., Heidari, M., Javedan, G., Ali, I. and Sillanpaa, M. (2020). Methods for preparation and activation of activated carbon: A review, *Environmental Chemistry Letters*, 18: 393–415.

[7] Ceyhan, A.A. ve Baytar, O. (2018). Metilen Mavisinin Magnetik NiFe2O4/Aktif Carbon Nanokompoziti İle Adsorpsiyonu: Kinetik ve İzoterm, *Selcuk Univ. J. Eng. Sci. Tech*, 6(2):227-241.

[8] Fındık, S. (2020). Congo Red Removal From Aqueous Solutions by Adsorption on Peanut Hull, *Müh.Bil.ve Araş. Dergisi,* 2(1):28-35.

[9] Polat, İ. ve Orhan, R. (2019). Şeftali Çekirdeği Kabuğu Kullanarak Metilen Mavisi Boyasının Giderilmesi İçin Sabit Yataklı Kolonun Adsorpsiyon Performansı, *AKU J. Sci. Eng*., 19:861-870.

NATURENGS
MTU Journal of Engineering and Natural Sciences
https://dergipark.org.tr/tr/pub/naturengs
DOI: 10.46572/nat.2020.15

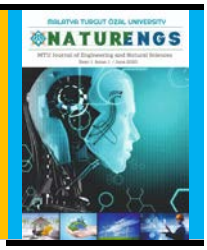

Correlations Between SPT, PMT and MASW on Quaternary Alluvial – Fluvial Sediments in Battalgazi, Malatya, Turkey

Çiğdem CEYLAN[1*], Mehmet ÖNAL[2]

[1]Department of Civil Engineering, Faculty of Engineering and Natural Sciences, Malatya Turgut Özal University, Malatya, Turkey.

[2]Department of Mining Engineering, Faculty of Engineering, İnönü University, Malatya, Turkey.

(**Received:** 04.12.2020; **Accepted:** 22.12.2020)

ABSTRACT: The field tests such as the standard penetration test (SPT), pressuremeter test (PMT), and Multi-Channel Analysis of Surface Waves (MASW) give information about the stratigraphic properties, structure, underground water level, bearing capacity, and liquefaction of soil. The studies investigating the correlations between these tests are quite common. Most of the studies found in the literature have focused on sand, silty, and clay soils, while the number of studies about gravelly soils is limited. In the study area, the gravel content ranged from 0% to 47% depending on local differences. Gravel sizes reached 80 mm at certain locations but remained below them in most locations. In this study, it has been discussed that how correlation studies will change in heterogeneous soils. Among the correlations between the field test results, with the highest R^2 value of 0.6847, the strongest correlation was obtained between the PMT-P_L value and SPT-N_{60} value, while, with an R^2 value of 0.3906, the weakest correlation was between the PMT-E_m value and MASW- V_s value. The low R^2 values were attributed to the exceedingly heterogeneous structure of the soil and locally changing gravel amounts.

Keywords: Correlation, Soil tests, Alluvial-fluvial sediments.

1. INTRODUCTION

During an earthquake, local geology plays an important role in the control of the effect of the earthquake on the surface. Soil properties can affect the amplitude, frequency, and duration of bedrock motion when it reaches the surface [1].

In geotechnical applications, as in situ tests that do not alter the soil stress conditions, field tests are preferred over laboratory applications. These tests are prevalently used in practices such as the design of foundations and other building structures, bearing capacity, and liquefaction analysis.

Within the scope of the in situ tests, various geophysical methods are also used, among them being the Multi-Channel Analysis of Subsurface Waves (MASW), which is a series of geophysical tests done on the ground surface and used to determine the shear wave velocity

*Corresponding Author: cigdem.ceylan@ozal.edu.tr
ORCID number of authors: [1] 0000-0002-5961-3085, [2] 0000-0002-4450-4417

(V_s) profile with depth for a certain site [2]. V_s is an important parameter revealing the stiffness of soil layers [3].

The study investigates whether there is a relationship between the SPT-N_{60} value (SPT N-value corrected for field procedures) obtained with the SPT, the E_m (Mernard deformation module) and P_L (Limit Pressure) values obtained with the PMT, and the V_s value obtained with the MASW test.

The study area was the Battalgazi Campus of Turgut Özal University located within the borders of Battalgazi District in the north of Malatya, Turkey (Figure 1). It has an area of about 600 decares. In the region, 15 boreholes were drilled at certain intervals and the SPT and PMT were performed in the boreholes at predetermined depths. The equations derived between the data obtained from the two tests were compared with the results found by other researchers. Again, in the same region, an MASW test was carried out at 32 points and the 15 closest MASW tests to the drilling points were used for comparison purposes. The relationship between the results and the results obtained with the SPT and PMT was examined and compared with the results found in the literature.

The maximum relation was obtained between SPT and PMT. But this relationship is quite weak. It is thought that such a result is due to the heterogeneous nature of the soil. Literature studies generally include studies on homogeneous soils and the relations obtained are quite high. However, it has been observed that as the heterogeneity of the ground increases, the relationship between SPT, PMT and MASW also gets weaker. In this study, it was investigated how the correlation studies in heterogeneous soils would yield results.

1.1. Geological Description of the Study Area

The study area involves the Quaternary alluvial-fluvial deposits of the Malatya basin located in the north of Battalgazi District, Malatya, Turkey. The alluvial deposits in the study area mostly comprised of treated-non-treated gravel, sand, silt, and clay-intercalated mud. The examination of the clay samples in the study area revealed that they were high-plastic clays. The pile stiffness examination showed that the pile was highly stiff. According to the seismic data, the pile had a thickness of 70 m. The evaluation of the lithological and stratigraphic properties and sedimentary geometry of the unit revealed that the unit reflected the sedimentation in alluvial fan and flood plain settings [4]. The underground water level (GW) in the region ranged from 2.29 m to 6.42 m depending on seasonal changes. The region mostly consists of agricultural lands and agricultural and education activities are carried out together in the campus site.

2. MATERIAL AND METHODS

2.1. Field Tests

In the study area total of 15 boreholes were drilled at 250 m intervals. The SPT and PMT were performed for the same boreholes and correlation studies were carried out between the results obtained from both tests. Among the measurements obtained with the MASW tests, the 15 closest measurements to the drilling points were used in the comparisons.

Figure 1. Location map of the study area [5]

2.1.1 SPT

The SPT is a simplistic and common test used in the calculations of the soil type, soil stiffness, resistance, liquefaction, and the bearing capacity for the foundation and estimated settlement. In the study, 15 boreholes were drilled and 7 SPTs were performed for each borehole to collect SPT samples. The drilling points of the study area are given in Figure 2. The standard penetration tests were carried out in the boreholes by ASTM D 1586 [6]. During the test, a hammer weighing 63.5 kg was dropped from 760 mm to achieve a free fall and the plunge of the SPT tube to 450 mm. The number of blows for the penetration of the SPT tube to the last 300 mm was recorded as N_{30}. Energy corrections were performed on the blow counts and the results were used in the comparisons. Among the samples collected during the SPT, the numbers of SPT blows (SPT-N) values obtained in the first 12 m were used. Each borehole had a diameter of 150 mm and the SPT-N values were measured for every 3 m. Figure 3 shows the histogram plot and distribution of the SPT-N_{60} values by depth. Sieve analysis according to ASTM D-422 and consistency limit tests according to ASTM D4318-17e1 were performed on disturbed samples taken from SPT [7, 8]. Table 1 shows the gravel and fine material contents and consistency values of the SPT samples and soil classification made according to USCS standard is given in Table 2 [9].

Figure 2. Study area drilling points

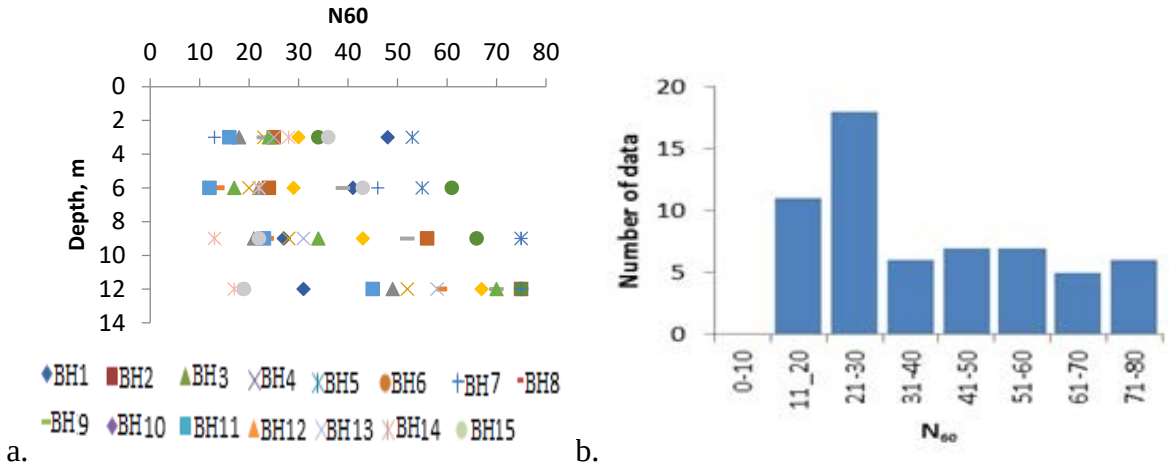

Figure 3. (a)SPT-N_{60} values for depths (BH: Bore Hole) (b) The histogram plot of the SPT-N_{60} values

2.1.2. PMT

The pressuremeter test was developed by Louis Menard and is frequently used in geotechnical projects to analyze soil properties. It is among the field tests used in the measurement of the characteristics of the lateral deformation of the test soil at a certain depth [10]. Compared with the SPT, the PMT is relatively costly and thus, is sometimes not preferred in small-scale or regular geotechnical applications [10]. Using the correlations established with the data obtained from the test, bearing capacity, internal friction angle, undrained shear stress, lateral stresses, elasticity module, and settlement can be calculated [11]. The PMT requires expertise and the SPT is a relatively more practical and easy test. Hence, correlations were also made between SPT results and the results from other field tests [12].

Table 1. Some Physical Properties of the SPT Samples

(BH: Bore Hole, NP: Non-plastic, LL: Liquid Limit, PI: Plasticity Index)

Depth (m)	Gravel (%)	Fine (%)	LL	PI	Depth (m)	Gravel (%)	Fine (%)	LL	PI	Depth (m)	Gravel (%)	Fine (%)	LL	PI
BH: 1					BH: 2					BH: 3				
3	0	23.32	47.1	19.95	3	1.43	20.82	36.38	16.14	3	23.29	5.56	50.12	29.57
6	0	15.75	50.03	21.23	6	8.26	5.82	31.61	14.05	6	25.91	9.64	39.22	18.83
9	6.09	15.44	43.5	67.38	9	12.35	7.70	39.61	18.04	9	30.28	33.48	18.87	7.24
12	13.83	21.28	35.25	14.70	12	29.63	7.56	30.75	9.15	12	47.49	4.06	22.24	7.30
BH: 4					BH: 5					BH: 6				
3	37.93	4.71	NP	NP	3	2.46	26.27	41.19	17.91	3	4.80	40.77	41.55	16.33
6	10.02	14.56	23.42	8.56	6	6.26	16.26	26.63	6.62	6	10.23	25.89	45.73	19.21
9	14.04	14.41	46.84	17.15	9	3.27	28.05	NP	NP	9	7.26	19.91	50.26	20.01
12	23.98	6.40	69.95	34.43	12	0.28	39.85	NP	NP	12	8.67	32.62	56.97	21.30
BH: 7					BH: 8					BH: 9				
3	22.79	15.78	41.10	17.52	3	0.80	34.61	41.58	17.60	3	11.91	15.75	40.85	23.08
6	26.44	17.27	NP	NP	6	15.16	31.27	37.75	14.01	6	15.63	17.31	28.71	13.35
9	18.55	14.51	15.72	6.14	9	16.33	19.74	53.68	21.65	9	21.65	15.91	32.42	10.69
12	18.93	8.69	38.67	16.79	12	4.38	24.01	70.96	29.69	12	28.71	9.90	42.05	16.16
BH: 10					BH: 11					BH: 12				
3	7.06	59.38	49.92	26.24	3	12.96	30.66	39.08	19.81	3	11.10	9.81	62.26	32.69
6	7.06	60.84	47.60	23.52	6	14.03	35.42	NP	NP	6	4.36	31.39	79.53	47.15
9	14.81	40.84	39.96	18.07	9	0	10.92	NP	NP	9	13.72	39.35	57.35	33.86
12	14.91	23.49	52.75	24.23	12	9.91	25.51	74.73	36.90	12	21.23	33.14	35.92	16.54
BH: 13					BH: 14					BH: 15				
3	2.14	58.82	48.65	24.04	3	4.79	45.90	61.07	34.34	3	26.80	52.62	47.96	26.91
6	0.07	62.42	50.41	25.95	6	4.82	38.13	66.97	37.95	6	0.78	44.71	46.57	26.09
9	20.25	38.14	44.54	24.22	9	0.14	57.64	57.46	31.39	9	1.21	30.65	NP	NP
12	38.80	12.14	NP	NP	12	0.21	73.97	NP	NP	12	0.55	28.13	33.85	13.22

Table 2. Soil classification according to depth

BH: 1		BH: 2		BH: 3		BH: 4		BH: 5		BH:6		BH:7	
Depth	USCS	Depth	USCS	Depth	USCS	Depth	USCS	Depth	USCS	Depth	USCS	Depth	USCS
3	SC	3	SC	3	SP-SC	3	GW	3	SC	3	SC	3	SC
6	SC	6	SP-SC	6	SP	6	SP-SM	6	SC	6	SM	6	SC
9	SM	9	SP-SC	9	SC	9	SM	9	SM	9	SC	9	SW-SC
12	SC	12	SP-SC	12	GW	12	SP-SM	12	SM	12	SM	12	SP-SC
BH: 8		BH: 9		BH: 10		BH: 11		BH: 12		BH:13		BH:14	
Depth	USCS	Depth	USCS	Depth	USCS	Depth	USCS	Depth	USCS	Depth	USCS	Depth	USCS
3	SC	3	SC	3	CH	3	SC	3	SC	3	CH	3	CH
6	SM	6	SW-SC	6	SC	6	SC	6	SC	6	CL	6	SC
9	SC	9	SC	9	CL	9	SC	9	SC	9	CH	9	SC
12	SM	12	SP-SM	12	SP-SC	12	SP-SM	12	SC	12	SC	12	CL
BH:15		GC: Clayey gravel, GW: Well-graded gravel, SC: Clayey sand, SM: Silty sand, SP: Poorly graded sand, CL: Clay of low plasticity, CH: Clay of high plasticity, SP-SC: Poorly graded sand and clayey sand, SP-SM: Poorly graded sand and Silty sand, SW-SC: well-graded sand and clayey sand											
3	GC												
6	CL												
9	SP												
12	SC												

In their study published in 2016, Naseem et al. developed a correlation between SPT-$N_{1,60}$ (Energy-corrected N-value normalized to effective overburden stress of one atmosphere) and P_L and E_m. In the tests predominantly carried out in sandy soils, the SPT-$N_{1,60}$ blow counts were between 6 and 23. Eq. (1) and (2) give the correlations derived by the researchers. The R^2 values were determined to be 0.857 and 0.8504, respectively [11].

$$P_L = 15.214.N_{1,60} + 89.276 \quad (1)$$

$$E_m = 165.88.N_{1,60} + 1364.1 \quad (2)$$

In 1990, in their study investigating sandy and clay soils, Kulhawy and Mayne correlated SPT blow count with E_m and carried out a PMT for the parameters used in foundation design [13].

Another correlation between the SPT and PMT was developed by Bozbey and Toğrol. In their study carried out in Istanbul in 2010, Bozbey and Toğrol performed the SPT and PMT for sandy and clay soils and found a linear relationship between the SPT-N_{60}, E_m, and P_L values concerning the soil type [10, 14]. The researchers determined that, in sandy soils, there was a correlation between the results of the SPT-N_{60} and PMT, which is as follows Eq. (3) [14]:

$$E_m = 1.33.(N_{60})^{0,77} \quad (r^2=0.2) \quad (3)$$

Again, in 2008, in their study on sandy, silty, and clay soils, Yağız et al. derived the following Eq. (4) [15]:

$$E_m = 388N_{60} + 4554 \quad (r^2=0.91) \quad (4)$$

In this study, 6 PMTs were carried out for each of the 15 boreholes with depths of 20 m. The test was carried out following the ASTM D 4719. SPT and PMT tests were made by "Garanti Temel Teknik Sondaj- Elazığ" company [16]. The PMT results for the depths between 0 m and 12 m were used in the tests. To compare the data obtained from the SPT with the data obtained from the PMT, the mean 3m-deep SPT blow counts were used. Figure 4 shows the histograms and the PMT results for depth.

2.1.3. MASW

The MASW method is one of the most common methods used in determining the shallow seismic velocity of soil [17]. The V_s value obtained with the MASW test is the fundamental parameter needed to identify the dynamic properties of soils [18]. It is conveniently used in the evaluation of certain parameters such as soil stiffness, liquefaction potential, soil density, soil classification, and foundation settlement [18].

The main goal of the MASW method is to obtain the dispersion of Rayleigh waves in which phase velocity is dependent on the frequency and convert it into S-wave velocity and layer depth using the inversion technique [17].

However, determining the V_s wave velocity in all field applications is not always cost-friendly. Establishing a correlation between the V_s and SPT blow counts reduces the cost of the field study. In 2014, Tumwesige et al. carried out a correlation study between V_s and SPT-N blow counts. The researchers collected 273 data measurements for the V_s and SPT-N at the same depth and showed that the relationship between the two parameters depended on the effective strain and ignoring this strain created a bias in the model [19]. In 2007, Anbazhagan et al. developed a correlation between the corrected SPT-N and V_s values and the results of the 38 MASW tests carried out at a fairly close location to the drilling points [20].

Furthermore, in the USA, similar studies investigating the correlation between V_s and N_{30} showed that corrected SPT-N values yielded better correlations compared with the uncorrected SPT-N values [21]. In Japan, a great number of researchers developed correlations between the SPT-N and V_s values by taking the geological age and soil type into account. Among these studies, some used corrected SPT-N values, while others used uncorrected SPT-N values.

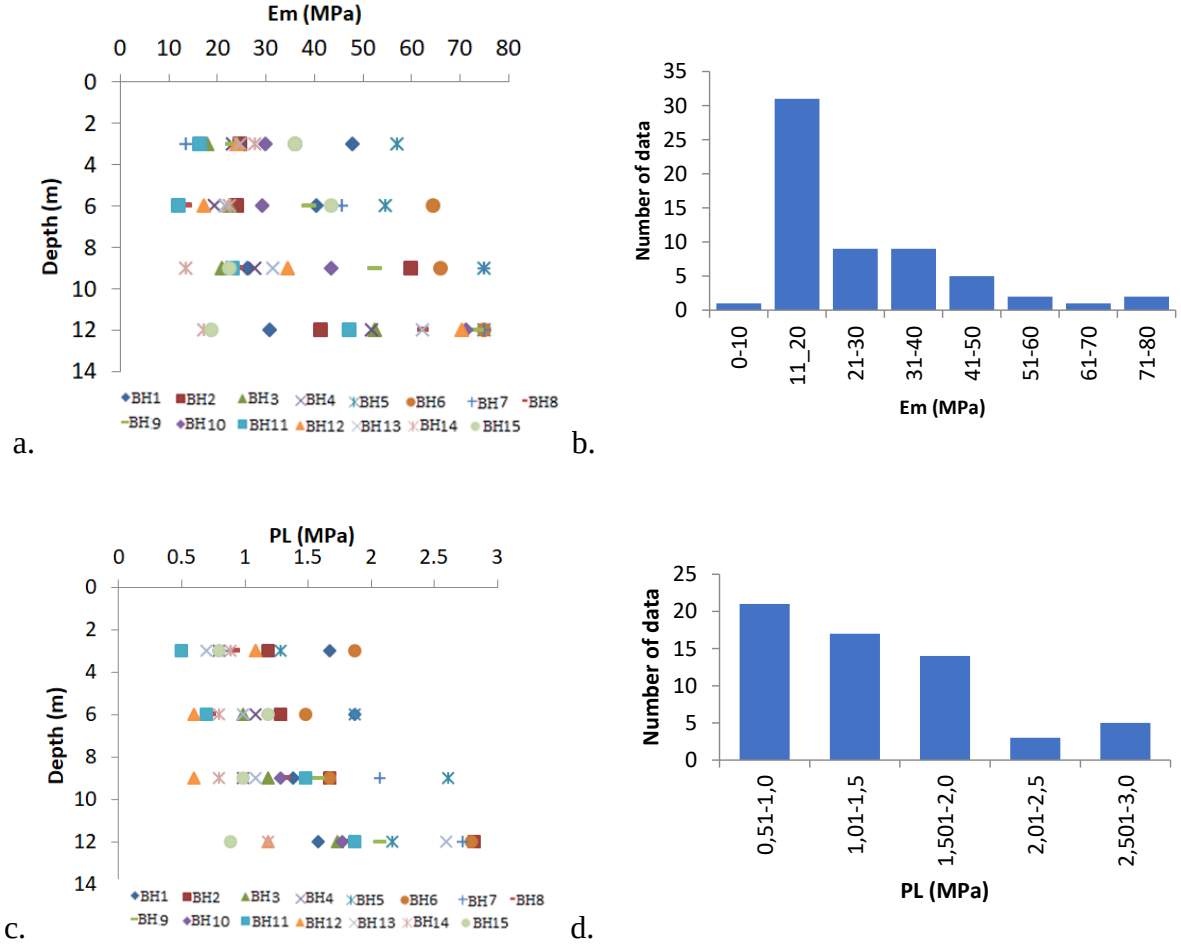

Figure 4. (a) E_m values (b) Histogram of E_m (c) P_L values (d) Histogram of P_L

In this study, MASW measurements were performed at 32 locations and the measurements from the 15 closest locations to the drilling points were used for comparison purposes. Furthermore, the same as the case for the SPT and PMT values, the values obtained at the first 12m were used for the comparisons. In the MASW test, a 12 channeled "Geometrics-Smartseis SE" model seismograph was used along with the use of an 8kg sledgehammer and a 30cmx30cm plate as the seismic energy sources. Geophone spacing is taken as 2m, minimum offset 4m and maximum offset 48m. MASW measurements were made by "Yerfiziği-Burhanettin TÜZÜN" company. Figure 5 shows the measurement results for MASW.

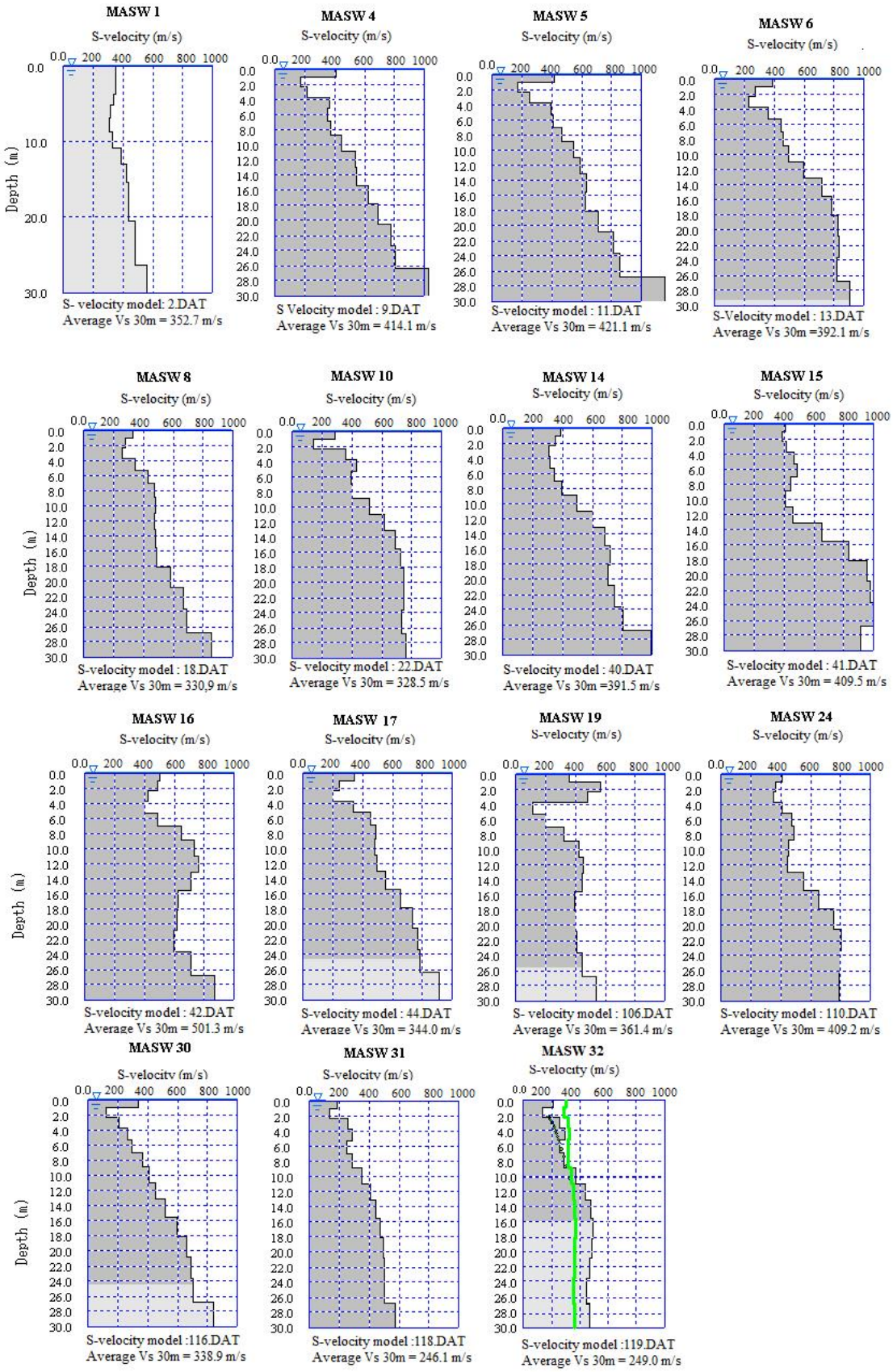

Figure 5. MASW measurement results

Table 3 shows a summation of the correlations between SPT and V_s found in the relevant literature. N_{30} was used in most of these correlations, while energy corrections (SPT-N_{60}) were made in some of the studies [18].

Table 3. Summary of the Empirical Correlations Based on SPT-N vs V_s [18]

Researcher(s)	V_s= (m/s. for all soils)	Researcher(s)	V_s= (m/s. for all soils)
Kanai (1966)	$19N^{0.6}$	Imai and Tonouchi (1982)	$97N^{0.314}$
Ohba and Toriumi (1970)	$84N^{0.31}$	Dikmen (2009)	$58N^{0.39}$
Imai and Yosimura (1970)	$92N^{0.329}$	Iyisan (1996)	$51.5N^{0.516}$
Fujiwara (1972)	$92.1N^{0.337}$	Kiku et al. (2001)	$68.3N^{0.292}$
Ohsaki and Iwasaki (1973)	$82N^{0.39}$	Hasançebi and Ulusay (2007)	$90N^{0.309}$
Imai and Yoshimura (1975)	$92N^{0.329}$	Uma et al. (2010)	$95.64N^{0.301}$
Imai (1977)	$91N^{0.337}$	Athanasopoulos (1995)	$107.6N^{0.36}$
Ohta and Goto (1978)	$85.35N^{0.348}$	Hanumantharao and Ramana (2008)	$82.6N^{0.43}$
Seed and Idriss (1981)	$61N^{0.50}$	Jafari et al. (1997)	$22N^{0.85}$

2.2. Correlations

2.2.1. The correlation between the PMT and SPT values

After the energy corrections to the SPT-N values obtained with the field tests, the results were compared with the E_m and P_L values obtained from the PMT results. The R^2 values for the correlations were 0.595 and 0.6847, respectively (Figure 6).

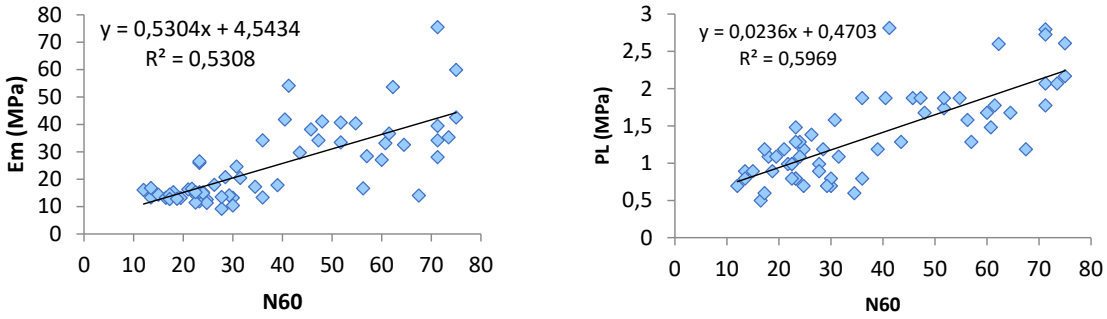

a. b.

Figure 6. Correlation between (a) SPT-N_{60}-Em, (b) SPT-N_{60}- P_L

2.2.2. The correlation between the SPT and MASW values

The SPT-N_{60} values were used in the comparisons with the MASW results and the R^2 value for the derived correlations was 0.5719 (Figure 7).

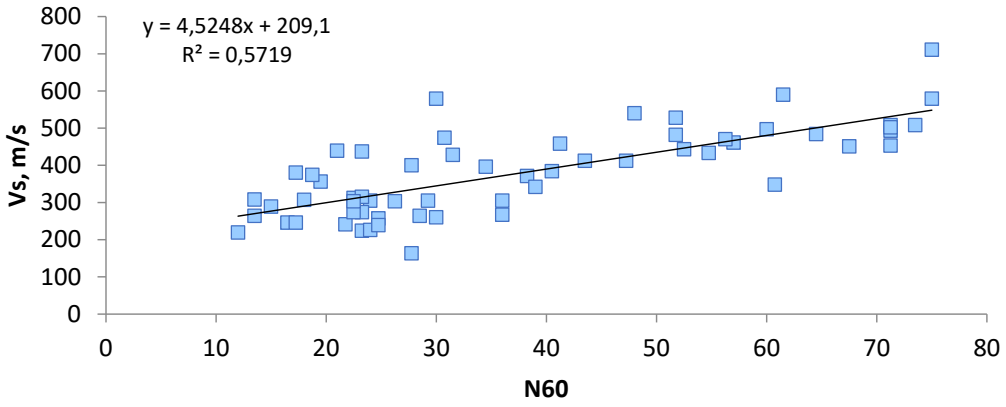

Figure 7. Correlation between SPT-N_{60}-V_s values

The results obtained from the tests were compared with the results found in the relevant literature and are given in Figure 8. In the study area, silty sand and clayey sand units are observed intensively. These units are concentrated in areas where the relationship is reduced relationship of the parts is also increased gravel unit. As the ratio of gravel increases, the soil becomes heterogeneous and the relationship becomes weak. When Figure 8 is examined; The measured values were found to be heavily compatible with Ohsaki and Iwasaki (1973) and Iyisan (1996). It is believed that the stiffening and gravel ratio in the remaining spots are effective.

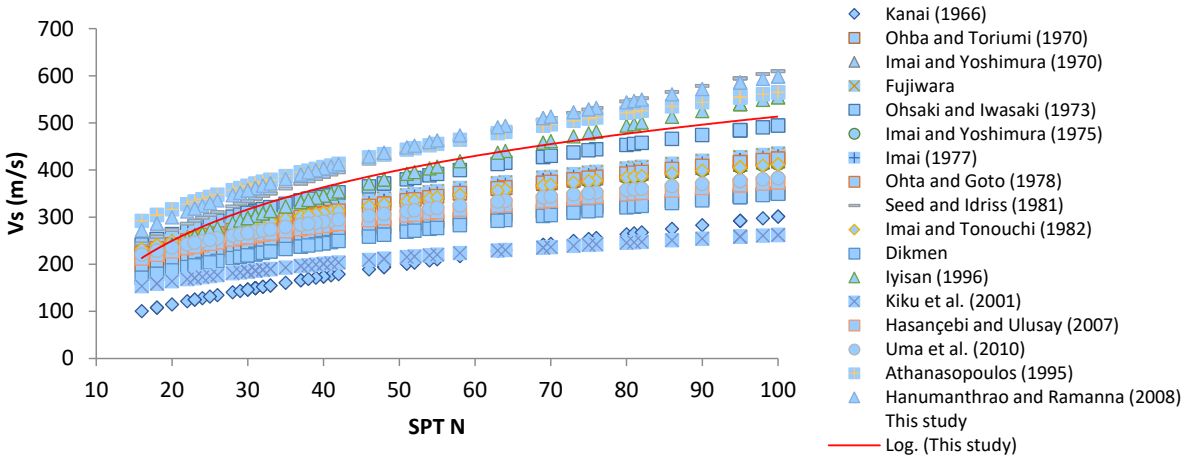

Figure 8. The comparison of the MASW and SPT results with the data found in the literature

2.2.3. The correlation between the PMT and MASW values

Figure 9 shows the correlations between the E_m and P_L values obtained with the PMT and the V_s values obtained with the MASW. The R^2 values were 0.3906 and 0.4524, respectively.

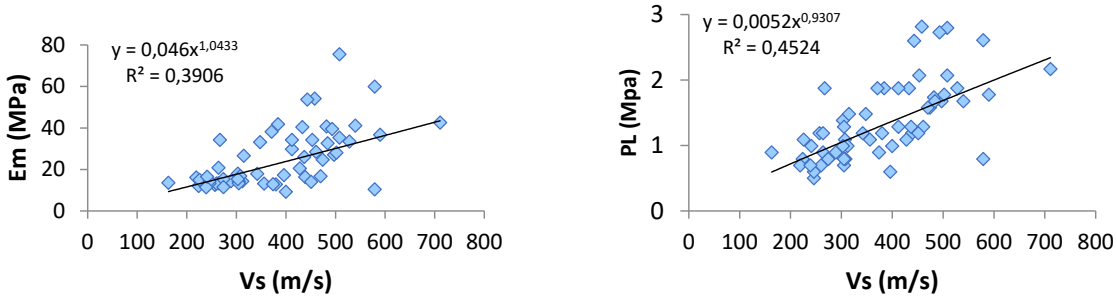

a. b.

Figure 9. Correlation between (a) V_s-E_m, (b) V_s- P_L

3. RESULTS AND DISCUSSION

The study investigates the relationship between the results obtained from the SPT, PMT, and MASW tests using simple regression analysis. A correlation study was carried out between the results obtained from the SPT and PMT tests performed for the 15 boreholes at certain intervals and the results obtained from the MASW test performed for the closest locations to the boreholes.

a. The study area is made up of the flood deposits from the Euphrates River. In light of the geophysical studies carried out across the field, the thickness of the unit was determined to be 70m. The unit has a complex structure that densely contains a silty sandy unit and in which large gravel blocks and clay bands are frequently encountered at different depths. According to the MASW test results, across the field, the north and northeast regions densely contained a silty clay unit, while, in the west and northwest regions, the silty clay units are accompanied by gravel (Figure 10).

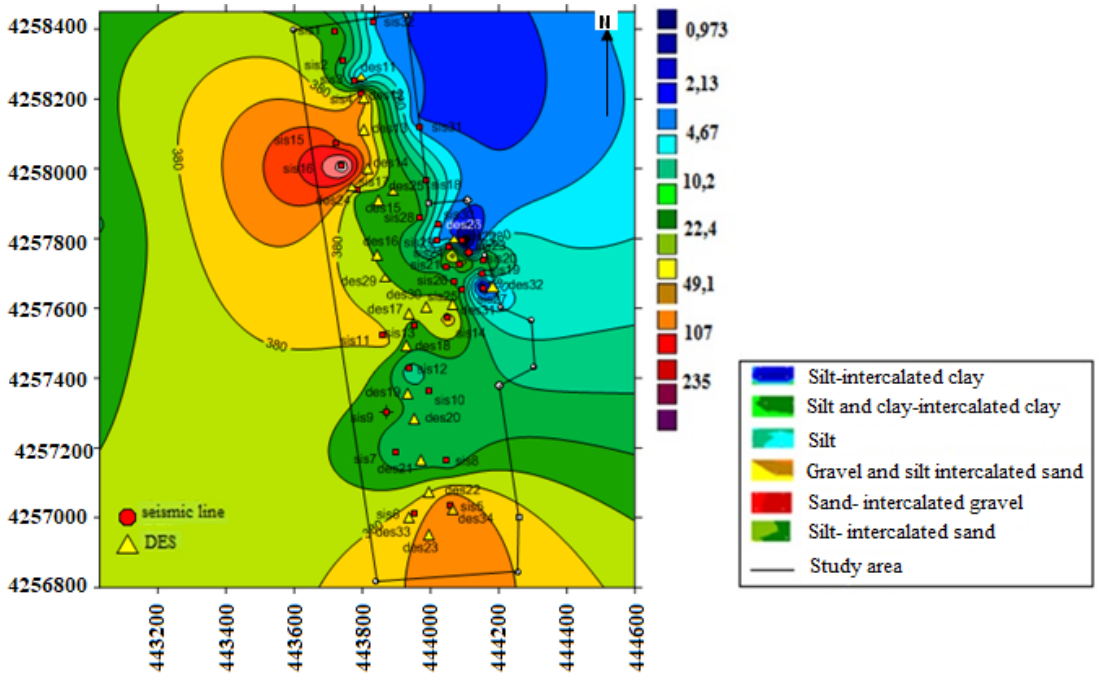

Figure 10. The lithological distribution of the study area according to the MASW test results

b. The correlations obtained in the study are given below. According to the table, the strongest correlation was determined between the P_L and SPT-N_{60} values, while the weakest correlation was determined between the E_m and V_s values (Table 4). as shown in Table 4, the highest relationship is between PMT and SPT. The fact that these tests were conducted in-situ in the same borehole may have increased the relationship. As seen in Table 2 and Figure 10, the study area is a very heterogeneous region. it is believed that R^2 values are therefore low. Other studies in the literature have mostly been done in homogeneous areas. These studies were mostly conducted in areas where sand or silt was dense. It is believed that R^2 values in the literature are therefore high.

Table 4. Correlation between the tests

Relation	E_m-V_s	P_L-V_s	SPT-N_{60} - V_s	E_m - SPT-N_{60}	P_L - SPT-N_{60}
R^2	0.3906	0.4524	0.5719	0.5950	0.6847

c. N_{30}, E_m, P_L, and V_s values increased depending on the depths. An increase in soil stiffness depending on depth can be cited as the reason for this.

d. The comparison of the V_s and SPT-N_{60} measured in the study area with the curves obtained in previous studies showed that they remained approximately in the same region (Figure 8). In the study area, silty sand and clayey sand units are observed intensively. These units are concentrated in areas where the relationship is reduced relationship of the parts is also increased gravel unit. As seen in Figure 8, this is thought to be the reason why the test results remain in the same area as previous studies.

4. CONCLUSIONS

This study emphasizes that homogeneity and tightness are effective in correlation studies. Studies in the literature were mostly conducted in homogeneous areas. Therefore, R^2 values are high. But because the heterogeneity of alluvial deposits is higher, the relationships established in these soils have also been weak. in studies conducted in heterogeneous areas, it is recommended that the relationship between these tests be evaluated in detail by other researchers.

Acknowledgments

We would like to thank the Inonu University Scientific Research Project Department, who financially supported this study with Project No. 2013/61.

REFERENCES

[1] Anbazhagan, P., Kumar, A. and Sitharam, T.G. (2013). Seismic site classification and correlation between standard penetration test *N* value and shear wave velocity for Lucknow City in Indo-Gangetic Basin. *Pure and Applied Geophysics* 170: 299-318.

[2] Samui, P. and Sitharam, T. (2010). Correlation between SPT, CPT and MASW. *Int J Geotechnical Eng* 4(2):279-288.

[3] Kirar, B, Maheshwari, B.K. and Muley, P. (2016). Correlation between shear wave velocity (*Vs*) and *SPT* resistance (*N*) for Roorkee Region. *Int J Geosynthetics and Ground Eng* 2(9):1-11.

[4] Onal, M. (1995). Miocene stratigraphy and lignite potential of the northern part of the Malatya graben basin Eastern Anatolia- Turkey. *International Earth Science Colloquium on the Aegean Region Proceedings, İzmir* 11:607-621.

[5]https://earth.google.com/web/@38.45696612,38.37107435,731.29476775a,8724.63210368d,35y,1.84813536h,0t,0r

[6] ASTM D1586 / D1586M-18, Standard Test Method for Standard Penetration Test (SPT) and Split-Barrel Sampling of Soils, ASTM International, West Conshohocken, PA, 2018, www.astm.org

[7] ASTM D 422-63, 2003. Standard Test Method for Particle-Size Analysis of Soils, In Annual Book of ASTM Standards, Volume 04.08, Philadelphia, PA, pp. 93-99.

[8] ASTM D4318-17e1. Standard Test Methods for Liquid Limit, Plastic Limit, and Plasticity Index of Soils; ASTM International: West Conshohocken, PA, USA, 2017.

[9] ASTM D2487-17e1. Standard Practice for Classification of Soils for Engineering Purposes (Unified Soil Classification System); ASTM International: West Conshohocken, PA, USA, 2017.

[10] Cheshomi, A. and Ghodrati, M. (2014). Estimating Mernard pressuremeter modules and limit pressure from SPT in silty sand and silty clay soils. A case study in Mashhad, Iran. *Geomechanics and Geoengineering* 10(3):194-202.

[11] Naseem, A. and Jamil, S.M. (2016). Development of correlation between standard penetration test and pressuremeter test for clayey sand and sandy soil. *Soil and Foundation Eng* 53(2): 98-102.

[12] Anwar, M.B. (2016). Correlation between *PMT* and *SPT* results for calcareous soil. *Housing and Building National Research Center* 14(1): 50-55.

[13] Kulhawy, F.H. and Mayne, P.W. (1990). Manual on estimating soil properties for foundation design. *Electric Power Research Institution Rep-EL-6800 Final report, August*, Project 1493-6.

[14] Bozbey, I. and Togrol, E. (2010). Correlation of standard penetration test and pressuremeter data a case study from Estunbol, Turkey. *Bulletin of Eng Geology and the Env* 69: 505-515.

[15] Yagiz, S., Akyol, E. and Sen, G..(2008). Relationship between the standard penetration test and the pressuremeter test on sandy silty clays: a case study from Denizli. *Bulletin of Eng Geology and the Env* 67(3): 405-410.

[16] ASTM D4719, Standard test method for pre-bored Pressuremeter Testing in soils ASTM International, West Conshohocken, 2000.

[17] Park, C.B., Miller, R.D. and Xia, J. (1999). Multichannel analysis of surface waves. *Presented at the 66th Annual Meeting, Society of Exploration Geophysicists* 64(3): 800-808.

[18] Akin MK, Kramer SL and Topal T (2011) Empirical correlations of shear wave velocity (*Vs*) and penetration resistance (SPT-N) for different soils in an earthquake-prone area (Erbaa-Turkey). *Eng Geology* 119: 1–17.

[19] Tumwesige, R., Gidudu, A., Bagampadde, U. and Ryan, C. (2014). An investigation of the relationship between standard penetration test and shear wave velocity for unsaturated soils (A case study of the earthquake prone area of The Albertıne Graben). *Second Conference on Earthquake Engineering and Seismology Istanbul*, Turkey pp 25-29.

[20] Sitharam, T.G. and Anbazhagan, P. (2007). Seismic hazard analysis for the Bangalore Region. *Natural Hazards* 40: 261–278.

[21] Mhaske, S.Y. and Choudhury, D. (2011). Geospatial contour mapping of shear wave velocity for Mumbai City, *Natural Hazards* 59: 317–327.

NATURENGS
MTU Journal of Engineering and Natural Sciences
https://dergipark.org.tr/tr/pub/naturengs
DOI: 10.46572/nat.2020.16

Investigation of Obesity Tendency of University Students with Bioelectric Impedance Body Analyzer

Aziz AKSOY[1*], Halime SELEN[2], Seda OĞUR[3]

[1] Department of Bioengineering, Faculty of Engineering and Natural Sciences, Malatya Turgut Özal University, Malatya, Turkey.

[2] Department of Nutrition and Dietetic, Faculty of Health Science, Ağrı İbrahim Çeçen University, Ağrı, Turkey.

[3]Department of Nutrition and Dietetic, Health Highschool, Bitlis Eren University, Bitlis, Turkey.

(**Received:** 06.12.2020; **Accepted:** 22.12.2020)

ABSTRACT: In this study, it was aimed to investigate the obesity tendency of the students of Bitlis Eren University with a Bioelectrical Impedance Body Analyzer. A total of 400 students volunteered comprised of 200 males and 200 females were enrolled in the study. According to Body Mass Index (BMI) values were found that 19.5% of the female l students were Underweight, 68.5% of them were normal weight, 11.0% of them were overweight and 1.0% of them were obese, 4.5% of the boy students were weak, 71.0% of them were normal weight, 22.0% of them were overweight and 2.5% of them were obese. The result of body fat ratio was indicated that while 48.0% of the female students were in the obese category, 40.0% of them were determined in the obesity tendency risk group, 56.0% of the boy students were in the obesity tendency risk group and 26.0% of them were obese. According to the waist/hip ratio were revealed that 95.5% of the girl students were in the obesity tendency group and 4.0% of them were obese, 85.5% of the boy students were in the obesity tendency group and 4.0% of them were obese. A significant difference was found between age and gender, fat ratio, waist/hip ratio, and BMI values ($p < 0.05$). University students participating in the study were evaluated. The overweight (Pre-obese) rate was found to be high in students (Female: 11%; Male: 22%).

Keywords: Obesity, Obesity tendency, Body mass index, Body fat ratio, Waist/hip ratio.

1. INTRODUCTION

Overweight and obesity are defined as abnormal or excessive fat accumulation that may impair health [1, 2]. Although the causes of obesity, which the World Health Organization (WHO) regards as an important public health problem, are not yet fully known, it is thought to be a complicated health problem caused by environmental and genetic factors [3]. It is known that obesity triggers cardiovascular diseases, causes degenerative effects on muscles, bones, and joints, and causes diseases such as dyslipidemia, hypertension, diabetes, arthritis, osteomalacia, osteoporosis, depression, and cancer [4-10]. The increase in the tendency to consume fast-food due to today's technology and especially the fact that the time spent actively is shortening invites obesity [11].

*Corresponding Author: aksoy_aziz@hotmail.com
ORCID number of authors: [1] 0000-0002-9683-6691, [2] 0000-0002-3705-0875, [3] 0000-0002-2041-0790

1.1. Body Mass Index (BMI)

The most common criterion that is utilized for obesity is Body Mass Index (BMI), which is accepted by the World Health Organization and can be used as a criterion for all individuals without the gender difference [12]. BMI is calculated by dividing body weight in kg by the square of height in meters (kg/m²) [13].

Table 1. BMI Classification in Adults

Classification	**BMI (kg/m²)**
Underweight	<18.5
Normal range	18.5–24.9
Overweight (Pre-obese)	25.0–29.9
1st degree obese	30.0–34.9
2nd degree obese	35.0–39.9
3rd degree obese	≥40

1.2.Waist/Hip Ratio

The waist/hip ratio is expected to be below 0.80 for females and below 0.95 for males [14]. According to WHO should the waist/hip ratio surpass 0.85 in women and 1.0 in men, it is considered as android type obesity [15].

1.3. Body Fat Ratio

The body fat ratio is between 18-24% in adult males and between 25-31% in adult females. This ratio surpassing 25% in men and 32% in women constitutes obesity [16].

1.4. Body Muscle Weight and Total Body Water

The muscle weight of the body is not a criterion for defining obesity. Although a high body muscle weight increases BMI, especially in athletes, it cannot be asserted that it demonstrates a tendency to obesity. WHO reports that obesity stems from the accumulation of excess adipose tissue and that this excess fat prompts diseases [16]. On the other hand, excessive body muscle weight provides flexibility, endurance, and dynamism to the body instead of causing diseases. And due to the water retention feature of creatine stores in muscle tissue [17], an increase in total body water is also observed in parallel with the increase in the body muscle.

1.5. Basal Metabolic Rate (BMR)

BMR, which is the energy needed for the circulation, respiration, and the continuation of body temperature while the individual is in the full resting state, may vary according to the factors such as body weight, the ratio of muscle and fat in body components, race, age, and genetics [18]. It decreases calorie expenditure via shortening the duration of physical activity of the individual and accordingly causes obesity by decreasing the basal metabolic rate [19].

2. MATERIAL AND METHODS

To this study; A total of 400 volunteer students, 200 female and 200 male, who studied at Bitlis Eren University between February and May 2015, were included in the study. Participants were informed about the measurement at least one day prior, and the measurement devices were introduced to them. The measurements were made at 09:30 in the morning while the students were hungry. The height measurements of the students were performed via a digital-display Ultrasonic Harpenden Stadiometer (ADE / Hamburg MZ10020) device with a precision degree of 0.1 cm, and no accessories or items that would affect the measurement were allowed [20]. Measurements were performed in the Inbody230 (MW160) Bioelectrical Impedance Body Analyzer [21] through the entrance of height, gender, and age values, and the measurements were made while the students were in a state of complete rest, while they were wearing nothing other than shorts, and at least 12 hours after the students ate the meal. As a result of the conducted measurement, BMI, body fat ratio, waist/hip ratio, body muscle weight, total body water, and basal metabolic rate values were determined.
The data obtained were analyzed through the utilization of IBM SPSS Statistics 20 package program, and Pearson chi-square test was performed to put forth whether the observed values were compatible with expected values, and the Spearman rank correlation coefficient test was utilized to determine the direction of the relationship between variables. Statistical significance level was accepted as $p < 0.05$ for the evaluation of the results.

3. RESULTS AND DISCUSSION

The number of female and male students participating in the study has been kept equal; A total of 400 (200F + 200M) volunteers, consisting of healthy students whose ages, diets are close to each other, participated in the study. The age range of the students is 18-25, and the mean age is 21.0 ± 1.65. In the study in which 400 students participated in total, 2.5% of the students (10 people) were 18 years old, 16.0% (64 people) of them were 19 years old, 25.5% (102 people) of them were 20 years old, 23.0% (92 people) of them were 21 years old 14.0% (56 people) of them were 22 years old, 9.75% (39 people) of them were 23 years old, 5.5% (22 people) of them were 24 years old, and 3.75% (15 people) of them were 25 years old.
Considering the distribution of BMI values of the students who participated in the study, of the female students, 19.5% (39 people) of them were underweight 68.5% (137 people) of them were normal, 11% (22 people) of them were slightly obese, 1% of them were obese; and of the male students, 4.5% (9 people) of them were thin, 71% (142 people) of them were normal, 22% (44 people) of them were slightly obese, and 2.5% (5 people) of them were obese. There was a significant difference ($p < 0.05$) between the gender of the students participating in the study and their value of BMI, and the correlation (r: 0.246) between this difference was weak. Accordingly, it can be asserted that BMI values of female students participating in the study were more normal and lower than those of the male students (Table 2).

Table 2. Percentage distribution of Body Mass Index by gender

Parameters			**Gender**		**p**	**r**
			F	**M**		
BMI	<18.5	n	39	9	p<0.05	r: 0.246
		%	19.5	4.5		
	18.5-24.9	n	137	142		
		%	68.5	71.0		
	25.0-29.9	n	22	44		
		%	11.0	22.0		

There was a significant difference ($p<0.05$) between the gender of the students who participated in the study and their body fat ratio (r: 0.891), waist/hip ratio (r: 0.979), total body water (r: 0.823), muscle weight (r: 0.826), and BMR (r: 0.819), and the correlation between this difference was immensely strong. According to this, while the body fat ratio and waist/hip ratio of the female students who participated in the study was concentrated above normal values compared to the male students, male students' muscle weight, total body water, and BMR values were concentrated above normal values compared to female students (Table 3).

Table 3. Percentage distribution of body fat ratio, waist/hip ratio, total body water, muscle weight and BMR by gender

Parameters			**Below Normal Value**	**Normal Value**	**Above Normal Value**	**p**	**r**
Body Fat Ratio	F	n	24	80	98	p<0.05	r: 0.891
		%	6.0	20.0	24.5		
	M	n	36	112	50		
		%	9.0	28.0	12.5		
Waist/Hip Ratio	F	n	1	191	8	p<0.05	r: 0.979
		%	0.3	47.8	2.0		
	M	n	21	171	8		
		%	5.3	42.8	2.0		
Total Body Water	F	n	39	139	22	p<0.05	r: 0.823
		%	19.5	69.5	11.0		
	M	n	9	147	44		
		%	4.5	73.5	22.0		
Muscle Weight	F	n	71	126	3	p<0.05	r: 0.826
		%	35.5	63.0	1.5		
	M	n	23	146	31		
		%	11.5	73.0	15.5		
BMR	F	n	65	129	6	p<0.05	r: 0.819
		%	32.5	64.5	3.0		
	M	n	29	160	11		
		%	14.5	80.0	5.5		

There was a significant difference ($p<0.05$) between the age of the students who participated in the study and their BMI (r: 0.204), body fat ratio (r: 0.255), and waist/hip ratio (r: 0.248), and the correlation between this difference was weak. No significant difference ($p>0.05$) between age and muscle weight, total body water, and BMR was found. When female and male students are grouped by age, it can be said that although BMI, body fat ratio, and waist/hip ratios are greater in the group of older students, they demonstrate similar distributions because the age groups are very close to each other and that they are associated with a weak correlation (Table 4).

According to the data gathered from the study, it can be interpreted by only looking at BMI values that overweight (pre-obese) rate was found to be high in students (Female: 11%; Male: 22%) (Table 2). In a similar study, it was reported that male students have higher BMI values than female students [22]. However, in different studies, it was found that adipose tissue was more in females than in males; more than average and muscle mass was significantly higher in boys than girls [23, 24]. Although BMI is a simple criterion used in the definition of obesity, it is not an adequate criterion [25].

Table 4. Change in BMI, body fat ratio and waist/hip ratio by age

Parameters / Clasification				Age								p	r
				18	19	20	21	22	23	24	25		
	BMI	<18.5	n	2	10	16	9	6	2	3	0	p<0.05	r: 0.204
			%	20.0	15.6	15.7	9.8	10.7	5.1	13.6	0.0		
		18.5-24.9	n	7	50	72	64	37	28	13	8		
			%	70.0	78.1	70.6	69.6	66.1	71.8	59.1	53.3		
		25.0-29.9	n	1	4	12	18	12	6	6	7		
			%	10.0	6.2	11.8	19.6	21.4	15.4	27.3	46.7		
		30-34.9	n	0	0	2	1	1	3	0	0		
			%	0.0	0.0	2.0	1.1	1.8	7.7	0.0	0.0		
Body Fat Ratio	Female Students	<%25	n	2	4	8	6	2	1	1	0	p<0.05	r: 0.255
			%	20.0	6.2	7.8	6.5	3.6	2.6	4.5	0.0		
		%25-31	n	4	19	22	15	11	7	2	0		
			%	40.0	29.7	21.6	16.3	19.6	17.9	9.1	0.0		
		≥%32	n	1	14	31	28	11	9	3	1		
			%	10.0	21.9	30.4	30.4	19.6	23.1	13.6	6.7		
	Male Students	<%18	n	1	3	11	5	5	7	3	1		
			%	10.0	4.7	10.8	5.4	8.9	17.9	31.8	6.7		
		%18-24	n	1	20	21	28	21	7	7	7		
			%	10.0	31.2	20.6	30.4	37.5	17.9	31.8	46.7		
		≥%25	n	1	4	9	10	6	8	6	6		
			%	10.0	6.2	8.8	10.9	10.7	20.5	27.3	40.0		
Waist/Hip Ratio	Female Students	<0.75	n	0	0	1	0	0	0	0	0	p<0.05	r: 0.248
			%	0.0	0.0	1.0	0.0	0.0	0.0	0.0	0.0		
		0.75-0.85	n	7	36	60	44	23	14	6	1		
			%	70.0	56.2	58.8	47.8	41.1	35.9	27.3	6.7		
		>0.85	n	0	0	0	4	1	3	0	0		
			%	0.0	0.0	0.0	4.3	1.8	7.7	0.0	0.0		
	Male Students	<0.80	n	0	4	6	4	1	5	1	0		
			%	0.0	6.2	5.9	4.3	1.8	12.8	4.5	0.0		
		0.80-0.90	n	3	24	34	39	30	14	14	13		
			%	30.0	37.5	33.3	42.4	53.6	35.9	63.6	86.7		
		>0.90	n	0	0	1	1	1	3	1	1		
			%	0.0	0.0	1.0	1.1	1.8	7.7	4.4	6.7		

This study along with similar studies [26] shows that using only BMI in the definition of obesity will not be sufficient. It can be said that body analysis devices are also important in this context. Because, according to the body analysis of the students, it was revealed that the number of females with a higher body fat ratio than normal was higher in those of male students. It is seen that the high BMI values in male students come from muscle mass [22, 26].

Although there are several studies on the prevalence of obesity in Turkey, the most comprehensive studies show that levels of obesity are higher in the female population than the male population [27-31].

It should not be forgotten that obesity is a complicated health problem and body composition is affected by factors such as dietary habits, levels of physical activity and social environment. Also, it is known that the hydration status of individuals in measurements made with bioelectrical impedance analysis devices is also a factor that can affect the measurements [32,

33]. Body analysis is an important criterion for healthy weight loss in the treatment and prevention of obesity and obesity-related diseases [34].

The fact that the students are away from the family environment during their university years results in them facing difficulties in terms of nutrition and health. Studies on university students have shown that students face significant problems when it comes to these issues. Fast food products consumed fondly by university students also cause obesity [35]. Fast-food foods are high in saturated fat and very low in fiber and nutrient content.

Besides, reasons such as irregularity in the nutrition, skipping meals or overeating at meals, consumption of junk food instead of meal, and eating disorders [36] are also among the causes of obesity of university students who stay away from the family environment.

4. CONCLUSIONS

In conclusion, obesity emerges as the main cause of most diseases at every stage of life, which can manifest itself since childhood. In this research, it was shown that methods other than the calculation of BMI values such as Bioelectric Impedance Body Analyzer by determining waist/hip ratio, body fat ratio, total body water, muscle weight and BMR values, obesity tendencies of university students were demonstrated more comprehensively. In chronological studies done within the university students in Turkey noted an increased prevalence of obesity and the results of our study were observed to be similar. Considering that the causes of obesity are dietary habits, levels of physical activity and social environment and genetic, it is clear that more enlightening information will be obtained with detailed studies about the nutritional status of university students and obesity status. The university students gaining the habit of sufficient and balanced nutrition and being directed to regular physical activity will be effective in reducing the prevalence of obesity among university students.

Acknowledgments

Acknowledgment (optional) of collaboration or preparation assistance may be included. Please note the source of funding for the research. The authors declare that there are no conflicts of interest. All authors approved the final version of the paper.

REFERENCES

[1] World Health Organization (WHO). (2020). https://www.who.int/health-topics/obesity#tab=tab_1

[2] T.C. Sağlık Bakanlığı Halk Sağlığı Genel Müdürlüğü Sağlıklı Beslenme ve Hareketli Hayat Dairesi Başkanlığı. (2020). https://hsgm.saglik.gov.tr/tr/obezite/obezite-nedir.html

[3] Serter R. (2003). *Obezite Atlası.* Roche Yayınevi, Ankara.

[4] Vecchié, A., Dallegri, F., Carbone, F., Bonaventura, A., Liberale, L., Portincasa, P., Frühbeck, G. and Montecucco, F. (2018). Obesity phenotypes and their paradoxical association with cardiovascular diseases, *European Journal of Internal Medicine,* 48: 6-17.

[5] Buch, A., Carmeli, E., Boker, L.K., Marcus, Y., Shefer, G., Kis, O., Berner, Y. and Stern, N. (2016). Muscle function and fat content in relation to sarcopenia, obesity and frailty of old age-an overview, *Experimental Gerontology*, 76: 25-32.

[6] Kaya A. (2013). Obezite ve Hipertansiyon, *Turkish Journal Endocrinology and Metabolism*, 2: 13-21.

[7] Verma, S. and Hussain, M.E. (2017). Obesity and diabetes: an update, *Diabetes & Metabolic Syndrome: Clinical Research & Reviews*, 11(1): 73-79.

[8] George, M.D. and Baker, J.F. (2016). The obesity epidemic and consequences for rheumatoid arthritis care, *Current Rheumatol Reports*,18(1): 6.

[9] Güleç Öyekçin, D., Yıldız, D., Şahin, E.M. and Gür, S. (2011). Depression and anxiety in obese patients, *Turk Journal of Emergency Medicine*, 15: 121-124.

[10] Koçak, M. and Erem, C. (2013). Obezite ve Kanser, *Türkiye Klinikleri Endokrinoloji Özel Dergisi*, 6: 40-44.

[11] Aksoy, A and Selen, H. (2018). The evaluation of body composition and anthropometric measurements of males aged 18-25 years, based on the regularity of physical exercise. *Progress in Nutrition*, 20(3): 338-343.

[12] Booth, M.L., Hunter, C., Gore, C.J., Bauman, A. and Owen, N. (2000). The relationship between body mass index and waist circumference: implications for estimates of the population prevalence of overweight, *International Journal of Obesity*, 24(8): 1058-61.

[13] World Health Organization (WHO). (2020). http://www.euro.who.int/en/health-topics/disease-prevention/nutrition/a-healthy-lifestyle/body-mass-index-bmi

[14] Türkiye Beslenme Rehberi 2015 (TÜBER). (2016). T.C. Sağlık Bakanlığı, Yayın No: 1031.

[15] T.C. Sağlık Bakanlığı Halk Sağlığı Genel Müdürlüğü Sağlıklı Beslenme ve Hareketli Hayat Dairesi Başkanlığı (2020). https://hsgm.saglik.gov.tr/tr/obezite/obezite-nasil-saptanir.html

[16] Mahan, L.K. and Raymond, J.L. (2019). *Krause, Besin ve Beslenme Bakım Süreci*. 14. Baskı. Nobel Tıp Kitabevleri, Ankara.

[17] Maughan, R.J. (1995). Creatine supplementation and exercise performance, *International Journal of Sport Nutrition and Exercise Metabolism*, 5(2): 94-101.

[18] Can, S., Arslan, E., and Ersöz, G. (2014). Güncel bakış açısı ile fiziksel aktivite, *SPORMETRE Beden Eğitimi ve Spor Bilimleri Dergisi*, 12(1): 1-10.

[19] Balcıoğlu, İ. and Başer, S.Z. (2008). Obezitenin psikiyatrik yönü, *İ.Ü. Cerrahpaşa Tıp Fakültesi Sürekli Tıp Eğitimi Etkinlikleri Sempozyum Dizisi,* 62: 341-348.

[20] Karaolis-Danckert, N., Buyken, A.E., Bolzenius, K., Perim de Faria, C., Lentze, M.J. and Kroke, A. (2006). Rapid growth among term children whose birth weight was appropriate for gestational age has a longer lasting effect on body fat percentage than on body mass index, *The American Journal of Clinical Nutrition*, 84(6): 1449-1455.

[21] McLester, C.N, Nickerson, B.S., Kliszczewicz, B.M. and McLester, J.R. (2018). Reliability and agreement of various inbody body composition analyzers as compared to dual-energy x-ray absorptiometry in healthy men and women, *Journal of Clinical Densitometry: Assesment&Management of Musculoskeletal Health*, 23(3): 443-450.

[22] Murathan, F. (2013). *Üniversite öğrencilerinde obezite sıklığı, fiziksel aktivite düzeyi ve sağlıklı yaşam biçimi davranışlarının incelenmesi*. Doktora Tezi, T.C. Fırat Üniversitesi Sağlık Bilimleri Enstitüsü Beden Eğitimi ve Spor Anabilim Dalı, Elazığ.

[23] Ramirez, E., Valencia, M.E., Bourges, H., Espinosa, T., Moya-Camarena, S.Y., Salazar, G. and Alemán-Mateo, H. (2012). Body composition prediction equations based on deuterium oxide dilution method in Mexican children: A national study, *European Journal of Clinical Nutrition*, 66(10): 1099-1103.

[24] Komiya, S., Eto, C., Otoki, K., Teramoto, K., Shimizu, F. and Shimamoto, H. (2000). Gender differences in body fat of low- and high-body-mass children: Relationship with body mass index, *European Journal Applied Physiology*, 82(1-2): 16-23.

[25] Eker, E. and Melih, Ş. (2004). Birinci basamakta obeziteye yaklaşım, *Sürekli Tıp Eğitimi Dergisi*, 11(7): 246-249.

[26] Ergün, A. and Erten, S.F. (2004). Öğrencilerde vücut kitle indeksi ve bel çevresi değerlerinin incelenmesi, *Ankara Üniversitesi Tıp Fakültesi Mecmuası*, 57(2): 57-61.

[27] Onat, A., Can, G., Yüksel, H., Ademoğlu, E., Erginel Ünaltuna, N., Kaya, A. and Altay, S. (2017). *Genetic Risk Factors for Coronary Heart Diseases and Metabolic Syndrome*, In TEKHARF 2017, Leadership to the Approach of Medicine World to Chronic Diseases, İstanbul: Logos Yayınevi, pp.262-275.

[28] Hatemi, H., Turan, N., Arık, N. and Yumuk, V. (2002). Türkiye obezite ve hipertansiyon çalışması (TOHTA), *Endokrinolojide Yönelişler Dergisi,* 11(1): 1-16.

[29] Bağrıaçık, N., Onat, H., İlhan, B., Tarakçı, T., Oşar, Z., Ozyazar, M., Hatemi, H.H. and Yıldız, G. (2009). Obesity profile in Turkey, *International Journal of Diabetes Metabolism,* 17: 5-8.

[30] *Türkiye nüfus ve sağlık araştırması 2018* (2019). Hacettepe Üniversitesi Nüfus Etütleri Enstitüsü, Ankara, Yayın No: NEE-HÜ-19.01.

[31] Erel, C., Uğurlu, M., Aydınlı, F., Kesici, C., Çakır, B., Özoğlu, F. and Kaplan, Y. (2004). *Sağlıklı beslenelim kalbimizi koruyalım projesi araştırma raporu 2004*. T.C. Sağlık Bakanlığı Temel Sağlık Hizmetleri Genel Müdürlüğü Gıda Güvenliği Daire Başkanlığı Toplum Beslenmesi Şubesi.

[32] Gültekin, T., Dasgupta, P. and Koca, Ö.B. (2014). Segmental bioelectrical impedance analysis in children aged 7-18 years living in Ankara-Turkey: age and sex difference in the measures of adiposity, *Papers on Anthropology*, 23(2): 23-36.

[33] Mialich, M.S., Sicchieri, F.J.M. and Jordao Junior, A.A. (2014). Analysis of body composition: a critical review of the use of bioelectrical impedance analysis, *International Journal of Clinical Nutrition*, 2(1): 1-10.

[34] Çetin, İ., Muhtaroğlu, S., Yılmaz, B. and Kurtoğlu, S. (2015). Biyoelektrik impedans analiz metodu ile obez çocuklarda cinsiyete göre vücut bileşimlerinin segmental olarak değerlendirilmesi, *Dicle Tıp Dergisi*, 42(4): 449-454.

[35] Satman, İ. (2016). The Obesity Problem in Turkey, *Turkiye Klinikleri Gastroenterohepatology - Special Topics*, 9(2): 1-11.

[36] Oğur, S., Aksoy, A. and Selen, H. (2016). Üniversite öğrencilerinin yeme davranışı bozukluğuna yatkınlıkları: Bitlis Eren Üniversitesi örneği, *BEÜ Fen Bilimleri Dergisi,* 5(1): 14-26.

NATURENGS
MTU Journal of Engineering and Natural Sciences
https://dergipark.org.tr/tr/pub/naturengs
DOI: 10.46572/nat.2020.17

Determination of Consumer Preferences for Goose Meat Using Conjoint Analysis

Selim GÜNDÜZ*

Department of Business, Faculty of Business Administration, Adana Alparslan Turkes Science and Technology University, Adana, Turkey.

(**Received:** 22.12.2020; **Accepted:** 30.12.2020)

ABSTRACT: This study examines the consumer preferences for goose meat purchases of consumers who had previously purchased goose meat. The main purpose of this study is to determine which factors are more important for consumers when purchasing goose meat. Accordingly, the conjoint analysis technique, which is one of the multivariate statistical analysis methods, is used to determine the factors affecting goose meat purchases and the reasons for preferring goose meat. According to data of the Turkish Statistical Institute (TURKSTAT) for 2019, 44.07% of the goose population of Turkey (1,157,049) spread among the provinces of Kars (27.26%), Ardahan (8.68%), and Mus (8.13%). A sample of 172 people was selected by using the convenience sampling technique, one of the non-probability sampling methods, among the people who lived or have been living in these provinces and consumed goose meat. Market research and a questionnaire, which was prepared to determine consumer preferences, were conducted on this sample. According to the results of the analysis, the most significant factor determining the consumer preference for goose meat was found to be the price of goose meat per kilo (37.3%). This was followed by the region where the goose was raised (32.8%), the place where the goose meat was sold (21.6%), and the presence of the product label (8.3%) with the identification information of the product. Considering the results of the data obtained from the study, it is thought that the market share of the goose meat will increase if its recognition is increased by applying a reasonable pricing strategy, and standardizing the quality of the product.

Keywords: Goose meat, Consumer preferences, Market research, Conjoint analysis.

1. INTRODUCTION

Contrary to popular belief, the development level of countries cannot be increased only by investment in industry and service sectors. Developed countries make serious investments in agriculture and animal husbandry as well, and they are observed to be at a level that at least meets their needs in these fields. As a result, the gains obtained from agriculture and animal husbandry and the budgets to be transferred to these sectors can be indirectly used in industry and service sectors [1]. It should also be kept in mind that the countries' dependence on foreign food products will be eliminated in this way. Considering the increase in the rural population in Turkey and the increase in investments in the production of agricultural and goose products that can create added value, the income obtained from these products can be used in industry and service sectors, thereby contributing to the country's development level. Accordingly, it is

*Corresponding Author: sgunduz@atu.edu.tr
ORCID number of author: 0000-0001-5289-6089

required to complete the infrastructure and technological equipment in the agriculture and animal husbandry sectors immediately. Also, diversifying the products, and ensuring the sustainability of natural resources in the production, and increasing the income from these products are required for these sectors.

The most important factors that make up the competitive power of countries and institutions are the capacity of making innovations and utilizing the resources efficiently. The issues of production with low added value and not being able to utilize the potentials sufficiently are among the main problems of the less developed countries. Accordingly, it is projected that geese husbandry, which has been on the agenda of Turkey in recent years and producing goose meat and products will be an efficient production line for the domestic and foreign markets. Also, market research in this sector is considered quite crucial.

In the present study, market research was conducted on goose meat and products, which are expected to reach a significant sales volume in both domestic and foreign markets. First, the current situation in the production and consumption of goose meat in Turkey was determined; then, the factors that affect the consumption preferences for goose meat and the effect sizes of these factors were determined by using the conjoint analysis technique, one of the multivariate statistical analysis methods. Within this context, the people who consumed goose meat or products were asked to answer the following questions: “For which features do you prefer these products?”, “The change of which parameters may increase the consumption? “Which features of these products should be brought to the fore if they are to be marketed in domestic and foreign markets?” This study is thought to contribute to the sector in terms of identifying the current status of goose husbandry and goose products consumption in Turkey, as well as determining the problems and providing solution proposals for the future. More research on goose husbandry will make important contributions to this production to be regarded as a sector. Goose husbandry, which has been carried out by traditional production methods, has not reached the desired level due to information pollution and lack of infrastructure [2]. It is important to carry out such studies to popularize this husbandry, which is highly competitive and value-added, as well as for promoting it as a sector. Moreover, it is thought that the studies in this field will provide important references for policymakers, executives who lead the sectors, institutions, and researchers.

The conjoint analysis used in the study is one of the multivariate analysis techniques preferred by researchers to determine the characteristics of consumer behavior [3]. The conjoint analysis provides important information to researchers on the following issues: matters to be considered in new product development studies; changes to be made in products or services and how these changes will be reacted by consumers; how and to what extent the general situation in the market will affect the products and services; how the balances in the market will change over time and with new products; how pricing will reflect on the market.

2. CURRENT STATUS OF GOOSE MEAT PRODUCTION AND CONSUMPTION

Many developing countries attach importance to animal husbandry in integrated production systems to achieve sustainable increases in the production of required food to meet the demands of a rapidly increasing population. Geese adapts well to this kind of systems and particularly to humid regions. They can be raised by natural grazing and are more resistant to diseases than other bird species. Even though goose has a long history dating back to 3000 BC in Egypt and it has inspired many books and stories, goose meat consumption has not been as popular as chicken and duck consumption [4]. The low economic significance of goose husbandry due to

low breeding levels compared to other poultry or the limited geographical spread is considered the reason for this case. Although geese can withstand winter conditions in minimal outdoor shelters and can also adapt to warmer climates, commercial goose production is important only in a few countries in Asia and Europe.

Geese, which were first domesticated in Egypt in history, have been now raised almost anywhere in the world. Domesticated geese are raised for their meat, fatty liver, fat, and feathers, and they are usually consumed widely on Christmas [4]. Although goose breeding can be carried out under all climatic and geographical conditions, it is believed that goose breeding is more yielding in cold and wetlands.

Goose production in Turkey is carried out only by small family businesses using traditional methods, and it seems that major investments have not been made in this field [5]. Goose production is carried out by these enterprises in many provinces, particularly in Kars and Ardahan, and consumed by the local people. Since a production system identified with this consumption understanding has been established, these enterprises have not grown [6]. However, thanks to the increasing demand for goose meat in recent years, it has been observed that the interest in goose husbandry has also increased. Therefore, it has been observed that gaggles of geese have been brought to Kars and Ardahan from various provinces for fattening. Moreover, the number of goose population has increased in many provinces [2]. The production can be extended by increasing the consumption network of goose meat and its products. This can be achieved by increasing the market share of the products. It is seen that goose meat has reached large cities in recent years due to the demands of people who have traditional consumption habits. Thus, traditional dishes are served in large cities. Thanks to this dynamism, the goose trade has emerged across Turkey, which has increased the interest in production [7].

The production cost of poultry such as chicken, turkey, duck, goose, and quail is lower compared to red meat. Moreover, the popularity of poultry has been increasing in many countries due to the short breeding period of these animals and the high nutritional value of their meat. Since poultry has high protein, low calorie, and low cholesterol levels, their consumption has been increasing each passing day across the world. Besides these features, the connective tissue rate of poultry is lower than that of red meat; therefore, it is easier to digest [8].

The goose, which is the first poultry fed by humans, grows later than other poultry. However, their immune system is better than that of other poultry; thus, they do not get sick easily and show more resistance to cold climatic conditions [8]. Goose meat has an important role in human nutrition since it is a good source of protein and contains essential amino acids, particularly arginine, and high unsaturated fatty acids [9].

Goose husbandry offers significant advantages since it can adapt to various climate conditions and utilize natural resources well. However, goose husbandry is limited in Turkey and carried out only in particular provinces. Table 2 presents the numbers of goose population by provinces according to TURKSTAT's data for 2019 [10]. The number of geese population is quite low compared to the numbers of chicken and turkey populations (Table 1). This is due to the insufficient retail consumption and consumer preference for goose products in the domestic market. However, it offers several advantages over substitute products in terms of nutritional values (Table 3).

Table 1. The numbers of poultry population by years in Turkey (x1000) (TURKSTAT)

Years	Broiler Chicken	Turkey	Goose	Duck and Guinea Fowl
2005	257,221	3,697	1,067	656
2006	286,121	3,227	830	525
2007	205,082	2,675	1,023	482
2008	180,916	3,230	1,063	470
2009	163,469	2,755	945	413
2010	163,985	2,942	716	397
2011	158,917	2,563	680	382
2012	169,034	2,761	676	357
2013	177,433	2,925	755	368
2014	199,976	2,990	912	400
2015	213,658	2,828	851	398
2016	220,322	3,183	933	414
2017	221,245	3,872	978	492
2018	229,507	4,043	1,080	533
2019	221,842	4,541	1,157	519

According to Table 1, the number of broiler chickens in Turkey decreased gradually between 2006 and 2011, however it has started to increase again after 2012. Table 2 also reveals that there is an increasing trend in the number of geese, particularly in the last 5 years. Moreover, the numbers of ducks and guinea fowls also increased in these years together with geese.

Table 2. Provinces with a geese population of more than 10,000 in 2019 and their percentages (TURKSTAT)

Rank	Province	Number	Percentage	Rank	Province	Number	Percentage
1	Kars	315,375	27.26%	14	Ankara	17,475	1.51%
2	Ardahan	100,429	8.68%	15	Cankiri	16,639	1.44%
3	Mus	94,036	8.13%	16	Erzincan	16,315	1.41%
4	Kutahya	42,321	3.66%	17	Agri	15,719	1.36%
5	Samsun	34,869	3.01%	18	Amasya	15,167	1.31%
6	Afyon	34,835	3.01%	19	Sirnak	14,528	1.26%
7	Yozgat	28,375	2.45%	20	Eskisehir	14,438	1.25%
8	Corum	28,264	2.44%	21	Aksaray	14,096	1.22%
9	Sanliurfa	22,967	1.98%	22	Kirsehir	12,025	1.04%
10	Diyarbakir	21,732	1.88%	23	Edirne	10,791	0.93%
11	Konya	18,401	1.59%	24	Elazig	10,747	0.93%
12	Erzurum	17,755	1.53%	25	Tokat	10,425	0.90%
13	Adana	17,629	1.52%	**Turkey**		**1,157,049**	

As shown in Table 2, 44.07% of the goose population in Turkey spread among the provinces of Kars (27.26%), Ardahan (8.68%), and Mus (8.13%). Table 1 also reveals that the goose population of 25 provinces is more than 10,000 and goose husbandry can be carried out in any region of Turkey. However, it is obvious that Northeastern Anatolia has a key role in goose husbandry, and it is distinguished from other regions in Turkey.

Table 3. The energy and nutritional values of edible parts of various meats (100 grams) [7]

Meat Type	Price (1 kg)	Energy (cal)	Protein (g)	Fat (g)	Calcium (mg)	Iron (mg)
Cattle (semi-fat)	50	240	18.7	18.2	8	2.6
Sheep (semi-fat)	55	267	17.0	21.0	7	2.2
Chicken	10	149	19.0	8.0	15	1.5
Rabbit	40	137	21.0	5.8	17	1.6
Goat	55	157	18.4	9.2	1	2.2
Turkey	25	144	19.5	6.7	17	1.7
Goose	70	161	22.8	7.1	13	2.6

3. LITERATURE REVIEW

With its ecological suitability, feasibility for small businesses, favorable geographical location for the EU and the Middle East market in terms of foreign trade, Turkey has ideal conditions for goose production. On the other hand, considering the changes in consumption patterns, increasing popularity of out-of-home consumption, increasing trend of healthy food consumption, being an alternative for the animal protein needs of the growing population, presence of consumers seeking for new products, the widespread use of local flavors as a touristic instrument, it reveals the existing goose production and consumption potential in Turkey. For these and similar reasons, many studies have been conducted recently to investigate the importance of goose breeding, goose meat and goose products. Some of these studies are given below.

Gunduz et al. (2019) conducted a sensory analysis on goose meat and the substitute products [7], while Boz and Sarica (2018) conducted a study on the current status and future of goose husbandry in Turkey [6]. Sarica (2018) performed applied research on increasing the yield of domestic goose [5], and Sekeroglu and Duman (2018) analyzed goose products and the ways of consuming them, and they researched their marketing structure and the current situation in the legislation [4]. Yamak (2018) performed studies on the breeding and incubation methods in geese [11], Kirmizibayrak (2018) studied the barriers for goose husbandry in Turkey [2], Arslan (2018) studied feeding methods according to goose production systems [12], Saatci (2018) examined hygiene and preventing diseases in goose husbandry [13]. Additionally, Tekbalkan (2017) studied traditional dishes of goose meat [14], Guner et al. (2002) compared goose salami with turkey salami and chicken salami to determine its suitability for consumption, thereby introducing goose meat to meat products technology [15]. Askin and Ilaslan (1976) researched Kars geese's several characteristics with economic importance [16].

Conjoint analysis, one of the multivariate statistical techniques, was used in this study, which can be regarded as market research on goose meat and its products. This analysis is a method that is frequently used especially in the field of marketing, and many academic studies have been conducted in market research in recent years using this method. The first studies on the conjoint analysis, which was used in the present study, were made in the 1920s. Then, R. Duncan Luce and John W. Tukey reported the importance of the "Conjoint Measurement" in their study in 1964 [17]. Although several studies were conducted and software applications were developed after this article, the first consumer-oriented study was carried out by Paul Green and Vithala R. Rao in 1971 [18]. The study conducted by Green and Srinivasan in 1978 has been a reference for many studies using conjoint analysis [3, 19].

Other studies using conjoint analysis are given below. These studies are presented in chronological order, and particularly, the studies conducted in recent years are presented.

Alvarez-Farizo and Hanley (2002) used conjoint analysis in their studies and showed how two choice modeling techniques can be used to estimate the potential environmental impacts of wind farm developments [20]. Poortinga et al. (2003) examined the preferences for various energy-saving measures using Part-worth conjoint analysis [21]. Sen and Cemrek (2004) conducted an applied study using conjoint analysis to determine the student preferences for private teaching institutions [22]. Saracli and Siklar (2005) examined the factors that affect the preference for Private Pension System using conjoint analysis [18]; Camlidere (2005) conducted a study on mobile phone purchases using conjoint analysis [23]; Tatlidil (2015) defined the political leader profile using conjoint analysis [24], and Catpinar (2005) researched preferences for private health insurances using conjoint analysis [25]. Dikici (2006) conducted a thesis study on determining consumer preferences for mobile phones using conjoint analysis [26]. Sonmez (2006) conducted a study on consumer preferences for computer purchases using conjoint analysis [27]. On the other hand, Akinci et al. (2007) made an application on adaptive conjoint analysis and discount markets in Istanbul. Soykan (2009) used conjoint analysis on purchasing decisions in the industry [28]. Dinc (2010) used conjoint analysis to determine the automobile selection criteria for consumers [29], and Filiz and Sengoz (2010) also examined the consumer preference for casco insurance using this analysis method [30]. Turanli et al. (2011) analyzed mobile phone consumer preferences for GSM plans and price elasticity using conjoint analysis [31], while Cevik and Yigit (2011) determined consumer preference for office furniture using conjoint analysis [32]. Bridges et al. (2011) presented the findings of their analysis as the following ten-item checklist: Research question, attributes and levels, construction of tasks, experiment design, preference elicitation, instrument design, data collection, statistical analyses, results, and conclusion, and the study presentation [33]. Aktas et al. (2012) conducted an applied study on the performances of conditional logit analysis and conjoint analysis in the modeling of the polychotomous dependent variable [34]. Sahinkanat (2013) analyzed the purchasing decisions of consumers using conjoint analysis in her master's thesis [35]. Yavuz and Cemrek (2013) examined the healthcare professionals' preferences for housing using conjoint analysis [36]. Turanli et al. (2013) identified the factors affecting consumer preferences for the newspaper using this analysis [31], and Ceylan (2013) published a study on market segmentation based on benefit in the retail sector by using conjoint and cluster analysis [37]. Baki et al. (2017) analyzed consumer preferences for honey in Izmir, Turkey by conjoint analysis [38]. Yildiz ve Kucukkancabas (2020) investigated the effects of eco-labels on consumer behaviors using conjoint analysis [39]. Finaly, Li et al. (2020) in their study examined the public preference for electric vehicle incentives in China based on a large sample (n = 1039) using the conjoint analysis for incentive policies [40]. The results of the study revealed that less than a third of consumers had a better understanding of incentive policies, while more than half had little information about these policies. According to consumers, the relative importance levels of various policy categories are ranked as follows: charging incentive policies, driving incentive policies, vehicle registering incentive policies, and purchasing incentive policies.

4. CONJOINT ANALYSIS

In the present study, conjoint analysis, which is one of the multivariate statistical techniques, was used to examine consumer preferences for goose meat. Also, the benefits attributed to the characteristics of this product (goose meat) by the consumers were determined. Because this analysis is based on the estimation of the utility functions of individuals, it measures the

relationship between the reactions of consumers to products or services and the features of these products and services. Determining consumer preferences using conjoint analysis allows the consumer to provide a preference degree for each quality level of the product or service, as well as to make preliminary preparation about possible future situations [3]. Due to this feature, it provides an opportunity to gain an insight into the product or service combinations that are planned to be released in the future, to determine the most important factor for the consumer, thereby offering the opportunity to run advertisement and promotion campaigns using the relevant variable.

The conjoint analysis allows determining the optimal features of a product or service, consumer choices, and estimating the weights attached to various factors in the decision-making process [38]. For example, consumers consider factors such as the number of rooms, location, price, transportation, etc. for house purchases and choose by evaluating them according to their importance levels. Similarly, the consumers determine the optimal choices for themselves when buying a car by considering the criteria such as body type, brand, fuel type, fuel consumption, brand, price, etc. If these tendencies of the consumers are determined accurately, the contractors can choose effective construction areas and types accordingly, and automobile manufacturers can revise their production lines in line with these demands.

What distinguishes Conjoint Analysis from other statistical analyses is that it provides the opportunity to compare the qualities quantitatively [18]. With the relationship between the variables determined for a particular product or service, the relationship levels between these variables, and the importance levels of these variables are converted into data that can be expressed numerically. In particular, conjoint analysis is used to understand how respondents develop their preferences for products and services [41]. Conjoint analysis is a common market research technique used in designing new products and improving existing products. Also, it is used for getting an advantageous position in the market compared to the competitors, measuring the effect of price on purchasing behavior, and estimating market share [42].

The value given by customers to each separable feature of a product is determined by conjoint measurement; thus, the most affordable product with the most suitable features is determined. The purpose of this study is not to measure the purchasing intentions of customers, but to determine the preference by evaluating the price and non-price features that are important in the choice of the product.

Multivariate statistical analysis techniques have been developed since multiple statistical techniques have to be used at the same time in many disciplines. The assumption of normality required in these techniques, the application of algorithms that generate complex and general results have led to the emergence of various issues and challenges. In some studies, modern methods were developed to determine relationships when several variables could not be measured actually and therefore they were defined qualitatively [43]. One of these modern methods is the conjoint analysis, which is also used in this study. As a multivariate statistical method developed by mathematician psychologists, conjoint analysis allows analyzing the effects of factors concerning human attitudes and behavior, as well as estimating the value of products and services for the consumers [17]. The conjoint analysis differs from other multivariate statistical methods in terms of reflecting consumer preferences and decisions more realistically. These differences can be observed in the following areas: segmentation/segregation difference, types of relationships between dependent/independent variables, and the possibility to make estimations at the individual level. In other words, consumer preferences can be divided according to each feature of the products using conjoint

analysis, and these discrete relationships can be easily calculated even if there is no linear relationship between dependent/independent variables. Moreover, estimations can be made at individual levels using different preference models for each unit instead of making a cumulative estimation.

Conjoint analysis can be expressed by the following equation. In this equation, the Y variable can be measured using a classifier, sorter, or an equidistant scale, while $X1, X2, \dots, Xp$ variables may be measured using a classifier or a sorting scale [44].

$$Y_i = X_1 + X_2 + \cdots + X_p, \qquad i = 1,2, \dots, n$$

Conjoint analysis is divided into the following three categories: Adaptive Conjoint Analysis, Selection-Based Conjoint Analysis, and Conjoint Value Analysis [18]. Determining the most appropriate Conjoint Analysis method for the research subject is important to obtain the desired results.

It is necessary to follow a specific strategy not to make the process complicated and to obtain accurate estimates when performing conjoint analysis. First of all, determinant factors of the product or service to be analyzed and the levels of these factors should be identified. Secondly, the combinations of these factors and levels should be determined. Considering that the number of combinations will be high when the number of these factors and levels are high, models that reduce these numbers should be used to facilitate consumer assessment. In the third step, determined combinations of various factors and levels should be presented in cards or opinion forms to the respondents. Finally, the estimation model is determined.

5. APPLICATION

According to data of the Turkish Statistical Institute (TURKSTAT) for 2019, the provinces of Kars (27.26%), Ardahan (8.68%), and Mus (8.13%) have the 44.07% of the goose population of Turkey (1,157,049). The primary material of the study is the data obtained by a questionnaire study conducted with people who lived or have been living in these cities and consumed goose meat. The questionnaire form, which was prepared after a detailed literature review, was revised after a pilot study. A sample of 172 people was selected by using the convenience sampling technique, one of the non-probability sampling methods, among the people who lived or have been living in these provinces and consumed goose meat. Then, the questionnaire was applied face-to-face. The data obtained from the responses of 172 people, whose responses were appropriate and complete, were used in the analysis. The number of participants meets the condition of the minimum number of responses (>150) for the Conjoint analysis [45]. Publications on goose meat consumption and conjoint analysis in national and international literature, reports, and statistics prepared by relevant institutions and organizations are other materials used in this study.

The first part of the questionnaire form includes questions to determine the socio-economic characteristics of the participants. Findings regarding the demographic characteristics of consumers are presented in Table 4. According to this table, 42% of the participants were women, 78.2% were married, and 25.3% had an associate degree or a higher degree. Moreover, it was determined that a significant part of the participants were housewives (42.9%) and the income level of the majority (62.1%) was 2,500 TRY or below.

Table 4. Demographic Features of the Participants

Gender	**Percentage**	**Marital Status**	**Percentage**
Female	42%	Married	78.2%
Male	58%	Single	21.8%
Age (years)	**Percentage**	**Level of Education**	**Percentage**
25 and below	10.2%	Primary school or below	37.6%
25 - 40	23.7%	High School	37.1%
41 - 65	58.9%	Associate Degree or Bachelor's Degree	24.5%
65 and above	7.2%	M.Sc. Degree or above	0.8%
Profession	**Percentage**	**Monthly Income (TRY)**	**Percentage**
Civil servant	22.7%	Up to 2,500	62.1%
Private sector/Self-employed	13.1%	2,501-5,000	28.3%
Housewife	42.9%	5,001-7,500	6.0%
Retired	12.2%	More than 7,500	3.6%
Student	9.1%		

As stated in the previous sections, the aim of this study is; to determine the order of importance of factors affecting consumer preferences while purchasing goose meat by using conjoint analysis. In this study, the order of preference was used as the dependent variable to determine the goose meat preferred by consumers. This variable has been measured with an interval scale and takes values between 1 and 16. Expert opinions and related literature were used while determining the independent variables and levels affecting goose meat purchasing preferences. The independent variables included in the analysis were determined as region, price, distribution and product label. The number of variables used in the study is 4 and the number of levels related to the variables is 3, 3,3, 2, respectively. The total number of cards containing all possible combinations of levels is 3 * 3 * 3 * 2 = 54. However, since the application of 54 cards is difficult, the orthogonal design was used. Syntax menu of SPSS package program was used to create the cards used in conjoint analysis. 18 cards were created using this program. 172 people in the study sample were asked to rank 18 cards from the most preferred to the least preferred. In the Conjoint analysis used in this study, the full concept technique was preferred as the data collection method. The full concept technique is a method where all features are evaluated together.

Table 5 presents the results of the conjoint analysis conducted to determine the goose meat purchasing preferences of the people who responded to the questionnaire. The features that the consumers consider when they buy goose meat such as the region where the goose is raised, the price, the place where the product is sold, and the presence of the product label, as well as the partial benefits and their relative importance values, are included in Table 5.

Table 5. Partial benefits and their relative importance values calculated by conjoint analysis

Feature	Sub-level	Utility (Benefit)	Relative Importance
Region	Eastern - Central Anatolia Regions	0.985	32.8%
	Mediterranean - Southeastern Anatolia Regions	0.326	
	Marmara – Aegean – Black Sea Regions	0.112	
Price (TRY/Kg)	40	0.385	37.3%
	60	1.128	
	80	-0.278	
Distribution	Grocery – Supermarket	0.358	21.6%
	Bazaar	0.058	
	House – Farm	0.296	
Product label	Available	0.218	8.3%
	Not available	-0.218	

According to the relative importance values of the features listed in Table 5, it is understood that the most effective factor in the consumer's preference for the purchase of goose meat is the price of goose meat per kilogram (37.3%). Following this factor, the region where the goose is raised (32.8%), where the product is sold (21.6%), and the presence of the product label (8.3%) affect consumer preferences.

The utility (benefit) coefficients are calculated to determine which levels of the variables each respondent desires most. Considering the partial benefit values of the price factor, which is the most effective factor on consumer preference, the highest benefit was found to be the price of 60 TRY per kg, while the lowest benefit was found to be the price of 80 TRY per kg. This can be interpreted that the consumers want to buy the goose meat cheaper than red meat, however, they do not prefer a product if the price per kg is very low considering the quality.

Following the price factor, the feature that most affects the purchasing preference is the region where the goose is raised. According to the levels of this factor, the highest benefit is obtained from the geese raised in the Eastern and Central Anatolia regions. According to the levels of the factor of the place where the product is sold, the highest benefit is obtained from the goose meat sold in popular supermarkets and the lowest benefit is obtained from the goose meat sold in bazaars. Finally, the presence of a product label that includes information on the expiration date of the goose meat and the place of slaughter was also found to have high benefit.

6. CONCLUSION

When the relevant literature is examined, it is obvious that goose meat will take place in the market, considering its superiority in terms of nutritional values compared to the substitute products and the positive evaluations of the participants according to the substitute products. Therefore, it will be beneficial to accelerate the production and sales process of goose meat and

goose products that will contribute to the national economy in terms of added value. To achieve this acceleration, it is necessary to increase academic studies and market research in this field. In this direction, using conjoint analysis, which is a method frequently used in marketing research, consumers' buying behavior of goose meat was investigated in this study.
The participants of this study, which was conducted with 172 people who had previously purchased goose meat, 42% were women, 78.2% were married, and 25.3% had an associate degree or a higher degree. Moreover, it was determined that a significant part of the participants were housewives (42.9%) and the income level of the majority (62.1%) was 2,500 TRY or below.

Considering the results of the conjoint analysis in terms of the relative importance values, the price of goose meat per kilogram was found to be the most effective factor (37.3%) affecting consumer preference for goose meat purchases. Following this, the factors of the region where the goose is raised (32.8%), where the product is sold (21.6%), and the presence of the product label (8.3%) were found to affect consumer preferences for goose meat purchases.

According to the partial benefit values of the levels of the price factor, which is considered to have the most effect on the consumer preference for goose meat purchase, it is observed that the highest benefit is obtained at the price of 60 TRY per kg. Also, considering the level of the factor of the region where the goose is raised, the highest benefit is obtained from the geese raised in the Eastern and Central Anatolia regions, as expected. On the other hand, considering the factor of the place where the product is sold, the highest benefit is obtained from the goose meat sold at popular supermarkets. Also, considering the level of the product label factor, the presence of the product label was found to provide a high level of benefit.

It is important to know which properties of the product are important for the consumer and whether the product is preferred or not. It is necessary to find answers to these questions for a successful product and service design. In this study, it was tried to answer these questions for goose breeders.

Acknowledgments

This research was supported by the Scientific Research Projects Coordination Unit of Adana Alparslan Turkes University of Science and Technology within the scope of the scientific research projects (Project No: 18113008).

REFERENCES

[1] Kilci, A. E. (2018). Önsöz, Türkiye Kaz Yetiştiriciliği Çalıştayı ve Kaz Günü Etkinliği Sonuç Raporu, 11.

[2] Kırmızıbayrak, T. (2018). Türkiye'de Kaz Yetiştiriciliğinin Ticari Bir Sektör Olmasının Önündeki Engeller. Türkiye Kaz Yetiştiriciliği Çalıştayı ve Kaz Günü Etkinliği Sonuç Raporu, 22-23 February 2018, Yozgat, 53-68.

[3] Green, P.E., ve Srinivasan, V., (1978). Conjoint Analysis in Consumer Research: Issues and Outlook, Journal of Consumer Research, 5, 103-123.

[4] Şekeroğlu, A. and Duman, M. (2018). Kaz Ürünleri Pazarlama Yapısı, Mevzuattaki Durum ve Sorunları. Türkiye Kaz Yetiştiriciliği Çalıştayı ve Kaz Günü Etkinliği Sonuç Raporu, 22-23 February 2018, Yozgat, 110-116.

[5] Sarıca, M. (2018). Yerli Kazlarımızda Seleksiyonla Verim Artışı Sağlanabilir mi? Bir Uygulama Projesi. Türkiye Kaz Yetiştiriciliği Çalıştayı ve Kaz Günü Etkinliği Sonuç Raporu, 22-23 February 2018, Yozgat, 45-52.

[6] Boz, M.A. and Sarıca, M. (2018). Türkiye'de Kaz Yetiştiriciliğinin Durumu ve Geleceği. Türkiye Kaz Yetiştiriciliği Çalıştayı ve Kaz Günü Etkinliği Sonuç Raporu, 22-23 February 2018, Yozgat, 36-44.

[7] Gündüz, S., Dölekoğlu, C. Ö., and Say, D. (2019). Sensory Analysis with Goose Consumption Preferences Substitute Products. European Journal of Science and Technology, (16): 32-40.

[8] Oz, F., Celik, T., 2015. Proximate Composition, Color and Nutritional Profile of Raw and Cooked Goose Meat with Different Methods. Journal of Food Processing and Preservation, 39: 2442-2454.

[9] Liu, B. Y., Wang, Z. Y., Yang, H. M., Wang, J. M., Xu, D., Zhang, R., Wang, Q. (2011). Influence of Rearing System on Growth Performance, Carcass Traits, and Meat Quality of Yangzhou. Poultry Science, 90(3): 653-659.

[10] TSI, 2019. Turkish Statistical Institute. www.tuik.gov.tr. Access Date: 10.10.2010.

[11] Yamak, U. S. (2018). Kazlarda Üreme ve Kuluçka. Türkiye Kaz Yetiştiriciliği Çalıştayı ve Kaz Günü Etkinliği Sonuç Raporu. 22-23 February 2018, Yozgat, 69-84.

[12] Arslan, C. (2018). Kazların Ekstansif, Yarı Entansif ve Entensif Üretim Sistemlerine Göre Belirlenmesi. Türkiye Kaz Yetiştiriciliği Çalıştayı ve Kaz Günü Etkinliği Sonuç Raporu, 22-23 February 2018, Yozgat, 85-94.

[13] Saatci, M. (2018). Kaz Yetiştirmede Hijyen ve Hastalıklardan Korunma. Türkiye Kaz Yetiştiriciliği Çalıştayı ve Kaz Günü Etkinliği Sonuç Raporu, 22-23 February 2018, Yozgat, 95-109.

[14] Tekbalkan, M. (2017). The Role of Local and Regional Food in Local Tourism: Sample of Samsun Kaz Tiridi. Journal of Tourism and Gastronomy Studies, 5(4): 155-169.

[15] Güner, A., Doğruer, Y., Uçar, G., Yörük, H. D. (2002). Salam Üretiminde Kaz Etinin Kullanılabilme İmkanları. The Turkish Journal of Veterinary and Animal Sciences, 26: 1303-1308.

[16] Aşkın, Y. and İlaslan, M. (1976). Kars Bölgesi Kazlarında Ekonomik Önemi Olan Bazı Karakterler Üzerinde Araştırmalar. Ankara Üniversitesi Ziraat Fakültesi Yıllığı, 26: 542-552.

[17] Dölekoğlu, C. Ö. (2002). Consumer Quality Preferences for Products, Attitude of Consumers on Health Risk and Nutritional Information (Adana Case). Unpublished Ph. D. Thesis, Çukurova University, Institute of Natural and Applied Sciences, Adana, 171 pp.

[18] Saraçlı, S. and Şıklar, E. (2005). Examining the Individual Retirement Account with Conjoint Analysis. Journal of Social Sciences, (2): 1-12.

[19] Erdoğan, C. (2006). Determining the Consumer Preference of Automobiles with Conjoint Analysis. Master Thesis, Gazi University, Institute of Natural and Applied Sciences, Ankara 75 pp.

[20] Álvarez-Farizo, B. and Hanley, N. (2002). Using Conjoint Analysis to Quantify Public Preferences over the Environmental Impacts of Wind Farms. An Example from Spain. Energy Policy, 30(2): 107-116.

[21] Poortinga W., Steg, L., Vlek, C., Wiersma, G. (2003). Household Preferences for Energy-Saving Measures: A Conjoint Analysis. Journal of Economic Psychology, 24(1): 49-64.

[22] Şen, H. and Çemrek, F. (2004). Konjoint Analizi ve Özel Dershane Tercihine Yönelik bir Uygulama. Eskişehir Osmangazi UniversityJournal of Social Sciences, 5(2): 105-120.

[23] Çamlıdere, Ö. (2005). Conjoint Analysis and an Application to Mobile Phones Preference. Master Thesis, Gazi University, Institute of Natural and Applied Sciences, Ankara, 64 pp.

[24] Tatlıdil, H. (2015). Siyasi Lider Profili-Konjoint Analizi Uygulaması. (Basılmamış Notlar).

[25] Çatpınar, H. (2005). Özel Sağlık Sigortalarında Konjoint Analizi ile Tüketici Tercihi. Sigorta Araştırmaları Dergisi, 1.

[26] Dikici, T. (2006). Conjoint Analysis and an Application in Connection with Determination of Mobile Phone Preference of Consumers. Master Thesis, Uludag University, Institute of Social Sciences, Econometrics Department, Bursa, 113 pp.

[27] Sönmez, H. (2006). An Application of Consumer Preferences Via Conjoint Analysis: How to Choose a Home PC. Journal of Social Sciences, 6(2): 185-196.

[28] Soykan, Y. (2009). Conjoint Analysis in Industrial Purchasing Decisions and an Application. Akademik Bakış, 16: 1-18.

[29] Dinç, Y. (2010). Conjoint Analysis and an Application on the Selection Criteria of Automobile. Master Thesis, Marmara University, Institute of Social Sciences, Department of Statistics, Istanbul, 93 pp.

[30] Filiz, Z. and Şengöz, M. (2010). Kasko Sigortası Tercihinin Konjoint Analizi ile İncelenmesi. "İşGüç" Industrial Relations and Human Resources Journal, 12(1): 107-121.

[31] Turanlı, M., Bağdatlı Kalkan, S., and Yazılı, N. (2011). Customers' Mobile Phone Package Choice and Price Flexibility Teste with Conjoint Analysis. Trakya University Journal of Social Science, 13 (2): 355-370.

[32] Çevik, O. and Yiğit, A. M. (2011). Determining Office Furniture Consumers' Preferences with Conjoint Analysis. Karamanoglu Mehmetbey University Journal of Social and Economic Research, 13 (20): 105-110.

[33] Bridges, J. F., Hauber, A. B., Marshall, D., Lloyd, A., Prosser, L. A., Regier, D. A., Johnson, F. R., and Mauskopf, J. (2011). Conjoint Analysis Applications in Health a Checklist: A Report of the ISPOR Good Research Practices for Conjoint Analysis Task Force. Value in Health, 14(4): 403-413.

[34] Aktaş, S., Akkuş, Ö. and Osmanoğlu, S. (2012). A Practical Study on the Performances of the Conditional Logit and Conjoint Analyses in the Modelling of the Polychotomous Dependent Variable. Istanbul Commerce University Journal of Science, 11(21): 25-40.

[35] Şahinkanat, E. (2013). Determination of Consumers' Purchasing Decisions with Conjoint Analysis. Master Thesis, Uludag University, Social Science Institution, Statistics Department, Bursa, 152 pp.

[36] Yavuz, S. and Çemrek, F. (2013). The Determination of Residental Preferences of Healthcare Workers Through Conjoint Analysis. Atatürk University Journal of Graduate School of Social Sciences, 17(2): 379-396.

[37] Ceylan, H. H. (2013). Market Segmentation Based on Benefit in Retail Sector by Using Conjoint and Cluster Analysis. CBU, Journal of Management and Economics, 20(1): 141-154.

[38] Baki, F., Saner, G., Adanacıoğlu, H., and Güler, D. (2017). A Conjoint Analysis of Consumer Preferences for Honeydew Honey in Turkey: A Case of İzmir Province. Balkan and Near Eastern Journal of Social Sciences, 3(2): 50-57.

[39] Yıldız, B. and Küçükkancabaş Esen, S. (2020). The Influence of Eco-Labelling on Consumer Behaviors: Examining Refrigerator Eco-Labels Using Conjoint Analysis. Productivity Journal (Verimlilik Dergisi), (1): 83-98.

[40] Li, W., Long, R., Chen, H., Dou, B., Chen, F., Zheng, X., and He, Z. (2020). Public Preference for Electric Vehicle Incentive Policies in China: A Conjoint Analysis. International Journal of Environmental Research and Public Health, 17(1): 318.

[41] Hair, J. F., Anderson, R., Tatham, R., and Black, W.C. (1992). Multivariate Data Analysis, Third Edition, U.S.A.: Prentice Hall (Higher Education Division, Pearson Education), 480 pp.

[42] Kuhfeld, W.F. (2005). Marketing Research Methods in SAS. SAS 9.1 Edition.

[43] Çetinel, B. and Yeniay, O. (1997). Konjoint Analiz ve Cep Telefonu Pazarı Üzerine Bir Araştırma. 3. Ulusal Ekonometri ve İstatistik Sempozyumu Bildiri Kitabı, Bursa, 15-24.

[44] Sönmez, H., (2001). The Usage of Conjoint Analysis in Marketing Research and an Application. Ph.D. Thesis, Anadolu University, Institute of Natural and Applied Sciences, Department of Statistics, Eskişehir, 183 pp.

[45] Orme, B. (2010). Getting Started with Conjoint Analysis: Strategies for Product Design and Pricing Research, 2nd Edition. Madison: Research Publishers LLC.

NATURENGS
MTU Journal of Engineering and Natural Sciences
https://dergipark.org.tr/tr/pub/naturengs
DOI: 10.46572/nat.2020.18

A Study on Chen-like Inequalities for Half Lightlike Submanifolds of a Lorentzian Manifold Endowed with Semi-Symmetric Metric Connection

Nergiz (ÖNEN) POYRAZ[1], Burçin DOĞAN[2*]

[1] Department of Mathematics, Faculty of Arts and Sciences, Çukurova University, Adana, Turkey.

[2*] Department of Engineering Basic Science, Faculty of Engineering and Natural Sciences, Malatya Turgut Özal University, Malatya, Turkey.

(**Received:** 18.12.2020; **Accepted:** 30.12.2020)

ABSTRACT: In this paper, Chen-like inequalities of a half lightlike submanifolds of a real space form $\tilde{N}(c)$ with constant sectional curvature c, equipped with semi-symmetric metric connection are established and some important characterization theorems for such submanifolds are proved using these inequalities.

Keywords: Chen inequality; Half lightlike submanifold; Lorentzian manifold; Semi-symmetric metric connection.

1. INTRODUCTION

Lightlike submanifolds theory is an important field of study as it is the mathematical modeling of black holes. The lightlike submanifolds theory was first studied by Kupeli [1] and Duggal-Bejancu [2]. Later many geometers have worked in this area [3-5].

The connection on the manifold is a very important concept geometrically, as it enables us to operate algebraically on the manifold. One of the different connections that can be defined on manifolds is the semi-symmetric metric connection. A semi-symmetric metric connection defined by Hayden in [6] was studied by Yano in [7]. The first studies on Riemannian, semi-Riemannian and Lorentzian manifolds with semi-symmetric metric connection belong to Z. Nakao [8], Duggal and Sharma [9] and Konar and Biswas [10], respectively. Yaşar, Çöken and Yücesan introduced lightlike hypersurfaces of a semi-Riemannian manifold with a semi-symmetric metric connection in [11]. Later, Akyol, Vanlı and Fernandez studied curvature properties of a semi-symmetric metric connection on S manifolds in [12].

The Chen inequalities established by Chen in [13] are inequalities that extrinsic and intrinsic curvatures of the manifold and are very useful in characterizing the manifold. Then, various non-degenerate manifolds have been studied by establishing Chen inequalities on them [14-26]. However, Chen inequalities in lightlike geometry were first studied by Gülbahar, Kılıç and Keleş in [27] and [28]. Then Poyraz, Doğan and Yaşar introduced inequalities on the lightlike hypersurface of a Lorentzian manifold with a semi-symmetric metric connection in [29].

*Corresponding Author: burcin.dogan@ozal.edu.tr
ORCID number of authors: [1] 0000-0002-8110-712X, [2] 0000-0001-8386-213X

Finally, some inequalities of screen conformal half lightlike submanifolds were derived by Gülbahar and Kılıç in [30].

In this paper, Chen-like inequalities of a half lightlike submanifolds of a real space form $\tilde{N}(c)$ with constant sectional curvature c, equipped with semi-symmetric metric connection are established and some important characterization theorems for such submanifolds are proved using these inequalities.

2. MATERIAL AND METHODS

Let $\tilde{\nabla}$ be a connection on a semi-Riemannian manifold $(\tilde{N},\tilde{g})$. $\tilde{\nabla}$ is called a semi-symmetric metric connection if it is metric, i.e., $(\tilde{\nabla},\tilde{g})=0$ and for $\forall \tilde{U},\tilde{V}\in\Gamma(T\tilde{N})$, its torsion tensor $\tilde{T}$ satisfies

$$\tilde{T}(\tilde{U},\tilde{V})=\tilde{\pi}(\tilde{V})\tilde{U}-\tilde{\pi}(\tilde{U})\tilde{V}, \tag{2.1}$$

where $\tilde{P}$ is a vector field on $\tilde{N}$, which called the torsion vector field and $\tilde{\pi}$ is a 1-form defined by

$$\tilde{g}(\tilde{P},\tilde{U})=\tilde{\pi}(\tilde{U}).$$

Now, suppose that the semi-Riemannian manifold $\tilde{N}$ admits a semi-symmetric metric connection which is given by

$$\tilde{\nabla}_{\tilde{U}}\tilde{V}=\overset{\circ}{\tilde{\nabla}}_{\tilde{U}}\tilde{V}+\tilde{\pi}(\tilde{V})\tilde{U}-\tilde{g}(\tilde{U},\tilde{V})\tilde{P} \tag{2.2}$$

for arbitrary vector fields $\tilde{U}$ and $\tilde{V}$ of $\tilde{N}$, where $\overset{\circ}{\tilde{\nabla}}$ denotes the Levi-Civita connection concerning the semi-Riemannian metric $\tilde{g}$ [7].

Let $(\tilde{N},\tilde{g})$ be a $(m+3)-$dimensional semi-Riemannian manifold of the index $q\geq 1$ and N be a lightlike submanifold of codimension 2 of $\tilde{N}$. Then the radical distribution $Rad(TN)=TN\cap TN^{\perp}$ of N is a vector subbundle of the tangent bundle TN and the normal bundle $TN^{\perp}$ of rank 1 or 2. If $rank(Rad(TN))=1$, then N is called half lightlike submanifold of $\tilde{N}$. Then there exist complementary non-degenerate distributions $S(TN)$ and $S(TN^{\perp})$ of $Rad(TN)$ in TN and $TN^{\perp}$, which are called the screen and the screen transversal distribution on N respectively. Thus we have

$$TN=Rad(TN)\perp S(TN),\quad TN^{\perp}=Rad(TN)\perp S(TN^{\perp}). \tag{2.3}$$

Consider the orthogonal complementary distribution $S(TN)^{\perp}$ to $S(TN)$ in $T\tilde{N}$. Then ξ and Z belong to $\Gamma(S(TN)^{\perp})$. Thus we obtain

$$S(TN)^{\perp}=S(TN^{\perp})\perp S(TN^{\perp})^{\perp}, \tag{2.4}$$

where $S(TN^{\perp})^{\perp}$ is the orthogonal complementary to $S(TN^{\perp})$ in $S(TN)^{\perp}$. For any null section

$\xi \in Rad(TN)$ on a coordinate neighborhood $U \subset N$, there exists a uniquely determined null vector field $L \in \Gamma(ltr(TN))$ satisfying

$$\tilde{g}(L,\xi)=1, \quad \tilde{g}(L,L)=\tilde{g}(L,U)=\tilde{g}(L,Z)=0, \ \forall U \in \Gamma(TN). \tag{2.5}$$

We call L, $ltr(TN)$ and $tr(TN)=S(TN^{\perp}) \perp ltr(TN)$ the lightlike transversal vector field, lightlike transversal vector bundle and transversal vector bundle of N concerning $S(TN)$, respectively. Hence we have

$$\begin{aligned} T\tilde{N} &= TN \oplus tr(TN) \\ &= \{Rad(TN) \oplus ltr(TN)\} \perp S(TN) \perp S(TN^{\perp}). \end{aligned} \tag{2.6}$$

Let $\tilde{\nabla}$ be the Levi-Civita connection of $\tilde{N}$. Using (2.6) we define the projection morphism $Q : \Gamma(TN) \to \Gamma(S(TN))$. Hence we derive

$$\tilde{\nabla}_U V = \nabla_U V + B(U,V)L + D(U,V)Z, \tag{2.7}$$
$$\tilde{\nabla}_U F = -A_F U + \nabla^t_U F, \tag{2.8}$$
$$\tilde{\nabla}_U L = -A_L U + \tau(U)L + \rho(U)Z, \tag{2.9}$$
$$\tilde{\nabla}_U Z = -A_Z U + \psi(U)L, \tag{2.10}$$
$$\nabla_U QV = \nabla^*_U QV + C(U,QV)\xi, \tag{2.11}$$
$$\nabla_U \xi = -A^*_\xi U - \tau(U)\xi, \tag{2.12}$$

for any $U,V \in \Gamma(TN)$, $\xi \in \Gamma(Rad(TN))$, $F \in \Gamma(tr(TN))$, $L \in \Gamma(ltr(TN))$ and $Z \in \Gamma(S(TN^{\perp}))$. Then ∇ and ∇^* are called induced linear connections on TN and $S(TN)$ respectively, B and D are called the local second fundamental forms of N, C is called the local second fundamental form on $S(TN)$. A_L, A^*_ξ and A_Z are called linear operators on TN. Also τ, ρ and ψ are called $1-$ forms on TN.

The induced connection ∇ of N is not metric and satisfies

$$(\nabla_U g)(V,W) = B(U,V)\eta(W) + B(U,W)\eta(V), \tag{2.13}$$

for any $U,V,W \in \Gamma(TN)$, where η is a $1-$form defined by

$$\eta(U) = \tilde{g}(U,L), \ \forall U \in \Gamma(TN). \tag{2.14}$$

But the connection ∇^* is metric. Using (2.1) and (2.13), we show that

$$T(U,V) = \pi(V)U - \pi(U)V \tag{2.15}$$

and B and D are symmetric, where T is the torsion tensor concerning ∇. From (2.13) and (2.15), we show that the induced connection ∇ of N is a semi-symmetric non-metric connection of N. From the facts $B(U,V)=\tilde{g}(\tilde{\nabla}_U V,\xi)$ and $D(U,V)=\tilde{g}(\tilde{\nabla}_U V,Z)$, we know that B and D are independent of the choice of $S(TN)$ and satisfy

$$B(U,\xi)=0,\ D(U,\xi)=-\varepsilon\psi(U),\ \forall U\in\Gamma(TN). \tag{2.16}$$

Therefore one obtains

$$B(U,V)=g(A^*_\xi U,V),\quad g(A^*_\xi U,L)=0, \tag{2.17}$$

$$C(U,QV)=g(A_L U,QV),\quad g(A_L U,L)=0, \tag{2.18}$$

$$D(U,QV)=g(A_Z U,QV),\quad g(A_Z U,L)=\rho(U), \tag{2.19}$$

$$D(U,V)=g(A_Z U,V)-\psi(U)\eta(V),\quad \forall U,V\in\Gamma(TN). \tag{2.20}$$

By (2.17) and (2.18), A^*_ξ and A_L are $\Gamma(S(TN))-$valued shape operators related to B and D, respectively and $A^*_\xi\xi=0.$

Using (2.7), (2.12) and (2.16), one derives

$$\tilde{\nabla}_U\xi=-A^*_\xi U-\tau(U)\xi-\varepsilon\psi(U)Z, \tag{2.21}$$

for any $U\in\Gamma(TN)$.

Definition 1. *A half lightlike submanifold (N,g) of a semi-Riemannian manifold $(\tilde{N},\tilde{g})$ is said to be irrotational [31] if $\tilde{\nabla}_U\xi\in\Gamma(TN)$ for any $U\in\Gamma(TN)$. From (2.16) and (2.21), the definition of irrotational is equivalent to the condition $\psi(U)=0$, that is, $D(U,\xi)=0$ for any $U\in\Gamma(TN)$.*

Definition 2. *A half lightlike submanifold (N,g) of a semi-Riemannian manifold $(\tilde{N},\tilde{g})$ is called umbilical N, if there is a smooth vector field $H\in\Gamma(tr(TN))$ on any coordinate neighborhood U such that*

$$h(U,V)=Hg(U,V) \tag{2.22}$$

for any $U,V\in\Gamma(TN)$, where

$$h(U,V)=B(U,V)L+D(U,V)Z \tag{2.23}$$

is the global second fundamental form tensor of N. In the case $H=0$ on U, we say that N is totally geodesic [32].

It is easy to see that N is totally umbilical iff, on each coordinate neighborhood U, there exist smooth vector functions λ and δ such that

$$B(U,V)=\lambda g(U,V),\quad D(U,V)=\delta g(U,V), \tag{2.24}$$

for any $U,V\in\Gamma(TN)$.

Definition 3. *We say that the screen distribution $S(TN)$ of N is totally umbilical [32] in N if there is a smooth function γ on any coordinate neighborhood $U\subset N$ such that*

$$D(U,QV)=\gamma g(U,V), \tag{2.25}$$

for any $U,V \in \Gamma(TN)$. *If* $\gamma = 0$ *on* U, *then we say that* $S(TN)$ *is totally geodesic in* N.

Furthermore, $(N,g,S(TN))$ is called minimal if it is irrotational and

$$trace_{S(TN)}h = 0, \tag{2.26}$$

where $trace_{S(TN)}$ denotes the trace restricted to $S(TN)$ concerning the degenerate metric g [33].

Let $(N,g,S(TN))$ be a $(m+1)-$dimensional half-lightlike submanifold and $\{e_1,...,e_m\}$ be an orthonormal basis of $\Gamma(S(TN))$. Let us consider

$$\mu_1 = \frac{1}{m}\sum_{j=1}^{m} B(e_j,e_j),\ \mu_2 = \frac{1}{m}\sum_{j=1}^{m} D(e_j,e_j). \tag{2.27}$$

Then it is clear from (2.26) and (2.27) that ∇ is minimal if and only if $\mu_1 = \mu_2 = 0$.

A lightlike hypersurface (N,g) of a semi-Riemannian manifold $(\tilde{N},\tilde{g})$ is called *screen locally conformal* if the shape operators A_L and A_ξ^* of N and $S(TN)$, respectively, are related by

$$A_L = \phi A_\xi^*, \tag{2.28}$$

i.e.,

$$C(U,PV) = \phi B(U,V),\ \ \forall U,V \in \Gamma(TN), \tag{2.29}$$

where ϕ is a non-vanishing smooth function on a neighborhood U in N. In particular, if ϕ is a non-zero constant, N is called screen homothetic [34].

We denote by $\tilde{R}$, R and R^* the curvature tensors of the semi-symmetric metric connection $\tilde{\nabla}$ on $\tilde{N}$, the induced connection ∇ on N and the induced connection ∇^* on $S(TN)$, respectively. Using the Gauss-Weingarten equations (2.7)-(2.12) for N and $S(TN)$, we obtain the Gauss-Codazzi equations for N and $S(TN)$:

$$\begin{aligned}\tilde{g}(\tilde{R}(U,V)W,QT) &= g(R(U,V)W,QT)\\ &\quad + B(U,W)C(V,QT) - B(V,W)C(U,QT)\\ &\quad + D(U,W)D(V,QT) - D(V,W)D(U,QT),\end{aligned} \tag{2.30}$$

$$\begin{aligned}\tilde{g}(\tilde{R}(U,V)W,\xi) &= (\nabla_U B)(V,W) - (\nabla_V B)(U,W)\\ &\quad + [\tau(U) - \pi(U)]B(V,W) - [\tau(V) - \pi(V)]B(U,W)\\ &\quad + \psi(U)D(V,W) - \psi(V)D(U,W),\end{aligned} \tag{2.31}$$

$$\begin{aligned}\tilde{g}(\tilde{R}(U,V)W,L) &= g(R(U,V)W,L)\\ &\quad + \rho(V)D(U,W) - \rho(U)D(V,W),\end{aligned} \tag{2.32}$$

$$\begin{aligned}\tilde{g}(\tilde{R}(U,V)\xi,L) &= g(A^*_\xi U, A_L V) - g(A^*_\xi V, A_L U) \\ &\quad -2d\tau(U,V) + \rho(U)\psi(V) - \rho(V)\psi(U),\end{aligned} \tag{2.33}$$

$$\begin{aligned}g(R(U,V)QW,QT) &= g(R^*(U,V)W,QT) + B(V,QT)C(U,QW) \\ &\quad -B(U,QT)C(V,QW),\end{aligned} \tag{2.34}$$

$$\begin{aligned}\tilde{g}(R(U,V)QW,L) &= (\nabla_U C)(V,QW) - (\nabla_V C)(U,QW) \\ &\quad +[\tau(V)+\pi(V)]C(U,QW) - [\tau(U)+\pi(U)]C(V,QW),\end{aligned} \tag{2.35}$$

for any $U,V,W,T \in \Gamma(TN)$ [35].

Now let us choose a $2-$dimensional non-degenerate plane section

$$\Pi = Span\{U,V\}, \tag{2.36}$$

in T_pN, $p \in N$. Then the sectional curvature at p is expressed by [36]

$$K(\Pi) = \frac{g(R(U,V)V,U)}{g(U,U)g(V,V) - g(U,V)^2}. \tag{2.37}$$

Let $p \in N$ and ξ be a null vector of T_pN. A plane Π of T_pN is said to be null plane if it contains ξ and e_i such that $g(\xi,e_i)=0$ and $g(e_i,e_i)=\varepsilon_i=\pm 1$. The null sectional curvature of Π is defined by

$$K_i^{null} = \frac{g(R_p(e_i,\xi)\xi,e_i)}{g_p(e_i,e_i)}.$$

The Ricci tensor $\overline{Ric}$ of $\tilde{N}$ and the induced Ricci type tensor $R^{(0,2)}$ of N are given by

$$\begin{aligned}\overline{Ric}(U,V) &= trace\{W \to \tilde{R}(W,U)V\}, \ \ \forall U,V \in \Gamma(T\tilde{N}), \\ R^{(0,2)}(U,V) &= trace\{W \to R(W,U)V\}, \ \ \forall U,V \in \Gamma(TN),\end{aligned} \tag{2.38}$$

where

$$R^{(0,2)}(U,V) = \sum_{i=1}^{m} \varepsilon_i g(R(e_i,U)V,e_i) + \tilde{g}(R(\xi,U)V,L) \tag{2.39}$$

for the quasi-orthonormal frame $\{e_1,...,e_m,\xi\}$ of T_pN. From the equations (2.30)-(2.33), it can be shown that the Ricci type tensor doesn't need to be symmetric as the sectional curvature map. This tensor is called Ricci tensor if it is symmetric.

One defines scalar curvature τ by

$$\tau(p) = \sum_{i,j=1}^{m} K_{ij} + \sum_{i=1}^{m} K_i^{null} + K_{iL}, \tag{2.40}$$

where $K_{iL} = \tilde{g}(R(\xi,e_i)e_i,L)$ for $i \in \{1,...,m\}$.

3. CHEN LIKE INEQUALITIES FOR HALF-LIGHTLIKE SUBMANIFOLDS

Let N be a $(m+1)-$dimensional half lightlike submanifold of a $(m+3)-$dimensional of a Lorentzian manifold $\tilde{N}$ with a semi-symmetric metric connection and $\{e_1,....,e_m,\xi\}$ be a basis of $\Gamma(TN)$ where $\{e_1,....,e_m\}$ be an orthonormal basis of $\Gamma(S(TN))$. For $k \le m$, we establish $\pi_{k,\xi} = sp\{e_1,....,e_k,\xi\}$ is a $(k+1)-$dimensional degenerate plane section and $\pi_k = sp\{e_1,....,e_k\}$ is $k-$dimensional non-degenerate plane section. The $k-$degenerate Ricci curvature and the $k-$Ricci curvature are defined by

$$Ric_{\pi_{k,\xi}}(U) = R^{(0,2)}(U,U) = \sum_{j=1}^{k} g(R(e_j,U)U,e_j) + \overset{\frown}{g}(R(\xi,U)U,L), \tag{3.1}$$

$$Ric_{\pi_k}(U) = R^{(0,2)}(U,U) = \sum_{j=1}^{k} g(R(e_j,U)U,e_j), \tag{3.2}$$

respectively for a unit vector $U \in \Gamma(TN)$. Also, $k-$degenerate scalar curvature and $k-$scalar curvature are at $p \in N$ are given by

$$\tau_{\pi_{k,\xi}}(p) = \sum_{i,j=1}^{k} K_{ij} + \sum_{i=1}^{k} K_i^{null} + K_{iL}, \tag{3.3}$$

$$\tau_{\pi_k}(p) = \sum_{i,j=1}^{k} K_{ij}, \tag{3.4}$$

respectively. For $k = m$, $\pi_m = sp\{e_1,....,e_m\} = \Gamma(S(TN))$, we have the screen Ricci curvature and the screen scalar curvature given by

$$Ric_{S(TN)}(e_1) = Ric_{\pi_m}(e_1) = \sum_{j=1}^{m} K_{1j} = K_{12} + ... + K_{1m}, \tag{3.5}$$

and

$$\tau_{S(TN)} = \sum_{i,j=1}^{m} K_{ij}, \tag{3.6}$$

respectively.

Let $\tilde{N}(c)$ be a real space form of constant sectional curvature c endowed with a semi-symmetric metric connection $\tilde{\nabla}$. The curvature tensor $\overset{\circ}{\tilde{R}}$ concerning the Levi-Civita connection $\overset{\circ}{\tilde{\nabla}}$ on $\tilde{N}(c)$ is expressed by

$$\tilde{g}(\overset{\circ}{\tilde{R}}(U,V)W,QT) = c\{g(U,T)g(V,W) - g(V,T)g(U,W)\}. \tag{3.7}$$

Using (2.2), we have the relation between the curvature tensor $\overset{\circ}{\tilde{R}}$ concerning the Levi-Civita connection $\overset{\circ}{\tilde{\nabla}}$ and the curvature tensor $\tilde{R}$ concerning the semi-symmetric metric connection $\tilde{\nabla}$ given by

$$\tilde{g}(\tilde{R}(U,V)W,QT) = \tilde{g}(\overset{\circ}{\tilde{R}}(U,V)W,QT) - \alpha(V,W)g(U,T) + \alpha(U,W)g(V,T) \\ -\alpha(U,T)g(V,W) + \alpha(V,T)g(U,W), \tag{3.8}$$

for any vector fields $U,V,W,T \in \Gamma(TN)$, where α is a $(0,2)$ tensor field defined by

$$\alpha(U,V) = (\overset{\circ}{\tilde{\nabla}}_U \pi)V - \pi(U)\pi(V) + \frac{1}{2}\pi(Q)g(U,V) \tag{3.9}$$

[20].

From (2.30), (3.6), (3.7) and (3.8), we can write

$$\tau_{S(TN)}(p) = m(m-1)c - 2(m-1)\lambda + \sum_{i,j=1}^{m} B_{ii}C_{jj} - B_{ij}C_{ji} + \sum_{i,j=1}^{m} D_{ii}D_{jj} - D_{ij}D_{ji}, \tag{3.10}$$

where λ is the trace of α and $B_{ij} = B(e_i,e_j)$, $C_{ij} = C(e_i,e_j)$, $D_{ij} = D(e_i,e_j)$ for $i,j \in \{1,...,m\}$.

Let N be a screen homothetic half lightlike submanifold of a $(m+3)-$dimensional Lorentzian space form $\tilde{N}(c)$. From the Gauss-Codazzi equations and using (2.29) and (3.10) we have the following equations:

$$\tau_{S(TN)}(p) = m(m-1)c - 2(m-1)\lambda + \phi m^2\mu_1^2 + m^2\mu_2^2 - \sum_{i,j=1}^{m}[\phi(B_{ij})^2 + (D_{ij})^2]. \tag{3.11}$$

Theorem 4. *Let N be a $(m+1)-$dimensional screen homothetic half lightlike submanifold of a $(m+3)-$dimensional Lorentzian space form $\tilde{N}(c)$ of constant sectional curvature c, endowed with a semi-symmetric metric connection $\tilde{\nabla}$.*

a) If $\phi > 0$, then

$$\tau_{S(TN)}(p) \le m(m-1)c - 2(m-1)\lambda + \phi m^2\mu_1^2 + m^2\mu_2^2. \tag{3.12}$$

The equality case of (3.12) holds if and only if $S(TN)$ is totally geodesic and for $\forall U,V \in \Gamma(S(TN))$, $D(U,V) = 0$.

b) If $\phi < 0$, then

$$\tau_{S(TN)}(p) \ge m(m-1)c - 2(m-1)\lambda + \phi m^2\mu_1^2 + m^2\mu_2^2 - \sum_{i,j=1}^{m}(D_{ij})^2. \tag{3.13}$$

The equality case of (3.13) holds if and only if $S(TN)$ is totally geodesic.

Proof. The proof is obvious from (3.11).

The following corollary is obtained from the previous theorem.

Corollary 5. *Let N be a $(m+1)-$dimensional irrotational screen homothetic half lightlike submanifold of a $(m+3)-$dimensional Lorentzian space form $\tilde{N}(c)$ of constant sectional curvature c, endowed with a semi-symmetric metric connection $\tilde{\nabla}$.*

a) If $\phi > 0$, then

$$\tau_{S(TN)}(p) \le m(m-1)c - 2(m-1)\lambda + \phi m^2\mu_1^2 + m^2\mu_2^2. \tag{3.14}$$

The equality of (3.14) holds if and only if N is totally geodesic.

b) If $\phi < 0$, then

$$\tau_{S(TN)}(p) \ge m(m-1)c - 2(m-1)\lambda + \phi m^2\mu_1^2 + m^2\mu_2^2 - \sum_{i,j=1}^{m}(D_{ij})^2. \tag{3.15}$$

The equality of (3.15) holds if and only if $S(TN)$ is totally geodesic on N.

Furthermore, the second fundamental form B and the screen second fundamental form C provide

$$\sum_{i,j=1}^{m} B_{ij}C_{ji} = \frac{1}{2}\left\{\sum_{i,j=1}^{m}(B_{ij}+C_{ji})^2 - \sum_{i,j=1}^{m}(B_{ij})^2 + (C_{ji})^2\right\} \tag{3.16}$$

and

$$\sum_{i,j=1}^{m} B_{ii}C_{jj} = \frac{1}{2}\left\{\left(\sum_{i,j=1}^{m} B_{ii} + C_{jj}\right)^2 - \left(\sum_{i=1}^{m} B_{ii}\right)^2 - \left(\sum_{j=1}^{m} C_{jj}\right)^2\right\}. \tag{3.17}$$

Theorem 6. *Let N be a $(m+1)-$dimensional half lightlike submanifold of a $(m+3)-$dimensional Lorentzian space form $\tilde{N}(c)$ of constant sectional curvature c, endowed with a semi-symmetric metric connection $\tilde{\nabla}$. Then*

$$\begin{aligned}\tau_{S(TN)}(p) \le{}& m(m-1)c - 2(m-1)\lambda + m\mu_1 trace(\tilde{A}_L) \\ &+ m^2\mu_2^2 + \frac{1}{4}\sum_{i,j=1}^{m}(B_{ij}-C_{ji})^2.\end{aligned} \tag{3.18}$$

The equality case of (3.18) satisfies if and only if either $\phi = -1$ or B vanishes on N and C and D vanish on $S(TN)$.

Proof Using (3.10) and (3.16), we have

$$\begin{aligned}\tau_{S(TN)}(p) &= m(m-1)c - 2(m-1)\lambda + \sum_{i,j=1}^{m} B_{ii}C_{jj} \\ &\quad -\frac{1}{2}\left\{\sum_{i,j=1}^{m}(B_{ij}+C_{ji})^2 - \sum_{i,j=1}^{m}(B_{ij})^2 + (C_{ji})^2\right\} \\ &\quad + \sum_{i,j=1}^{m} D_{ii}D_{jj} - (D_{ij})^2.\end{aligned} \tag{3.19}$$

since

$$\frac{1}{2}((B_{ij})^2 + (C_{ji})^2) = \frac{1}{4}(B_{ij}+C_{ji})^2 + \frac{1}{4}(B_{ij}-C_{ji})^2, \tag{3.20}$$

from (3.19) and (3.20)

$$\begin{aligned}\tau_{S(TN)}(p) &= m(m-1)c - 2(m-1)\lambda + m\mu_1 trace(\tilde{A}_L) - \frac{1}{4}\sum_{i,j=1}^{m}(B_{ij}+C_{ji})^2 \\ &\quad + \frac{1}{4}\sum_{i,j=1}^{m}(B_{ij}-C_{ji})^2 + m^2\mu_2^2 - \sum_{i,j=1}^{m}(D_{ij})^2\end{aligned} \tag{3.21}$$

is obtained. Thus, we get equation (3.18). The equality case of (3.18) satisfies if and only if $B_{ij} = -C_{ij}$ and $D_{ij} = 0$, in the other word, either $\phi = -1$ or local second fundamental form B vanishes on TN and local second fundamental forms C and D vanish on $S(TN)$.

Theorem 7. *Let N be a $(m+1)-$dimensional half lightlike submanifold of a $(m+3)-$dimensional Lorentzian space form $\tilde{N}(c)$ of constant sectional curvature c, endowed with a semi-symmetric metric connection $\tilde{\nabla}$. Then we have*

$$\begin{aligned}\tau_{S(TN)}(p) &\le m(m-1)c - 2(m-1)\lambda + \frac{1}{2}trace(\tilde{A}_L)^2 \\ &\quad + m^2\mu_2^2 + \frac{1}{4}\sum_{i,j=1}^{m}(B_{ij}-C_{ji})^2\end{aligned} \tag{3.22}$$

where

$$\tilde{A}_L = \begin{pmatrix} B_{11}+C_{11} & B_{12}+C_{12} & \dots & B_{1m}+C_{1m} \\ B_{21}+C_{21} & B_{22}+C_{22} & \dots & B_{2m}+C_{2m} \\ & & & \\ B_{m1}+C_{m1} & B_{m2}+C_{m2} & \dots & B_{mm}+C_{mm} \end{pmatrix}. \tag{3.23}$$

The equality case of (3.23) holds for all $p \in N$ if and only if $\mu_1 = \mu_2 = trace(\tilde{A}_L) = 0.$

Proof. Using (3.17) and (3.21), we obtain

$$\begin{aligned}\tau_{S(TN)}(p) &= m(m-1)c - 2(m-1)\lambda \\ &+\frac{1}{2}\left\{\left(\sum_{i,j=1}^{m}(B_{ii}+C_{jj})\right)^2 - \left(\sum_{i=1}^{m}B_{ii}\right)^2 - \left(\sum_{j=1}^{m}C_{jj}\right)^2\right\} \\ &-\frac{1}{4}\sum_{i,j=1}^{m}(B_{ij}+C_{ji})^2 + \frac{1}{4}\sum_{i,j=1}^{m}(B_{ij}-C_{ji})^2 \\ &+\sum_{i,j=1}^{m}D_{ii}D_{jj} - (D_{ij})^2.\end{aligned} \tag{3.24}$$

From equation (3.24), the inequality (3.22) is obtained and it is clear that the equality case of (3.22) holds if and only if $\mu_1 = \mu_2 = trace(\tilde{A}_L)$, $B_{ij} = -C_{ji}$ and $D_{ij} = 0$.

The following corollaries is obtained from the previous theorem.

Corollary 8. *Let N be a $(m+1)-$dimensional irrotational half lightlike submanifold of a $(m+3)-$dimensional Lorentzian space form $\tilde{N}(c)$ of constant sectional curvature c, endowed with a semi-symmetric metric connection $\tilde{\nabla}$. Then we have*

$$\begin{aligned}\tau_{S(TN)}(p) &\le m(m-1)c - 2(m-1)\lambda + \frac{1}{2}trace(\tilde{A}_L)^2 \\ &+m^2\mu_2^2 + \frac{1}{4}\sum_{i,j=1}^{m}(B_{ij}-C_{ji})^2,\end{aligned} \tag{3.25}$$

where $\tilde{A}_L$ is as defined in (3.23). The equality case of (3.25) holds for all $p \in N$ if and only if N is minimal.

Corollary 9. *Let N be a $(m+1)-$dimensional irrotational screen homothetic half lightlike submanifold of a $(m+3)-$dimensional Lorentzian space form $\tilde{N}(c)$ of constant sectional curvature c, endowed with a semi-symmetric metric connection $\tilde{\nabla}$. Then we derive*

$$\begin{aligned}\tau_{S(TN)}(p) &\le m(m-1)c - 2(m-1)\lambda + \frac{(\phi+1)^2}{2}m^2\mu_1^2 \\ &+m^2\mu_2^2 + \frac{(\phi-1)^2}{4}\sum_{i,j=1}^{m}(B_{ij})^2.\end{aligned} \tag{3.26}$$

The equality case of (3.26) holds for all $p \in N$ if and only if N is minimal. That is, $S(TN)$ is umbilical in N. The converse is trivial.

REFERENCES

[1] Kupeli, D. N., (1996). *Singular semi-Riemannian Geometry*, Kluwer Academic Publishers, Dordrecht.

[2] Duggal, K. L., Bejancu, A., (1996). *Lightlike Submanifolds of Semi-Riemannian Manifolds and Applications*, Kluwer Academic Publishers, Dordrecht.

[3] Duggal, K. L., Jin, D. H. (2007). *Null curves and Hypersurfaces of Semi-Riemannian Manifolds*, World Scientific.

[4] Duggal, K. L. and Sahin, B., (2010). *Differential Geometry of Lightlike Submanifolds*, Birkhäuser, Basel.

[5] Jin, D. H. (2010). Half lightlike submanifolds with totally umbilical screen distributions, J. *Korean Soc. Math. Educ. Ser. B Pure Appl. Math.*, 17(1): 29-38.

[6] Hayden, H. A., (1932). Subspace of a space with torsion, *Proceedings of the London Mathematical Society II Series*, 34: 27-50.

[7] Yano, K., (1970). On Semi-Symmetric Metric Connection, *Rev. Roum. Math. Pures Et Appl.*, 15: 1579-1586.

[8] Nakao, Z., (1976). Submanifolds of a Riemannian manifold with semi-symmetric metric connections, *Proc. Amer. Math. Soc.*, 54: 261-266.

[9] Duggal, K. L., and Sharma, R., (1986). Semi-Symmetric metric connection in a Semi-Riemannian Manifold, *Indian J. Pure appl Math.*, 17: 1276-1283.

[10] Konar, A. and Biswas, B., (2001). Lorentzian Manifold that Admits a type of Semi-Symmetric Metric Connection, *Bull. Cal. Math., Soc.*, 93(5): 427-437.

[11] Yaşar, E., Çöken, A. C., Yücesan, A., (2007). Lightlike Hypersurfaces of Semi-Riemannian Manifold with Semi-Symmetric Metric Connection, *Kuweyt Journal of Science and Engineering*, 34(2A): 11-24.

[12] Akyol, M. A., Vanlı, A. T. And Fernandez, L. M., (2013). Curvature properties of a semi symmetric metric connection on S manifolds., *Annales Polonici Mathematici*, 107(1): 71-86.

[13] Chen, B. Y., (1993). Some pinching and classification theorems for minimal submanifolds, *Arch. math.*, (Basel), 60(6): 568-578.

[14] Tripathi, M. M., (2003). Certain Basic Inequalities for Submanifolds in (;) Space, *Recent Advances in Riemannian and Lorentzian Geometries*, Baltimore, 187-202.

[15] Chen, B. Y., (1998). Strings of Riemannian invariants, inequalities, ideal immersions and their applications, *The Third Pacific Rim Geometry Conference* (Seoul, 1996), 7-60, *Monogr. Geom. Topology*, 25, Int. Press, Cambridge, MA,.

[16] Chen, B. Y., (2000). Some new obstructions to minimal and Lagrangian isometric immersions, *Japanese J. Math.*, 26: 105-127.

[17] Chen, B. Y., (2008). $\delta-$invariants, Inequalities of Submanifolds and Their Applications, in Topics in Differential Geometry, Eds. A. Mihai, I. Mihai, R. Miron, *Editura Academiei Romane*, Bucuresti, 29-156.

[18] Chen, B. Y., Dillen, F., Verstraelen, L. and Vrancken, V., (2000). Characterizations of Riemannian space forms, Einstein spaces and conformally flat spaces, *Proc. Amer. Math. Soc.*, 128: 589-598.

[19] Hong, S., Matsumoto K. and Tripathi, M. M. , (2005). Certain basic inequalities for submanifolds of locally conformal Kaehlerian space forms, *SUT J. Math.*, 4(1): 75-94.

[20] Imai, T., (1972). Hypersurfaces of a Riemannian Manifold with Semi-Symmetric Metric Connection, *Tensor, N.S.*, 23: 300-306.

[21] Imai, T., (1972). Notes on Semi-Symmetric Metric Connection, *Tensor, N.S.*, 24: 293-296.

[22] Kim, J. S., Choi, J., (2003). A basic inequality for submanifolds in a cosymplectic space form, *Int. J. Math. Math. Sci.*, 9: 539-547.

[23] Matsumoto, K., Mihai, I., Oiaga, A., (2001). Ricci curvature of submanifolds in complex space forms, *Rev. Roumaine Math. Pures Appl.*, 46: 775-782.

[24] Mihai, A. and Özgür, C., (2010). Chen inequalities for submanifolds of real space form with a semi-symmetric metric connection, *Tawanese Journal of Mathematics*, 14(4): 1465-1477.

[25] Oiaga, A., Mihai, I., Chen, B. Y., (1999). Inequalities for slant submanifolds in complex space forms, *Demonstratio Math.*, 32: 835-846.

[26] Zhang, P., Zhang, L. and Song, W., (2014). Chen's inequalities for submanifolds of a Riemannian manifold of quasi-constant curvature with a semi-symmetric metric connection, *Taiwanese Journal of Mathematics*, 18(6): 1841-1862.

[27] Gülbahar, M., Kılıç, E. and Keleş, S., (2013). Chen-like inequalities on lightlike hypersurfaces of a Lorentzian manifold, *J. Inequal. Appl.*, 266.

[28] Gülbahar, M., Kılıç, E. and Keleş, S., (2013). Some inequalities on screen homothetic lightlike hypersurfaces of a Lorentzian manifold, *Taiwanese Journal of Mathematics*, 17(6): 2083-2100.

[29] Poyraz, N. Ö., Doğan, B. and Yaşar, E., (2017). Chen Inequalities on Lightlike Hypersurface of a Lorentzian manifold with semi-symmetric metric connection, *Int. Electronic Journal of Geometry*, 10(1): 1-14.

[30] Gülbahar, M., Kılıç, E., (2017). Some optimal inequalities for screen conformal half-lightlike submanifolds, *Acta Mathematica Academiae Paedagogicae Nyíregyháziensis*, 33(2): 315-329.

[31] Duggal, K. L. and Jin, D. H., (1999). Half lightlike submanifolds of codimension 2, *Math. J. Toyama Univ*, 22: 121-161.

[32] Bejan, C. L. and Duggal, K. L., (2005). Global lightlike manifolds and harmonicity, *Kodai Math. J.*, 28(1): 131-145.

[33] Duggal, K. L. and Sahin, B., (2004). Screen conformal half-lightlike submanifolds, *Int. J. Math. and Math. Sci.*, 68: 3737-3753.

[34] Jin, D. H., (2011). Geometry of half lightlike submanifolds of a semi-Riemannian space form with a semi-symmetric metric connection, *J. Chungcheong Math. Soc.*, 24(4): 769-780.

[35] Beem, J. K., Ehrlich, P. E. and Easley, K. L., (1996). Global Lorentzian geometry, *Volume 202 of Monographs and Textbooks in Pure and Applied Mathematics*, Marcel Dekker, Inc., New York.

[36] De Smet, P. J., Dillen, F., Verstraelen, L. and Vrancken, V., (1999). A pointwise inequality in submanifold theory, *Arch. Math. (Brno)*, 5(2): 115-128.

NATURENGS
MTU Journal of Engineering and Natural Sciences
https://dergipark.org.tr/tr/pub/naturengs
DOI: 10.46572/nat.2020.19

The Effect of Align Parameter on Scattering Parameter for Pseudomorphic High Electron Mobility Transistor

Gökhan SATILMIŞ*
Electric and Electronic Engineering, Engineering and Architecture, Muş Alparslan University, Muş, Turkey

(**Received:** 06.12.2020; **Accepted:** 30.12.2020)

ABSTRACT: In this paper, various physical device simulation of pseudomorphic High Electron Mobility Transistors are realized to show the effect of aligning parameter on scattering parameters. S parameters are complex numbers, so both real and imaginer part of scattering parameters are plotted concerning frequency at different align parameters. In all figures, a brief explanation about the change of the S parameter for frequency and align parameter is provided. The effect of the align parameter, which has a value of 0.4 differs from other align parameter values such as 0.45, 0.5, 0.55 and 0.6 on scattering parameters of the transistor structure.

Keywords: PHMET, Scattering parameters, Align parameter, Device simulation.

1. INTRODUCTION

The name HEMT transistor is referred to as High Electron Mobility Transistor. The transistor is a type of field-effect transistor. The HEMT transistor is structured with a narrow channel, which enables operating at high frequencies. The device structure incorporates a junction of two materials with different energy band gaps. The development of HEMT transistor goes back to the 1980s, when its cost is high, so the applications of the transistor are limited. Nowadays, the production cost of HEMT transistor is low comparing to the past, so the application of the transistor are common in communication technologies such as microwave radio communication, mobile communication, and RF (Radio Frequency) design circuits [1-4]. The pseudomorphic High Electron Mobility Transistor (pHEMT) [5-9] is modeled and used for various applications such as low noise amplifier, power amplifier, oscillator or mixers. Transistors are considered as two-port networks for designing circuits, and scattering (S) parameters are the main parameters for calculating the performance of the design circuits. In other words, transistors are modeled as two-port networks, where the input port gate electrode and the output port is a drain electrode. S parameters of these two-port networks affect the performance of the designed circuits. S parameters are modeled with various optimization algorithms and neural networks [10]. Physical parameter based modeling of S parameter is realized in this study [11, 12] using symbolic regression, and novel classification algorithms. The power gain and stability of the microwave circuit can be defined by S parameters [13-17]. S parameters are dependent on various parameters such as bias condition parameters, device parameters and frequency. The effect of the align parameter on the S parameter is studied in this paper.

*Corresponding Author: g.satilmis@alparslan.edu.tr
ORCID number of authors: 0000-0002-8188-7242

Bandgap, which is the difference between two material energy bands cause conduction and valence band discontinues. The distribution of bandgap difference on conduction and valence band has an impact on charge transport, and so forth S parameters of the device. Align parameter is defined as a portion of the energy bandgap difference, that is applied to the conduction band of the transistor. For instance, %80 percent of the bandgap difference can be assigned to material 1 and material 2 to the conduction band offset by setting the align parameter to 0.8.

In this study, the effect of the align parameter on S parameters is expressed from 1 GHz to 100 GHz for pHEMT structure. The align parameter is ranged from 0.4 to 0.6 with a step of 0.5. This study is realized using a physical device simulator. S parameters are complex numbers, so real and imaginer parts of S parameters are calculated and plotted on a cartesian coordinate system.

2. DEVICE SIMULATION

A physics-based device simulator is chosen in this study. Physics-based device simulators calculate the electrical characteristics of the structure given bias conditions. The simulator uses a numerical method such as Newton, Gummel or Block method. [18]. As a result, the device can be modeled in AC for S parameter analysis. The major advantages of a physical-based device simulator are being predictive, providing insight into the structure. Moreover, physics-based device simulation is compared to actual experiments, it has many advantages such as being faster, being cheaper and providing information, that requires extensive work using experimental work.

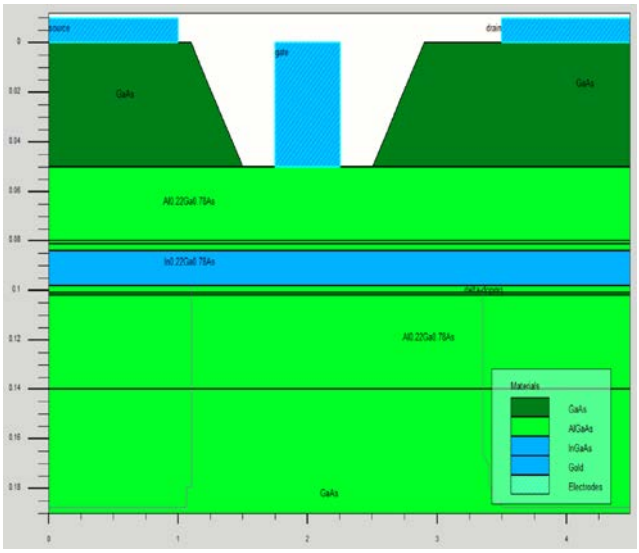

Figure 1. pHEMT Structure [19]

In Figure 1, the pHEMT structure is shown and the architecture of the transistor is referenced in [19]. Source, gate and drain electrodes are placed at the top of the structure. Source and drain electrodes are in contact with GaAs material, whereas the gate electrode in contact with $Al_{0.22}Ga_{0.78}As$ material. Delta doping, which is a very thin layer is used between $In_{0.22}Ga_{0.78}As$ material. $Al_{0.22}Ga_{0.78}As$ material is placed on GaAs substrate, and the device is symmetrical to $In_{0.22}Ga_{0.78}As$ material region if the electrodes and their contact with GaAs substrate are omitted.

The transistor is considered as two-port networks, where the gate electrode is the input port, and the drain electrode is the output port. Small signal analysis of the transistor is realized from 1 GHz to 100 GHz to exhibit the entire potential use on various applications.

3. RESULTS AND DISCUSSION

5 different physical device simulations are realized for showing the effect of the align parameter. The values of these parameters are listed in Table 1. Drain voltage and gate voltage are set to 2(V) and 0 (V), respectively. The effect of the align parameter on S parameters is plotted both real and imaginer values on cartesian coordinates, separately. The effect of the align parameter on S parameters is plotted from Figure 2 to Figure 9. In all figures, the absolute value of real and imaginer part of S parameters are analyzed.

Table 1. Align Parameter Range

Align Parameter	Frequency
0.4	1,2, … 100 GHz
0.45	1,2, … 100 GHz
0.5	1,2, … 100 GHz
0.55	1,2, … 100 GHz
0.6	1,2, … 100 GHz

In Figure 2, the real part of S_{11} is plotted from 1 GHz to 100 GHz with all aligned parameters listed in Table 1. It can be seen in Figure 1 that the real part of S_{11} steadily decreases as the frequency increase. The minimum value is around 20 GHz, which makes a good return loss value. All align parameter values has almost no effect on the real part of the S_{11} parameter.

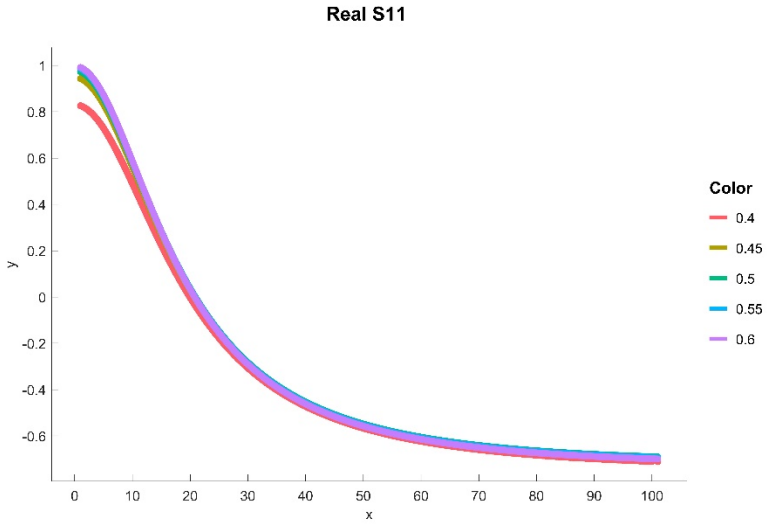

Figure 2. The effect of aligning parameter on the real part of the S_{11} parameter

In Figure 3, the imaginer part of S_{11} is plotted from 1 GHz to 100 GHz with all aligned parameters listed in Table 1. It can be seen in Figure 2 that the imaginer part of S_{11} increments until frequency reaches 20 GHz, and decrement again. All align parameter values has almost no effect on the imaginer part of the S_{11} parameter.

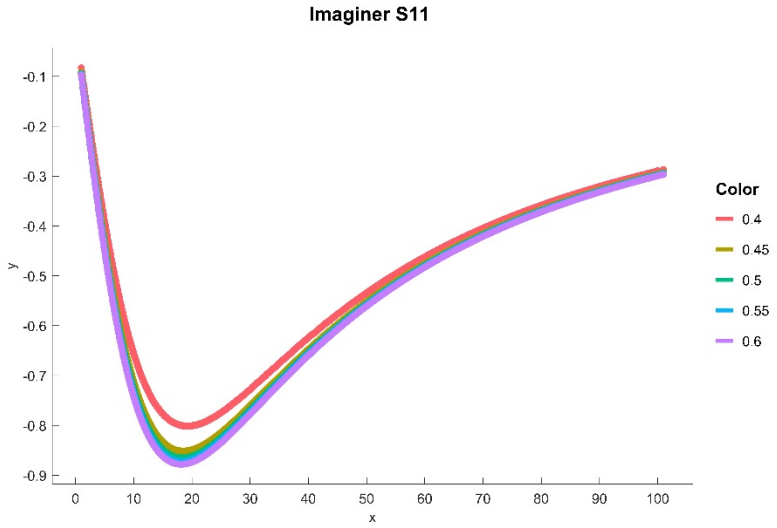

Figure 3. The effect of aligning parameter on the imaginer part of the S_{11} parameter

In Figure 4, the real part of S_{12} is plotted from 1 GHz to 100 GHz with all aligned parameters listed in Table 1. It can be seen in Figure 2 that the real part of S_{11} steadily increments as the frequency increase. Align parameter, which has a value of 0.4 has an effect on the imaginer part of the S_{11} parameter around 20 GHz, and it has no effect on other aligned parameters.

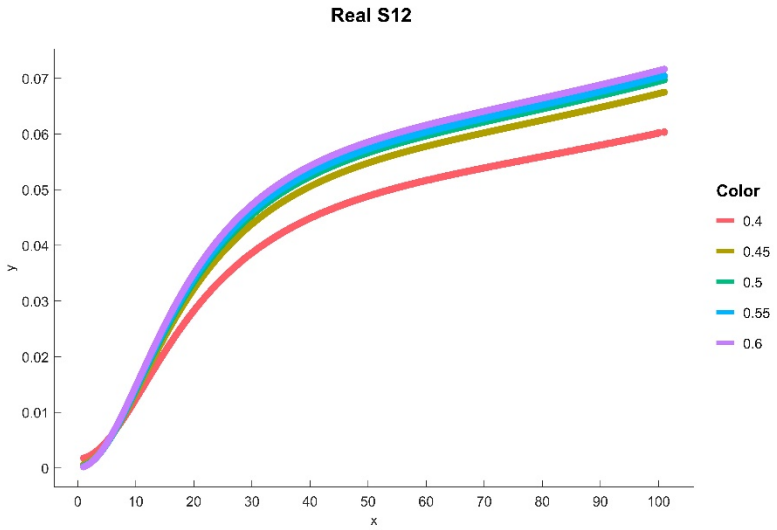

Figure 4. The effect of aligning parameter on the real part of the S_{12} parameter

In Figure 5, the imaginer part of S_{12} is plotted from 1 GHz to 100 GHz with all align parameters listed in Table 1. It can be seen in Figure 5 that the imaginer part of S_{12} increments as the frequency increase. Align parameter, which has a value of 0.4 has an effect on the real part of the S_{12} parameter, and it does not affect other aligned values.

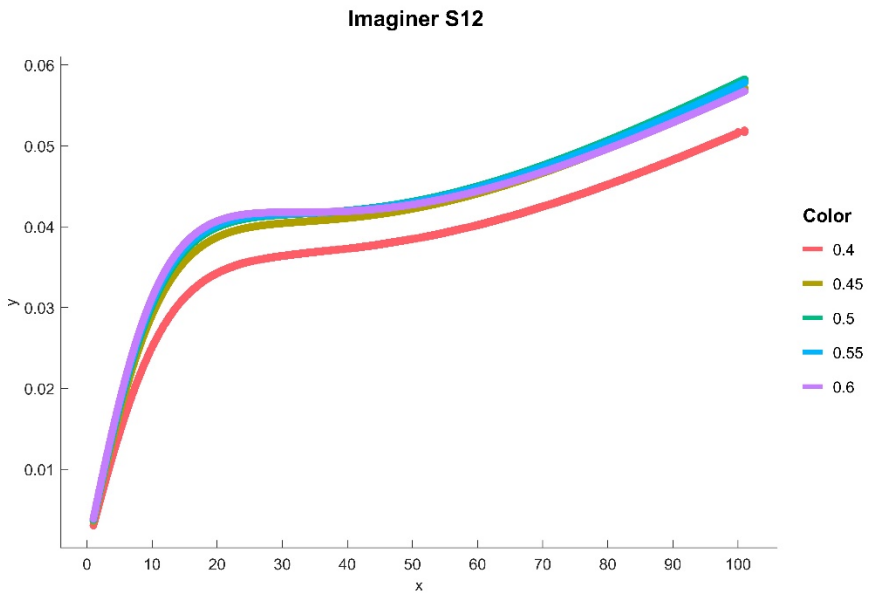

Figure 5. The effect of aligning parameter on the imaginer part of the S_{12} parameter

In Figure 6, the real part of S_{21} is plotted from 1 GHz to 100 GHz with all aligned parameters listed in Table 1. It can be seen in Figure 2 that the real part of S_{11} steadily decrements until 50 GHz, and then its sutures. All align parameter values has almost no effect on the real part of the S_{21} parameter.

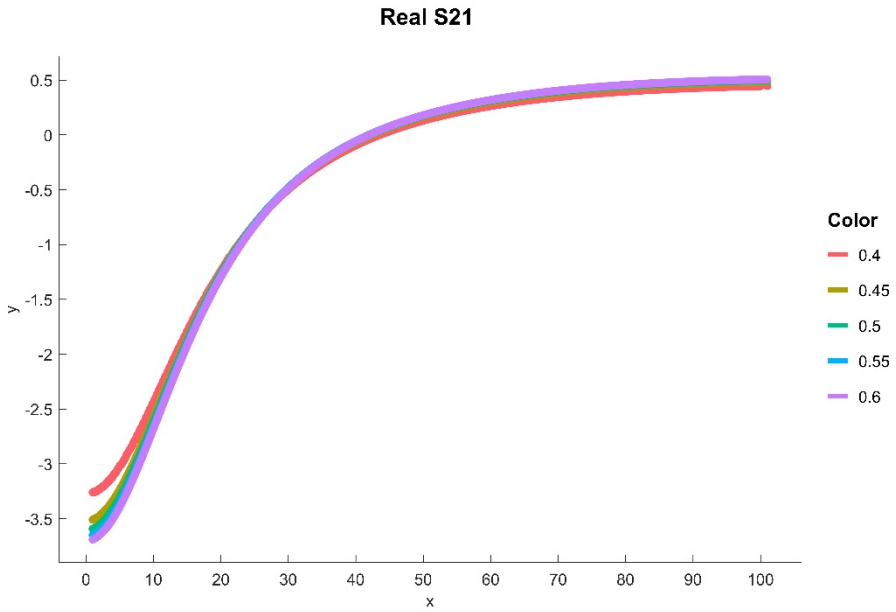

Figure 6. The effect of aligning parameter on the real part of the S_{21} parameter

In Figure 7, the imaginer part of S_{21} is plotted from 1 GHz to 100 GHz with all aligned parameters listed in Table 1. It can be seen in Figure 7 that the imaginer part of S_{21} increments until frequency reaches 20 GHz and it drops as frequency increases. Align parameter, which has a value of 0.4 has an effect on the imaginer part of the S_{21} parameter around 20 GHz, and it has no effect on other aligned parameters.

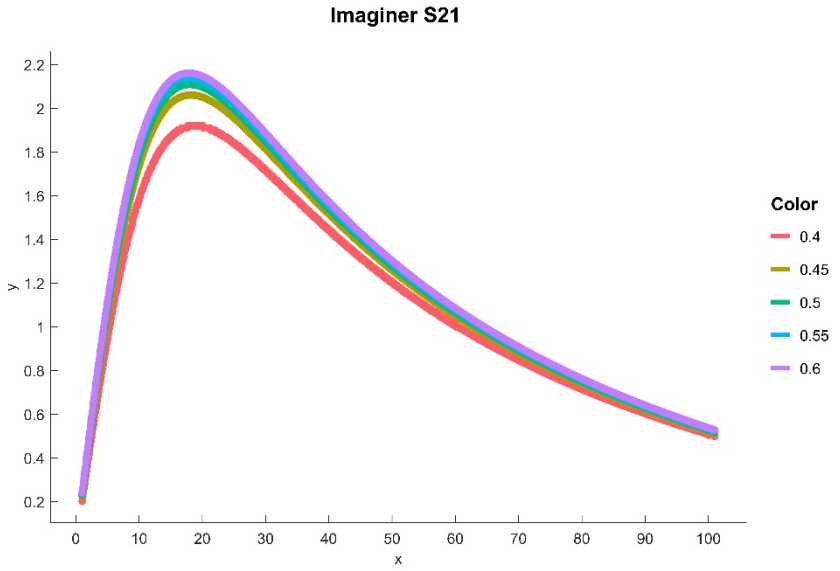

Figure 7. The effect of aligning parameter on the imaginer part of the S_{21} parameter

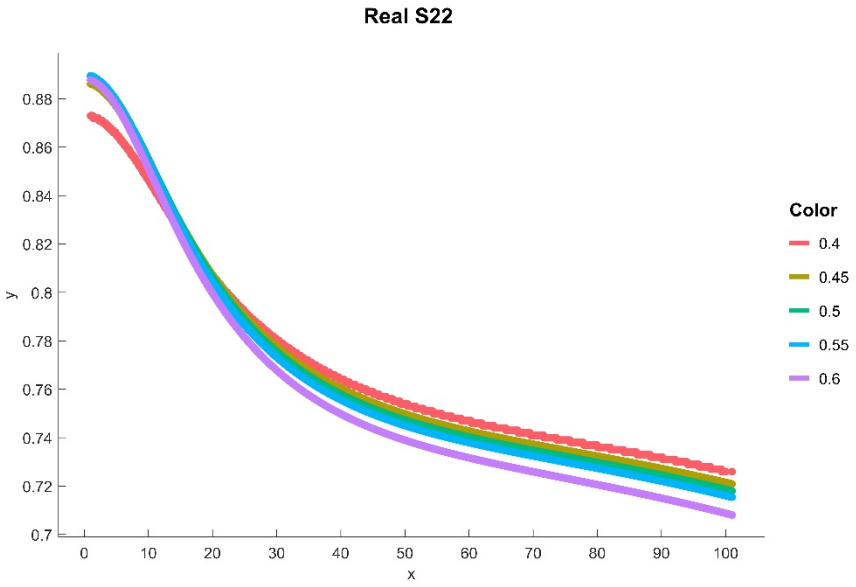

Figure 8. The effect of aligning parameter on the real part of the S_{22} parameter

In Figure 8, the real part of S_{22} is plotted from 1 GHz to 100 GHz with all aligned parameters listed in Table 1. It can be seen in Figure 8 that the real part of S_{22} steadily decreases as the frequency increase. All align parameter values has almost a limited effect on the real part of the S_{22} parameter.

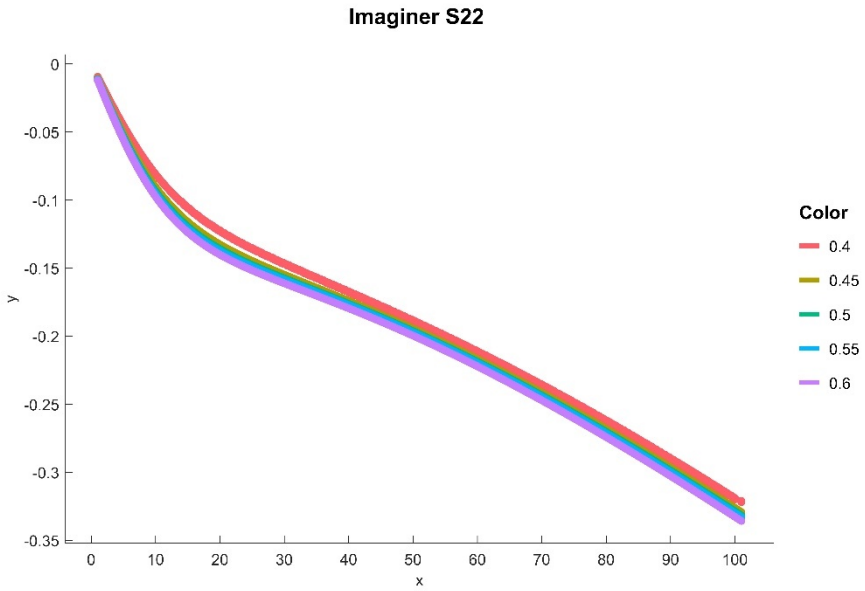

Figure 9. The effect of aligning parameter on the imaginer part of S_{22} parameter

In Figure 9, the imaginer part of S_{22} is plotted from 1 GHz to 100 GHz with all aligned parameters listed in Table 1. It can be seen in Figure 9 that the imaginer part of S_{22} increments until as frequency increase. All align parameter values has almost a limited effect on the imaginer part of the S_{22} parameter.

4. CONCLUSIONS

In this paper, two-port S parameters analysis of pHEMT structure is realized from 1 GHz to 100 GHz. 8 different both real and imaginer part of S parameters are plotted from Figure 2 to Figure 9. In all figures, a brief explanation about the change of the S parameter concerning frequency is given. Also, the effect of the align parameter on S parameters is explained in detail. In conclusion, the effect of the align parameter, which has a value of 0.4 differs from other align parameter values such as 0.45, 0.5, 0.55 and 0.6 on S parameters of pHEMT structure. The parameter range of the align parameter can be scaled up, and further analysis can be realized. An optimization algorithm, which maximizes both real and imaginer part of S_{21} while minimizing the both real and imaginer part of S_{11} and S_{22} parameter would help circuit designers for satisfying low noise amplifier circuit performance criteria.

REFERENCES

[1] Demirel, S. and Güneş, F. (2013). Performance characterization of a microwave transistor for the maximum output power and the required noise. *IET Circuits, Devices & Systems*, 7(1): 9-20.

[2] Güneş, F. and Çetiner, B.A. (1988). Smith chart formulation of performance characterization for a microwave transistor. *IEE Proceedings - Circuits, Devices and Systems*, 145(6): 419-428.

[3] Güneş, F., Güneş, M. and Fidan, M. (1994). Performance characterization of a microwave transistor. *IEE Proceedings-Circuits, Devices and Systems*, 141(5): 337-344.

[4] Güneş, F., Türker, N. and Gürgen, F. (2007). Signal-noise support vector model of a microwave transistor. *International Journal of RF and Microwave Computer-Aided Engineering*, 17(4): 404-415.

[5] Ahmad, M., Butt, H. T., Tauqeer, T. and Missous, M. (2012). *DC characterization of InGaAs/InAlAs/InP based pseudomorphic HEMT (pHEMT).* Paper presented at The Ninth International Conference on Advanced Semiconductor Devices and Microsystems.

[6] Ahmad, N., Arshad, S., and Missous, M. (2010). *New InP based pHEMT double stage differential to single-ended MMIC low noise amplifiers for SKA.* Paper presented at The Eighth International Conference on Advanced Semiconductor Devices and Microsystems.

[7] Arshad, S., Mohiuddin, M., Bouloukou, A., and Missous, M. (2008). *Physical Modelling of the Kink Effect in Strained InGaAs/InAlAs pHEMTs.* Paper presented at the 2008 International Conference on Advanced Semiconductor Devices and Microsystems.

[8] Aziz, A. A., and Missous, M. (1996). InGaP/InGaAs/GaAs pseudomorphic HEMT grown by solid source MBE. Paper presented at the Proceedings of EDMO '96.

[9] Aziz, A. A., and Missous, M. (1997). *Fabrication and characterization of AlGaAs/InGaAs/GaAs pseudomorphic HEMT with in-situ epitaxial aluminum grown by MBE.* Paper presented at the IEEE MTT/ED/AP/LEO Societies Joint Chapter United Kingdom and the Republic of Ireland Section. 1997 Workshop on High Performance Electron Devices for Microwave and Optoelectronic Applications.

[10] Güneş, F., and Demirel, S. (2016). Performance characterization of a microwave transistor subject to the noise and matching requirements. *International Journal of Circuit Theory and Applications,* 44(5): 1012-1028.

[11] Satılmış, G., Güneş, F., and Mahouti, P. (2019). Calculation of Scattering Parameters for a MESFET Transistor. *Paper presented at the 4th International Conference On Advances in Natural & Applied Sciences.*

[12] Satılmış, G., Güneş, F., and Mahouti, P. (2020). Physical parameter-based data-driven modeling of small signal parameters of a metal-semiconductor field-effect transistor. *Int J Numer Model El.*, e2840.

[13] Gao, J. (2015). *Heterojunction Bipolar Transistors for Circuit Design: Microwave Modeling and Parameter Extraction*. Wiley.

[14] Abdullah, M.R.R.B. (2018). GaAs/AlAs ASPAT Diodes for Millimetre and Sub-Millimetre Wave Applications, Ph.D., The University of Manchester (United Kingdom), Ann Arbor, 11015556.

[15] Devabhaktuni, V.K., Yagoub, M.C.E., Fang, Y., Xu, J. and Zhang, Q.Z. (2001). Neural networks for microwave modeling: Model development issues and nonlinear modeling techniques. *International Journal of RF and Microwave Computer-Aided Engineering,* 11(1): 4-21.

[16] Jegadheesan, V. and Sivasankaran, K. (2017). RF stability performance of SOI junctionless FinFET and impact of process variation, *Microelectronics Journal*, 59: 15-21.

[17] Jubadi, V.M., Zawawi, M.A.M. and Missous, M. (2014). Simulative study on physical modeling of submicrometer highly-strained In0.8Ga0.2As/AlAs resonant tunneling diode, *The Tenth International Conference on Advanced Semiconductor Devices and Microsystems*, 1-4.

[18] Dragica Vasileska, S. M. G. (2006). *Computational Electronics*: Morgan &Claypool Publishers.

[19] PHEMT High Frequency Analysis. 2020 [cited 2020 17.01.2020]; Available from: https://silvaco.com/examples/tcad/section10/example6/index.html

NATURENGS
MTU Journal of Engineering and Natural Sciences
https://dergipark.org.tr/tr/pub/naturengs
10.46572/nat.2020.20

Obtaining Activated-Carbon from Zivzik (Siirt) Pomegranate Waste by Chemical Activation and Model Dye Adsorption

Ali Ender KUYUCU[1*], Ahmet SELÇUK[2], Yunus ÖNAL[3]

[1]Chemistry, Faculty of Science, Yüzüncü Yıl University, Van, Turkey
[2]Sciences and Mathematics Education, Faculty of Education, Yüzüncü Yıl University, Van, Turkey
[3]Department of Chemical Engineering, Faculty of Engineering, Inönü University, Malatya, Turkey

(**Received:** 25.12.2020; **Accepted:** 30.12.2020)

ABSTRACT: In this study, activated carbon, obtained from Zivzik Pomegrate (Siirt-TURKEY), has been used as adsorbent matter. The activated-carbon has been prepared with chemical activation using $ZnC1_2$. BET surface area has been measured as 1513.05 m^2/g. Methylene Blue and Crystal Violet have been used as dyestuffs. It has been investigated the effect of initial pH, initial dye concentration and temperature on adsorption. Four different initials concentrations have been used for both dyestuffs. It has been observed that the initial pH does not affect the adsorption capacity. The compatibility with four different adsorption isotherms has been investigated and it is approved that it fits the Langmuir adsorption isotherm. For both dyes; R_L value, which is the dimensionless separation factor found using K_L value from Langmuir parameters, was found to be 0.001. This result shows that the adsorption process is efficient. Also, it was seen that the correlation factor R^2 for both dyes calculated from the graph drawn according to the Langmuir isotherm has a high value such as 0,999. Three different kinetic models (the pseudo first order model, the pseudo second order model and the Elovich equation) have been investigated by doing experimental studies at three different temperatures with different initial concentrations. Correlation coefficient R^2 is; for Methylene Blue 0.99 and for Crystal Violet 0.99. Since the q_e values calculated with the experimental q_e values are compatible with each other, it was observed that our study is more suitable for the Pseudo 2nd Order Kinetic model. The entropy (ΔS°) values are 51.717 J/molK for Methylene Blue and 70.817 J/molK for Crystal Violet, respectively. The positive values of ΔS° reflect the affinity of adsorbent material towards Methylene Blue and Crystal Violet. In addition, it has been observed that adsorption is reversible and endothermic.

Keywords: Adsorption, Activated carbon, Dye, İsotherm, Kinetic.

1. INTRODUCTION

Textile industry wastewaters contain a wide variety of organic materials, heavy metals, dissolved salts, color, turbidity, and discharging to the external environment at different pH's and require first degree treatment. Uncontrolled delivery of textile industry waste water to the environment without treatment is dangerous for both human health and the ecosystem [1].

Many methods and materials have been developed by scientists to remove pollution due to increasing environmental pollution. One of these methods is the adsorption technique.

*Corresponding Author: ali.ender@hotmail.com
ORCID number of authors: [1] 0000-0001-6247-4285, [2] 0000-0002-1566-6089, [3] 0000-0001-6342-6816

Studies in the field of adsorption have been showing a rapid increase in proportion with environmental awareness since the 1970s. In this context, adsorption is a very good technique to remove pollutants and is widely used in gas and liquid phase applications.

In addition to removing contaminants, adsorption has become an important separation technique with the potential for regeneration, recovery and recycling of adsorbent materials [2] Therefore, the development of new adsorption systems and porous materials constitutes great importance. Active carbon is one of the most important of these porous materials that have been researched extensively [3].

Activated carbons are frequently used in industry and daily life for various purposes such as environmental pollution control, bleaching, deodorization due to their high porosity and good adsorbent properties. Commercially activated carbons are obtained by activating the carbons obtained from wood, peat, lignite, coal, charcoal, bone, coconut shell, rice husk, nut shell and oil products through various processes [4].

Activated carbon is commonly defined as an amorphous material with high surface area and high porosity, which is generally prepared from carbon-based materials in a waste state [5]. There has not been a formula showing the active carbon structure yet. This structure can be used as a good absorbent owing to its high surface area and high porosity. In addition, the pore volumes of activated carbons vary between 3 angstroms and several thousand angstroms, so they have high adsorption capacity. Generally, organic-based activated carbons contain 87-97% carbon and the remaining part consists of oxygen, sulfur, nitrogen and hydrogen. Also, this ratio varies depending on the material to be synthesized activated carbon [6]. Although activated carbon is the oldest among the adsorbents available [7], it is still the most used material in the industry. Therefore, studies continue to prepare activated carbon with the most appropriate method and to understand its pore structure [8].

Different processes are used for the preparation of activated carbon. In the physical activation method, raw materials, such as CO_2, N_2 or water vapor, are activated at 700–1100 ^{0}C to produce activated carbon. Whereas, during the process of chemical activation carbonization is conducted at 400–900 ◦C in the presence of a chemical agent (e.g., $ZnCl_2$, KOH, K_2CO_3, H_3PO_4 or H_2SO_4) [9].

In this study, Zivzik pomegranate waste was used as a raw material in preparing activated carbon.

According to pomegranate production ranking between countries; Iran first, India second and Turkey ranks third. Pomegranate is grown in the coastline of the Aegean and Mediterranean Regions and the Southeastern Anatolia Region in our country. According to statistical data, pomegranate production is carried out in 48 cities in Turkey. In terms of pomegranate production amounts by cities; Antalya 71, Muğla 22, Denizli 13, Mersin 11, Gaziantep 8,8 and Aydın stand out with 8,5 thousand tons. The pomegranate production ranking of the Southeastern Anatolia Region (GAB) provinces as of 2009 is, Gaziantep is the first, Sanlıurfa is the second and Siirt is the third [10].

Zivzik pomegranate wastes are dried in the laboratory and they have been activated by chemical activation using $ZnCl_2$. The activation temperature was 800 ^{0}C and it has been activated for 1 hour. Methylene blue and Crystal violet have been used as model dyes in adsorption experiments.

1.1 Kinetic parameters of adsorption

Several kinetic models have been put forward to determine what role the mechanism characterizing the adsorption process plays. In this study, Pseudo 1st and 2nd order kinetic equations and Elovich equation are used [11-16].

The pseudo-first-order equation is expressed as

$$\frac{dq_t}{dt} = k_1(q_e - q_t) \quad (1)$$

The integrated form of Eq. (1) becomes:

$log(q_e - q_t) = log\ q_e - \frac{k_1}{2.303}t$ where q_e and q_t are amounts of dye adsorbed (mg/g) at equilibrium and time *t* (min), respectively, and k_1 is the rate constant os pseudo-first-order (min^{-1})

The pseudo-second-order kinetic model of Ho and McKay is

$$\frac{dq_t}{dt} = k_2(q_e - q_t)^2 \quad (2)$$

The integrated form of Eq.(2) becomes:

$$\frac{t}{q_t} = \frac{1}{k_2 q_e^2} + \frac{1}{q_e}t$$

Where k_2 is the rate constant of pseudo-second-order adsorption (g/(mg min)) and $h = k_2 q_e^2$, where h is the initial adsorption rate (mg/g min).

The Elovich equation is given as follows:

$$\frac{dq_t}{dt} = \alpha . e^{-\beta . q_t} \quad (3)$$

Where α is the initial rate (mg/g min) because (dq_t/dt) approaches α when q_t approaches zero, and the parameter β is related to the extent of surface coverage and activation energy for chemisorptions (g/mg).

Given that $q_t = 0$ at $t = 0$, integrated form of Eq. (3) is

$$q_t = \frac{1}{\beta} ln\alpha\beta + \frac{1}{\beta} lnt$$

2. MATERIAL AND METHODS

2.1. Materials

Two dyes were used in the study. The dyes, Methylene Blue (MB) (Chemical Formula = $C_{16}H_{18}N_3SCl$, MW = 319.85 g/mol, λ_{max} = 660 nm) was supplied by Merck; Crystal Violet (CV) (Chemical Formula = $C_{25}N_3H_{30}Cl$, MW = 407.979 g/ mol, λ_{max} = 594 nm) was supplied by Merck. One thousand milligrams per liter of stock solution was prepared by dissolving the required amount of dye in double distilled water. Working solutions of the desired concentrations were obtained by successive dilutions.

2.2. Preparation of activated carbon

Activated carbon used as an adsorbent in experimental studies was obtained by subjecting Zivzik Pomegranate to the carbonization process in a tubular reactor after the chemical activation process.

In the first step; dried Zivzik Pomegranate waste has been dried in an oven by mixing with $ZnCl_2$ in weight of 1:1 with a sufficient amount of water. The dried mixture has been activated in a nitrogen atmosphere in a tubular reactor in a tubular furnace. The activation process has been carried out by keeping under nitrogen atmosphere (100 ml / min) at 10 ^oC / min at a heating rate of 800 ^0C for 1 hour at a maximum temperature. The sample has been taken from the oven cooled to room temperature.

In the second stage, enough 0.5N HCl has been added to the sample taken after activation and boiled on the heater. The sample has filtered until it is sure that no chloride ions are left in the pure water. A chlorine ion test has been done with $AgNO_3$. After the washing process, the activated carbon has been dried in the oven at 105 °C for 24 hours. After grinding and sifting processes, activated carbon has been separated by waiting in a desiccator to be used in experimental studies.

2.3. Instrumentation

A Tri Star 3000 (Micromeritics, USA) surface analyzer was used to measure nitrogen adsorption isotherm at 77 K in the range of relative pressure 10^{-6} to 1. Before measurement, the sample was degassed at 300 ^oC for 2 h. The BET surface area, total surface area and volume of the total surface were measured by the surface analyzer.

The spectrophotometric determination of dyes was done on a Boeco UV – vis spectrophotometer (model UV – S22, Germany).

2.4. Adsorption experiments

In studies that the effect of temperature and mixing time on adsorption was investigated, the solutions prepared as 200 ppm, 400 ppm, 600 ppm and 800 ppm by diluting from 1000 ppm stock solution. Activated carbon was added 0.1 gram and prepared as 500 ml solutions in 1000 ml beakers. It was mixed in the water bath at 25 °C, 35 °C and 45 °C. The moment when adsorbents were added to the solution was accepted as t = 0 and samples were taken at time intervals of 1,3,5,7,9,13,17,23,30,40,50,60,70,90 and 120 minutes.

3. RESULTS AND DISCUSSION

3.1. Characterization of the prepared activated carbon

Activated carbon surface measurements were made by BET device. Its total surface area, total surface volume and BET surface area were measured as 429,044 m^2/g, 0,59232 cm^3/g and 1513,05 m^2/g, respectively.

3.2. Effect of temperature on adsorption

In order to examine the effect of temperature on the adsorption mechanism, both dyes (Methylene Blue - Crystal Violet) were prepared in 1000 ml of solution using 0.1 g of activated carbon at three different temperatures and mixed for the equilibrium period (1 hour). Results are shown in Figure 1 and Figure 2. As can be seen from the figures, similar graphics have emerged for both dyestuffs. As can be seen from the graphics, dye removal increased with the increase in temperature. This means that the adsorption mechanism is endothermic.

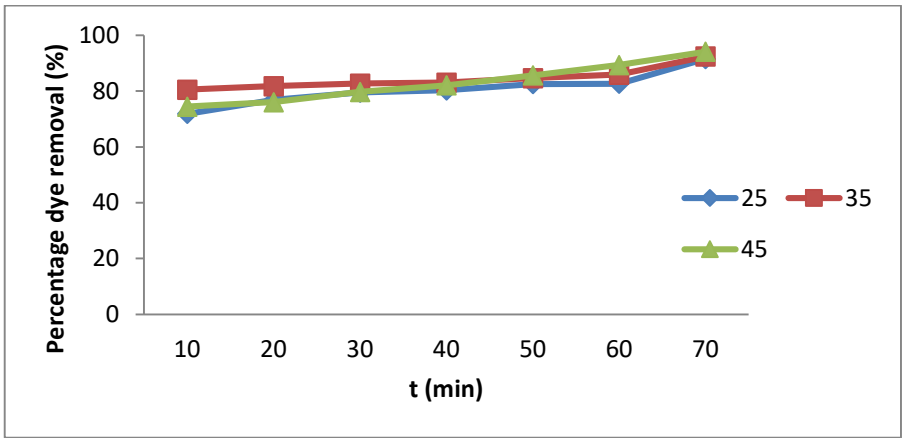

Figure 1. Effect of contact time and temperature on the adsorption of MB

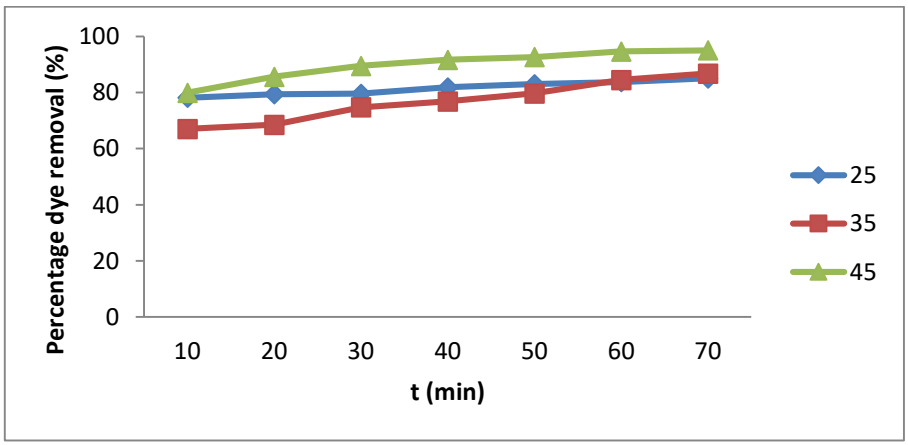

Figure 2. Effect of contact time and temperature on the adsorption of CV

Three basic kinetic models were used for adsorption kinetics. The equality giving the best fit was determined by looking at the regression coefficient (R^2). Methylene Blue and Crystal Violet dyestuffs used in experiments to examine adsorption kinetics at different time intervals (C0 = 200 mg / L, 400 mg / L, 600 mg / L and 800 mg / L, Adsorbent amount = 0.1 g / L, pH = 7.11, Stirring Speed = 300 rpm) adsorption data were used.

The first model used in the investigation of adsorption kinetics is the Pseudo 1st order kinetic equation. Log (qe-qt) values were calculated from dye removal plots to time. Log (qe-qt) versus t graphics drawn at Figure 5, correlation coefficients (R^2) with k_1 values were calculated from these graphs and shown in the Table 1. K_1 values calculated as ; for Methylene Blue at a concentration of 200 mg / L 0,0322, for Crystal Violet at a concentration of 200 mg / L 0,0184 respectively. Correlation coefficient R^2 calculated as 0,88 for Methylene Blue and 0,86 for Crystal Violet respectively. However, it was observed that the adsorption kinetics did not fit the Pseudo 1st order kinetic model because the calculated q_e values with the experimental q_e values did not match with each other.

In Pseudo 2nd order kinetic equation, t / qt 'versus t graphs are drawn in Figure 4. From these graphs, k_2 values and correlation coefficients (R^2) were calculated and shown in Table 1. Correlation coefficient R^2 is; for Methylene Blue 0.99 at 200 mg / L and for Crystal Violet 0.99 at 200 mg / L. Since the q_e values calculated with the experimental q_e values are compatible with each other, it was observed that the adsorption kinetics fit the Pseudo 2nd order kinetic model.

Finally, the Elovich equation is examined. As can be seen in Figure 3, Int graphs were drawn against q_t values. From these graphs α and β values and correlation coefficients (R^2) were calculated and shown in Table 1. However, since the correlation coefficients calculated from the graphs are low, it was observed that the adsorption kinetics did not fit the Elovich equation.

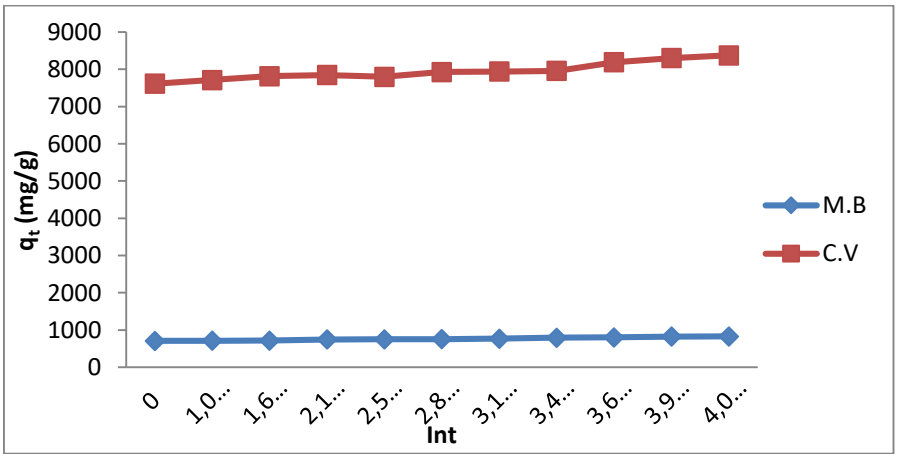

Figure 3. The Elovich equation for adsorption of MB and CV at different temperatures

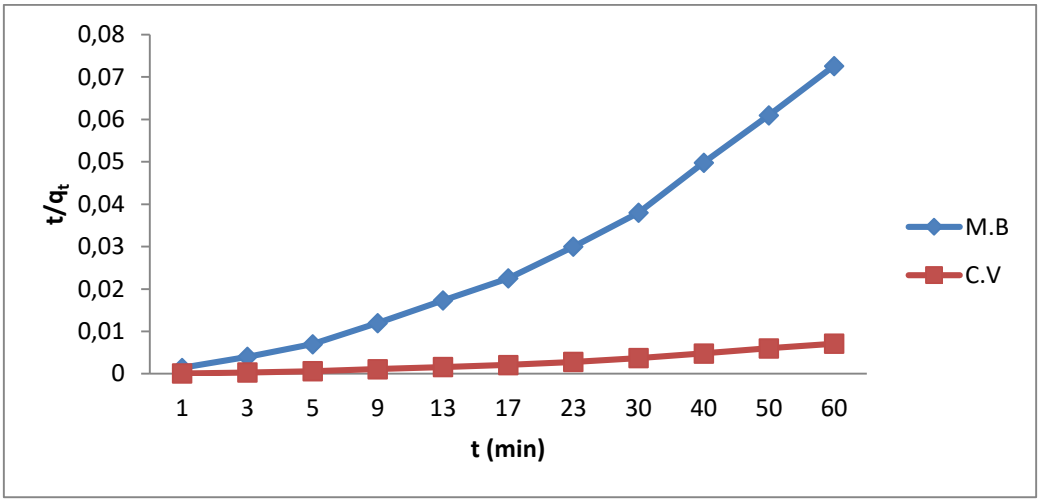

Figure 4. The pseudo-second-order adsorption kinetics of MB and CV at different temperatures

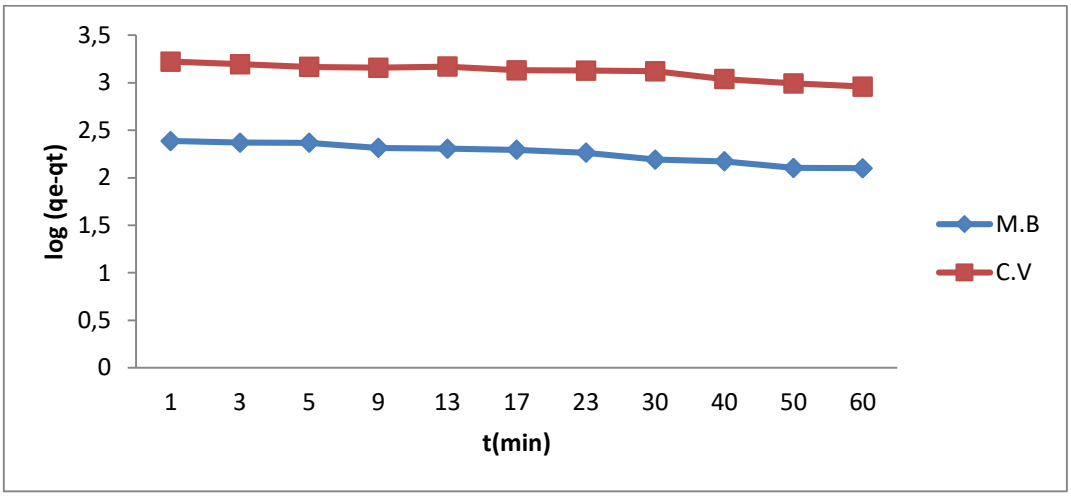

Figure 5. The pseudo-first-order adsorption kinetics of MB and CV at different temperatures

Table 1. Kinetic parameters for the effect of temperatures on the adsorption of MB and CV

T(K)	**q_e(Exp.) (mg/g)**	**Pseudo 1st order kinetic model**			**Pseudo 2 nd order kinetic model**			**Elovich equation**			**Dye**
		(qe)calc. (mg/g)	k1 (l/min)	R^2	(qe)calc. (mg/g)	k1 (g/mg min)	R^2	α (mg/g min)	β (g/mg)	R^2	
298	900.04	391.832	0.0322	0.88	909.09	0.00031	0.99	61.941	0.0215	0.73	M.B
298	9285	1969.246	0.0184	0.86	10000	0.000005	0.99	72.9643	0.0035	0.72	C.V

3.4. Adsorption thermodynamics

The effect of temperature on the Methylene Blue and Crystal Violet adsorption is shown in Figure 1. While the temperature increases, the percentage of dye removal increases lightly. The change in Standard free energy (ΔG°), enthalpy (ΔH°) and entropy (ΔS°) of adsorption were calculated from the following equation:

$$\Delta G° = -RT \ln KC \quad (4)$$

Table 2. Thermodynamic parameters of MB (800 mg/L)

T(K)	lnKc (kJ/mol)	ΔG° (kJ/mol)	ΔH° (J/mol K)	ΔS° (J/mol K)
298	1.864	-4.565		
308	1.926	-5.082	10.846	51.717
318	2.151	-5.600		

Table 3. Thermodynamic parameters of CV (800 mg/L)

T(K)	lnKc (kJ/mol)	ΔG° (kJ/mol)	ΔH° (J/mol K)	ΔS° (J/mol K)
298	1.720	-4.3231		
308	1.991	-5.0313	16.780	70.817
318	2.164	-5.7395		

where R is gas constant, K_c the equilibrium constant and T is the temperature in K. The K_c value is calculated from Eq. (5):

$$K_C = \frac{C_A}{C_S} \quad (5)$$

where C_A and C_S is the equilibrium concentration of dye ions on adsorbent (mg/L) and in the solution (mg/L), respectively.

Standard enthalpy (ΔH°) and entropy (ΔS°) of adsorption can be estimated from van't Hoff equation given in

$$\ln K_C = \frac{\Delta S°}{R} - \frac{\Delta H°}{RT} \quad (6)$$

The slope and intercept of the van't Hoff plot is equal to -ΔH°/RT and ΔS°/R , respectively. The van't Hoff plot for the adsorption of Methylene Blue and Crystal Violet onto Zivzik pomegranate is given in Figure 6 and Figure 7.

Thermodynamic parameters are summarized in Table 2 and Table 3.
It is seen in Table 2 and Table 3 that the ΔH°values were in 10.846 kJ/mol for Methylene Blue and 16.780 kJ/mol for Crystal Violet. The positive values of enthalpy change conform to the

endothermic nature of the adsorption process. The positive values of ΔS˚reflect the affinity of adsorbent material towards Methylene Blue and Crystal Violet. The entropy (ΔS˚) values were 51.717 J/molK for Methylene Blue and 70.817 J/molK for Crystal Violet, respectively. Despite being endothermic nature, the spontaneity of the adsorption process was decreased in the Gibbs energy of the system. The ΔG˚values varied in range with the mean values showing a gradual increase from 1.864 to 2.151 kJ/mol for Methylene Blue and 1.720 to 2.164 kJ/mol for Crystal Violet, respectively, in the temperature range of 25-45 ^{o}C by endothermic nature of the adsorption process.

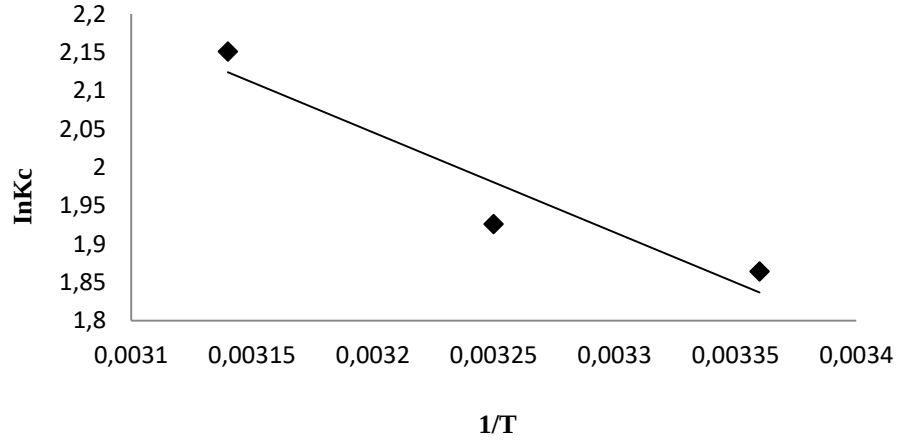

Figure 6. Van't Hoff plots of MB adsorption onto activated carbon from Zivzik pomegranate for 800 mg/L

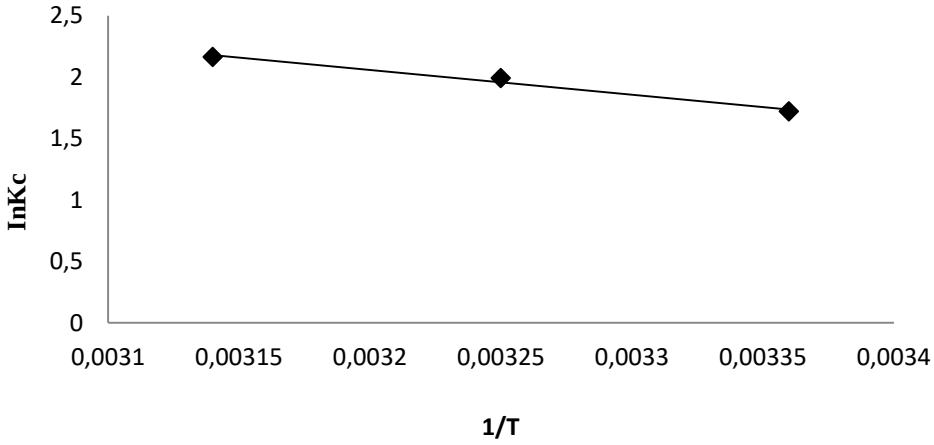

Figure 7. Van't Hoff plots of CV adsorption onto activated carbon from Zivzik pomegranate for 800 mg/L

4. CONCLUSIONS

The results of this work can be summarized as follows :

- The N_2 adsorption isotherm of Zivzik Pomegranate is of type IV. The values of S_{BET}, V_t and S_t are 1513,05 m^2/g, 0,59 cm^3/g and 429,044 m^2/g respectively. Results show that activated carbon includes micropores and mesopores.

- When the adsorption isotherm models for Methylene Blue were examined, it was found to be suitable for the Langmuir model. The constants obtained by the Langmuir equilibrium model have been examined. R_L value, which is the dimensionless separation factor found using K_L value from Langmuir parameters, was found to be 0.001. This result shows that the adsorption process is efficient. In addition, it was seen that the correlation factor R^2 calculated from the graph drawn according to the Langmuir isotherm has a high value such as 0,999. When the adsorption isotherm models for Crystal Violet are examined, their suitability to the Langmuir model was determined. Constants obtained by the Langmuir equilibrium model have been examined. R_L value, which is the dimensionless separation factor found using K_L value from Langmuir parameters, was found to be 0.001. This result shows that the adsorption process is efficient. It was seen that the correlation factor R^2 calculated from the graph drawn according to the Langmuir isotherm has a high value such as 0,999. In addition, the correlation factor R^2 calculated from the graphs drawn according to the Freundlich and Temkin isotherms for Crystal Violet was found to be 0.910 and 0.913, respectively. This shows that the Crystal Violet dye is also suitable for Freundlich and Temkin isotherm models.

- For the Methylene Blue and Crystal Violet dyestuffs, the system's compliance with the adsorption rate expressions was investigated by making use of the time-dependent variation of the amount adsorbed on activated carbon at different temperatures. When comparing the results of the Pseudo 1st Order kinetic model, Pseudo 2nd Order kinetic model and Elovich kinetic models, it was determined that the Pseudo 2nd Order kinetic model was more appropriate. It has been observed that the correlation factor R^2 calculated from the graphs drawn using the Pseudo 2nd order kinetic model is greater than the R^2 calculated from the graphs drawn using other kinetic models.

REFERENCES

[1] Kuyucu A.E., (2013). *Characterızatıon of activated carbon obtained from Zivzik Pomegranate (Siirt) and adsorptıon of dye***,** Master's Thesis, Yüzüncü Yıl University, Department of Primary Education, Van.

[2] Önal, Y., (2006). Kinetics of adsorption of dyes from aqueous solution using activated Carbon prepared from waste apricot, *Journal of Hazardous Materials B,* 137: 1719-1728.

[3] Saygılı H., (2015). *The productıon of nano-porous actıvated carbon from some vegatable pulps and ınvestıgatıon of avaılabılıty ın some adsorptıon practıces,* Phd Thesis, Dicle University, Instıtute of natural and applıed scıences department of chemistry, Diyarbakır

[4] Selçuk, A., Kuyucu, A. E., Kul, A.R, Önal, G., (2015). Investıgatıon of Isothermal Parameters of Dye Adsorptıon onto Actıve Carbon, *International Journal of Ecosystems And Ecology Sciences*, Albania.

[5] R.C. Bansal, M. Goyal (1992). *Activated carbon adsorption*, CRC pres,.

[6] Enver Y. K. (2004). Ticari aktif karbon üretimi ve özelliklerinin belirlenmesi, *Dokuz Eylül Mühendislik Bilimleri Dergisi*, İzmir.

[7] J.W. Hassler, Activated carbon, (1951). *ChemicalPub*, Co.

[8] R. Wirasnita, (2014). Removal of bisphenol A from aqueous solution by activated carbon derived from oil palmempty fruit bunch, *Water, Air, & SoilPollution*, 225(10), p. 2148.

[9] Sarıcı-Özdemir Ç., Önal Y., (2010). Study to investigate the importance of mass transfer of naproxen sodium onto activated carbon, *Chemical Engineering and Processing*, 49: 1058–106.

[10] Vardin H., Karaaslan M., Yılmaz F. M., (2011). *Zivzik ve görümlü narlarının özelliklerinin ve katma değerli ürünlere işlenebilirliğinin belirlenmesi,* Harran University, Siirt.

[11] Lagergren, S., (1898). *Zurtheorie der sogenannten adsorption gelösterstoffe*, Kungliga Svenska Vetenskaps akademiens, Handlingar, pp. 1-39.

[12] Ma, X.,Li, L., Yang, L., Su, C., Wang, K., Yuan, S., Zhou, J., (2012). Adsorption of heavy metal ions using hierarchical $CaCO_3$–maltose meso/macro porous hybrid materials: Adsorption isotherms and kinetic studies. *Journalof Hazardous Materials*, 209– 210**:**467–477.

[13] Elovich, S.Y.,Larionov, O.G., (1962). Theory of adsorption from solutions of non electrolytes on solid (I) equation adsorption from solutions and the analysis of its simplest form (II), verification of the equation of adsorption isotherm from solutions**,** *Izv. Akad. Nauk. SSSR*, 209-216.

[14]Tunalı, S., Akar, T., Özcan, A.S., Kıran, İ., Özcan, A., (2006). Equilibrium and kinetics of biosorption of lead(II) from aqueous solutions by Cephalosporiumaphidicola, *Separation and Purification Technology*, 47: 105-112.

[15] Tunalı, S., Akar, T., (2006). Zn(II) biosorption properties of Botrytisc in area biomass, *Journal of Hazardou sMaterials*, 131: 137-145.

[16] Selçuk A., Kuyucu A. E., Kul A.R. , Ocak S., (2014). Adsorption of dye on to activated carbon obtained from Zivzik Pomagranate, *International Environmental Sciences Symposium of Van,*Van.